ACIBADEM MEHMET ALI AYDINLAR UNIVERSITY
INSTITUTE OF HEALTH SCIENCES

DEVELOPMENT OF TARGETED DRUG RELEASE SYSTEMS AS AN EFFECTIVE THERAPY FOR COVID-19

ASLI AKGÜL

M.Sc. THESIS

DEPARTMENT OF MEDICAL BIOTECHNOLOGY

SUPERVISOR
Assist. Prof. Özgül Gök Özatay

ISTANBUL-2023

ACIBADEM MEHMET ALI AYDINLAR UNIVERSITY
INSTITUTE OF HEALTH SCIENCES

DEVELOPMENT OF TARGETED DRUG RELEASE SYSTEMS AS AN EFFECTIVE THERAPY FOR COVID-19

ASLI AKGÜL

M.Sc. THESIS

DEPARTMENT OF MEDICAL BIOTECHNOLOGY

SUPERVISOR
Assist. Prof. Özgül Gök Özatay

ISTANBUL-2023

Department:	Medical Biotechnology
Program:	Medical Biotechnology
Thesis Title:	Development of Targeted Drug Release Systems as an Effective Therapy for Covid-19
Student's name and Surname:	Aslı Akgül
Date of Defence:	20/06/2023

This is to certify that I have examined this copy of master thesis. I have found that she/he prepared after fulfilling the specified requirements in the associated legislations before the final examining committee whose signatures are below.

Jury Member (Head of the Defense)	Assoc. Prof. Gülen Melike Demirbolat Acıbadem Mehmet Ali Aydınlar University
Jury Member (Thesis Supervisor)	Assist. Prof. Özgül Gök Özatay Acıbadem Mehmet Ali Aydınlar University
Jury Member	Assist. Prof. Ayşe Dulda Yeditepe University

DECLARATION

I declare that this thesis is the result of my own work, and I conducted myself ethically throughout all stages, including planning and writing. I gathered all the information for this thesis in compliance with academic and ethical guidelines, properly acknowledging and citing any external sources or contributions. Furthermore, I ensured that there was no infringement on any patents or copyrights during the course of this study and the writing of the thesis.

25/05/2023

Aslı Akgül

PREFACE AND ACKNOWLEDGEMENT

With all the effort made and attention paid this thesis work has been such a devotion to me and my dedicated supervisor Assist. Prof. Dr. Özgül Gök Özatay. She has been sincerely giving and always there whenever I needed her. I made my experiments and wrote my thesis during Covid-19 pandemic disease which is a difficult period for me. I succeed to finish my project and I am highyl motivated to continue new projects.

I am thankful to Prof. Dr Tanıl Kocagöz to accept me Medical Biotechology Program and I am thankful to Acıbadem Mehmet Ali Aydınlar University to supported me as a full-scholarship student .

TABLE OF CONTENTS

LIST OF FIGURES

LIST OF TABLES

ÖZET

Covid-19 için Kombinasyonal Tedavi Sunabilen Hedefe Yönelik İlaç Salım Sistemlerinin Geliştirilmesi

Bu tezde, SARS-CoV-2 virüsüne bağlanarak hücre enfeksiyonuna neden olan viral hastalıklar için yeni ilaç taşıma sistemleri geliştirilmiştir. Özellikle virüslerin yayılma ve çoğalma hızları göz önünde bulundurularak ve ölüme neden olarak, Covid-19 pandemisi sırasında daha etkili ve odaklı tedavilerin geliştirilmesi hayati hale gelmiştir. İlaç taşıma aracı olarak niosomlar kullanılmıştır. Çünkü onlar non-iyonik, biyolojik olarak parçalanabilir, biyokompatibl, non-immünojenik ve yapısal karakterizasyonları bir spesifik molekülle bağlanarak ayarlanabilir. Ayrıca hedefe yönelik taşıma ve viral hastalıkların tedavisi için kontrollü salınım imkanı sağlarlar. Bu projede kullanılan bu yeni ilaç taşıma sistemleri, tedavi için daha etkili olan hedefe yönelik ve ilaç yüklü niosomları içerir. Benzer ACE2 reseptörlerinin tasarımı, hedefe yöneliklik ve özgüllük sağlar. Bu amaçla, etkin ilaç moleküllerinin sadece enfekte olmuş veya enfekte olma eğiliminde olan hücrelere taşınmasını sağlayacak nanometre boyutlu bir hedefe yönelik ilaç taşıma sistemi tasarlandı; ve bu hedefe yönelik ilaç yüklü nanopartiküller, alınan ilaç dozunu ve ilgili yan etkileri azaltır. P4 peptidi olarak adlandırılan bir özel peptid, özellikle virüs enfeksiyonuna yatkın hücrelere yüksek afiniteli olarak ACE2 reseptörlerine seçici bağlanmayı sağlamaktadır. Bir anti-enflamatuar ajanla ilaç yüklemesi, olası enfeksiyon hasarına bağlı iltihabı azaltmaya yardımcı olur ve hastalığın süresini azaltır. Sonuç olarak, ACE2 reseptörüne yönlendirilen yeni bir ilaç yüklü nanopartikül tasarımı, tedavi sırasında hızlı iyileşmeyi, ölüm oranının ve yan etkilerinin azalmasını sağlayabilir.

Anahtar Sözcükler: SARS-CoV-2, ACE2 reseptörü, Nanoparçacık, İlaç yüklü ve Hedefli Niozom, Deksametazon

ABSTRACT

Development of Targeted Drug Release Systems which can offer Combinatorial Therapy for Covid-19

In this thesis, new drug delivery systems has been developed for viral diseases that cause cell infection by binding to SARS-CoV-2 virus. Especially considering the spread and proliferation rates of viruses and causing death, the development of more effective and focused treatments has become crucial during the Covid-19 pandemic. Niosomes were used as a vehicle for drug delivery. Because, they are non-ionic, biodegradable, biocompatible, nonimmunogenic and their structural characterization can be adjusted by binding a specific molecule. They also enable targeted delivery and controlled release for the treatment of viral diseases. These new drug delivery systems used in this project include targeted and drug-loaded niosomes that provide more efficacy for the treatment. The design of similar ACE2 receptors enables targeting and specificity. For this purpose, a nanoSized targeted drug delivery system was designed to provide the delivery of active drug molecules only to the infected or tended to be infected cells; and these targeted drug-loaded niosomes reduce the dose of drug taken and related side effects. A specific peptide called as P4 peptide conjugation provided selectively binding to ACE2 receptors with high affinity, especially to cells prone to virus infection. Drug loading with an antiinflammatory agent help reduce inflammation caused by possible infection damage and and decrease the duration of the disease. As a conclusion, a new drug loaded niosome design targeted to the ACE2 receptor may enable rapid improvement, decreased mortality rate and decreased side effects during the treatment.

Key Words; SARS-CoV-2, ACE2 receptor, Nanoparticle, Drug-loaded and Targeted Niosome, Dexametasone

1. INTRODUCTION AND AIM

Coronavirus is a family of the virus and It causes a disease such as the common cold, the Middle East respiratory syndrome (MERS) and severe acute respiratory syndrome (SARS). the World Health Organization described the COVID-19 as a pandemic disease on 11 March 2020 (1).

The extremely transmissible SARS-CoV-2 virus quickly led to a global pandemic. It caused various severe health issues such as multi-organ failure, acute respiratory distress syndrome, and a significant number of deaths, particularly among the elderly. The clinical symptoms of SARSCoV-2 infection can vary from mild to moderate to severe, progressing rapidly and causing a sudden and severe illness. Common signs include fever, cough, fatigue, sore throat, muscle pain, headache, difficulty breathing, and conjunctivitis. (2-6).

SARS-CoV-2 which originates from bats, is an RNA virus. It spreads through aerosol droplets generated when an infected person coughs or sneezes. Once inside the body, it specifically attacks alveolar epithelial cells that express the angiotensin-converting enzyme 2 (ACE2) (7-8).

The virus causes damage specifically to the lungs, with cytokines playing a role in lung damage. The spike (S) protein of the coronavirus binds to ACE2 receptors found on the surface of lung cells, facilitating viral entry (9-11).

Antiviral medications are utilized to treat viral infections and are effective for many individuals. In the case of COVID-19 treatment, corticosteroids are also recognized as potent therapeutic drugs. (12,13).

Aspirin can effectively reduce inflammation and the release of proinflammatory cytokines. Additionally, aspirin is utilized for its protective effects on patients with COVID-19 (14,15).

Chloroquine/hydroxychloroquine, known for its antimalarial properties and immunomodulatory activities, has been used to treat Covid-19. Favipiravir, an oral medication approved for influenza treatment, has been used to treat Covid-19 (17,18).

Also, an antiinflammatory drug prevents the release of pro-inflammatory cytokines which are responsible for lung damage. Dexamethasone which is one of the antiinflammatory drugs inhibits the cytokine growth or storms which cause hyperinflammation (19,20).

The drugs like favipiravir and dexamethasone showed effective results in Covid-19 treatment (21). Recently, These drugs are more popular for the treatment of Covid-19 disease because they reduces the mortality rate and to increase treatment effiiciency. They decrease the cytokine storm and provide early recovery of Covid-19 patients. The side effects of the drug cause embryotoxicity teratogenicity and gastrointestinal disorders (22-24).

In spite of all efforts for the treatment, COVID-19 is still threatining for the health because of no specifically approved therapy. There is a serious need for new therapeutic approach to overcome this pandemic (25).

Nanomaterials can be benefical in fighting COVID-19 (26). There are two lipid nanoparticle-formulated mRNA vaccine candidates (moderna and biontech) (27). Nanomaterials can enhance the sustained release because they enhance to protect them from degradation and prolong their bioavailability (28-32).

There is a novel approach for the treatment of Covid-19, which is based on nanomedicine using Niosomes as drug carrier platforms. Niosomes, primarily composed of cholesterol as an excipient. They offer structural flexibility, controlled release biodegradability, biocompatibility, and non-immunogenicity. Niosomes have the capability to encapsulate both hydrophilic and lipophilic drugs and can prolong the circulation of the drug within the body (33-35).

A niosome is a non-ionic surfactant-based liposome Niosomes have a microscopic size, typically ranging from 10nm to 100nm in particle size (36-39). Cholesterol is used to provide rigidity and proper shape, conformation to the niosomes preparations. The major function of surfactant is in the formation of niosomes. The non-ionic surfactants have a hydrophilic head and a hydrophobic tail (40-42).

Purpose of the Study

In this project, targeted and drug-loaded niosomes that can be used in the treatment of viral diseases that cause cell infection by binding to SARS-CoV-2 virus and similar ACE2 receptors will be designed. Especially considering the spread and proliferation rates of viruses, the development of more focused and effective treatments has gained importance with the Covid-19 pandemic.

Therefore, in our project, the delivery of active drug molecules only to the infected or tended to be infected cells; and a nanosized targeted drug delivery system with drug load is designed to reduce the dose of drug taken and related side effects.

This niosome-based drug delivery system has the capacity to be conjugated with the P4 peptide, which can selectively bind to ACE2 receptors with high affinity, especially to cells prone to virus infection.

A niosome is designed that can selectively deliver an anti-inflammatory (Dexamethasone) drug to cells infected or likely to be infected by SARS-derived viruses. This niosome-based delivery system, thanks to its compartmentalized structure, will be able to guarantee the entry of drugs into the same cell by trapping the hydrophilic anti- inflammatory drug in the core in the membrane part. Therefore, these niosomes, which can reduce inflammation after infection and improve the treatment efficiency, will also be selectively directed to cells with ACE2 receptors.

2. BACKGROUND

2.1. Drug Delivery Systems

Nanotechnology involves making physical and chemical modifications to create materials in nano-scale size. These innovative materials have extensive applications in various fields such as pharmaceutical technology, scientific research, diagnostic imaging, drug delivery, and biosensors. Nanoscale devices used in medicine are referred to as nanomedicines or nanoparticles, which have a size of less than 1 μm. Nanosystems have shown significant advancements in treatment by providing effective drug delivery, targeting specific areas, and overcoming multi-drug resistance. They can also bind with antibodies for active drug targeting. The application of nanotechnology in drug delivery has the potential to revolutionize the future of pharmaceuticals and biotechnology (1-4).

Drug delivery indicates the delivery of a pharmaceutical to a specific illness location so as to obtain efficient and safer therapeutic results. One of the major desirable targets of clinicians is drug release at the point of action. Nevertheless, safe delivery of drugs to the pathogenic locations and controlled release are the major problems of Drug Delivery Systems (DDS) (5– 8).

The effectiveness of drug therapy is enhanced by controlling blood circulation and eliminating the drug from the body. The main objective of employing nanobiotechnology in drug delivery is to prolong the lifespan and concentration of the drug at the affected site while minimizing its concentration in healthy cells, thereby increasing the therapeutic effect. For instance, She et al. proposed a potential nanoscale drug delivery system that exhibited potent anti-tumor activity with minimal adverse effects in breast cancer treatment (9).

Nanodrug delivery systems have appeared to enhance administrative paths and biodistribution of drugs with low side effects and low immunogenicity (10).

Similarly, in recent times, several innovative drug delivery technologies have surfaced, presenting a promising avenue for combating COVID-19. Nano-based therapeutics present numerous possibilities for addressing the limitations of existing treatments. These systems have the potential to modify the properties of pharmacokinetics/pharmacodynamics, leading to decreased toxicity, lower dosages, and enhanced drug availability. As a result, they can retain their immunomodulatory effects and effectively suppress viral propagation. The importance of effectively localizing therapies to specific targets is underscored by previous understanding of respiratory viruses (11).

2.1.1. Passive targeting

Passive targeting refers to the utilization of the body's physiological and anatomical conditions by the bioactive-carrier complex to reach its desired target. Specific delivery to a particular site is determined by the properties of the bioactive agent itself, eliminating the need for an additional targeting approach. The size, charge, and hydrophobicity of the carrier system play a role in its in vivo distribution and clearance kinetics, and these characteristics can be adjusted to achieve passive targeting. Despite the complex mechanism involved, the term "passive targeting" is used because no additional ligand is attached for targeting purposes (12).

EPR effect

The enhanced permeability and retention (EPR) effect refers to the phenomenon where macromolecules like drugs, liposomes, and nanoparticles (NPs) tend to accumulate more in tumors compared to normal tissues. This is due to the leaky vasculature and dysfunctional lymphatic system present in tumor areas, which allows easier access for these agents. In contrast, the tight junctions between endothelial cells in normal tissues prevent the transport of therapeutics across them (13).

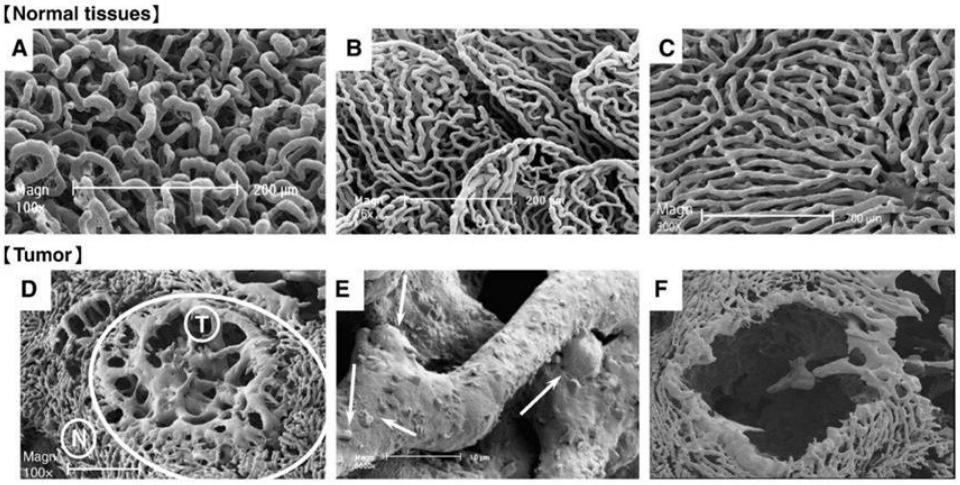

Fig. 4. SEM images of blood vessels in various normal tissues (A–C) and metastatic liver tumors (D–F). Normal capillaries of the pancreas (A), colon (intestinal villi) (B), and liver (sinusoid) (C) are shown. (D) Metastatic tumor nodule (circled area identified with T) in the liver, the normal liver tissue is indicated with "N." (E) Tumor vessels at the capillary level (larger magnification), with a rough surface and an early phase of polymer-extravasating vessels (arrows). Normal tissues show no leakage of polymeric resin (A–C), whereas the tumor nodules clearly demonstrate tumor-selective extravasation of polymer (via the EPR effect) (D, E). After i.v. injection of the macromolecular anticancer drug (SMA-pirarubicin micelles), the tumor vascular bed (visible in D) was completely disintegrated, as shown by an empty void (F).
Modified from Ref. [11] with kind permission of J. Daruwalla and C. Christophi.

Figure 2.1.1. SEM images of blood vessels in various normal tissues(A-C) and metastatic liver tissues (D-F)

Proteins larger than 40 kDa have shown a tendency to selectively accumulate in tumor tissues and normal tissues. Moreover, these proteins tend to remain in tumor tissues for extended periods of time. The accumulation of polymeric macromolecular drugs in tumor tissues is significantly higher compared to their accumulation in normal organs and tissues, such as muscle, heart, skin, and kidney, following intravenous injection. This suggests a potential for targeted drug delivery and preferential drug retention in tumor tissues (14,16,17,23-25,26–31).

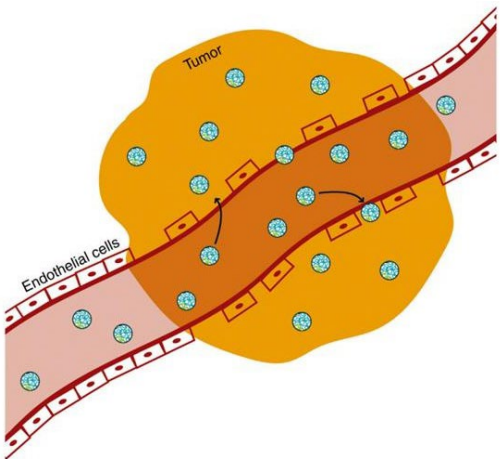

Figure 2.1.2. Passive Targeting: enhanced permeability and retention effect

The EPR effect was discovered not only with proteins involving immunoglobulin G (IgG), but also with drug–polymer conjugates, nanoparticles of PLGA, micelles, liposomes, DNA polyplexes and lipid particles (14-21,33).

2.1.2. Targeted drug delivery systems

Targeted drug delivery systems carry the drug to the diseased tissue through a particular interaction over a long period of time. Targeted drug delivery is a group of mechanisms that help the aggregation of drugs in a particular part of the body (e.g. organ, tissue, cells) that has been attacked by diseases. From a theoretic point of view, each drug delivery system has two main targets: first, improving drug efficiency, and second, preventing drug enterance to healthy parts of the body. The process of drug delivery is achieved by way of using suitable carriers for the drugs. Type, size, shape, chemical compound, morphology, and the surface chemistry of these carriers directly influence their distribution, behavior, and so the process of targeted drug delivery (35).

Due to the lack of specific treatments for preventing COVID-19, it is important to explore different strategies for delivering and formulating repurposed drugs. This may involve making changes to the dosing schedule or administration route. Regardless of the route used, the primary goal is to deliver effective concentrations of the drugs to vulnerable cells and tissues, both locally and systemically (36).

Most repurposed drugs are typically administered systemically through oral or injectable routes. However, there is also interest in delivering drugs through inhalation and intranasal routes, with a focus on achieving effective concentrations at the infection sites, particularly in the upper respiratory tract/lungs and the mucous membranes of the throat and nasal cavity. By using appropriate delivery devices or formulations, it is possible to achieve directly targeting to the primary infection sites (37). Inhaled immunomodulatory drugs show promise due to the genetic similarity between SARS-CoV-2 and its parent virus, SARS-CoV. Inhalation-based drug delivery often requires lower doses compared to systemic delivery (injection or oral administration), resulting in milder and fewer adverse effects (38).

Nanotherapy's principal demand/ goal is to reduce and get rid of the side effects of bioactive agents. Bioactive agents will be very beneficial if they attack only the particular targets, without troubling other mechanisms. An important target of nanotherapy is known to be targeting the therapeutic chemicals to the involved tissues and organs by means of special Nano-carrier systems (39,40). For instance, the nanoliposomes are able to deliver many drug molecules at once in comparison to other nanocarriers and they have the capacity to exhibit encouraging results when targeting moieties are fastened to their surface. Targeted delivery can be performed either passively or actively (41).

2.1.3. Active targeting

Liposomes can be modified by coating their surface with hydrophilic chains, allowing them to avoid opsonization, which leads to reduced elimination from the bloodstream and an extended circulation time. This modification improves drug intake as the liposomes migrate to the infected area, where the stealth liposomes are reduced and release the drugs into the surrounding environment. To achieve active targeting, various conjugating moieties such as monoclonal antibodies, small molecule ligands, and peptides can be attached to the surface of the liposomes or nanocarriers. This enables specific targeting of the liposomes/nanocarriers to desired locations. (42-46). In order to manage targeted delivery, the particular ligands of these receptors are fastened to the surface of the liposomes, this will in turn improve the binding capacity and affinity of the liposomes to the targeted cells, and therefore it ends up with targeted delivery (47,48).

2.2. Polymer-Lipid Nanoparticles as Drug Delivery System

2.2.1. Micelles

Micelles play a significant role as nanocarriers, effectively trapping functional components to improve their stability and bioavailability. These nanometer-sized aggregates are formed through the self-assembly of amphiphilic polymers in an

aqueous solution. By encapsulating volatile components, micelles can reduce their degradation and evaporation, enhancing the stability of sensitive compounds during production, storage, and ingestion. Initially, the amphiphilic polymers exist as individual unimers at low concentrations. However, when the concentration reaches the critical micelle concentration (CMC), the unimers combine to form micelles (49-53). Micelles are effective carriers for hydrophobic food functional components due to their hydrophilic shell and hydrophobic core. The hydrophobic core binds and adsorbs hydrophobic components, while the hydrophilic shell enhances their solubility. Different types of micelles can be utilized for this purpose. Polysaccharide-based micelles are formed through self-assembly of hydrophobic moieties attached to a polysaccharide backbone. Chitosan-based micelles are produced by modifying chitosan with hydrophobic groups, and they self-assemble into spherical micelles. Dextrans and starch can also be modified to create amphiphilic polymers for functional component delivery systems. Dextrins, derived from natural starch, can be used as substrates for hydrophobic modification. Casein, the principal element of milk protein, forms micelles with hydrophobic and hydrophilic segments, providing binding sites for hydrophobic functional components. Overall, micelles offer versatile and efficient carriers for delivering hydrophobic food functional components (54-59).

Surfactants and bile salts are commonly used materials for the delivery of functional components. Surfactants, such as sodium dodecyl sulfate (SDS), Tween, and Brij, form self-assembled micelles when their concentration exceeds the critical micelle concentration (CMC). Bile salts, along with lipid hydrolysates, can form bile salt mixed micelles during digestion, which can encapsulate hydrophobic functional components and improve their absorption by small intestinal epithelial cells. The use of bile salt-based micelles has shown promising results in achieving high bioavailability during digestion (60-62).

Micelles can be delivered through transcellular and paracellular transport. While polymer micelles are usually unable to pass through the tight junctions of cells via paracellular transport, their micellar structure enhances the bioavailability of loaded active components. The hydrophobic core of polymer micelles encapsulates

hydrophobic active components, ensuring their release in the gastrointestinal tract. Additionally, the particle size of polymer micelles is typically between 10 and 200 nm, allowing them to be absorbed intact through endocytosis. These properties make micelles suitable carriers for oral delivery (63,64).

2.2.2. Liposomes

Liposomes are double-layer structured vesicles and varying sizes ranging from nanometers to micrometers. When amphiphilic molecules like sphingolipids and phospholipids are present in water, the hydrophilic heads face the water while the hydrophobic tails minimize contact with water molecules (65).

Liposomes disperse hydrophobic molecules within their phospholipid bilayers, while hydrophilic molecules are encapsulated within the hydrophilic phase of liposomes. By doing so, liposomes enhance the stability of enclosed nutrients, reduce their toxicity, and provide long-lasting effects. They also possess properties such as cell affinity, targeting capabilities, and histocompatibility (66).

Liposomes are widely utilized for delivering small molecules and nucleic acids, offering several advantages. They can easily produce controlled-sized particles, achieve high drug-to-lipid ratios, exhibit long circulation with stealth coating, and resemble biological membranes due to their composition of natural phospholipids (67). An additional benefit is their ability to encapsulate both lipophilic and hydrophilic drugs. Liposomes can be tailored to a size range of 50-150 nm, enabling them to penetrate blood vessels and accumulate in tumor areas through the enhanced permeability and retention (EPR) effect (68-70). However, conventional liposomes are quickly recognized by the immune system, particularly the mononuclear phagocytic system, leading to their clearance by the reticuloendothelial system. To overcome this, nanoliposomes are extensively employed as nanosystems for delivering various substances such as long and small nucleic acids, proteins, peptides, and small molecules (71).

These materials are formed through the spontaneous organization of phospholipids, including phosphatidylserine, phosphatidylglycerol, phosphatidylethanolamines, phosphatidylcholine, as well as other molecules like cholesterol. Natural lipid bilayers are commonly utilized to create liposomes. Bilayer liposomes consist of a hydrophobic tail and a hydrophilic head, allowing hydrophobic drugs to be embedded within the lipid bilayer membrane and hydrophilic drugs to be encapsulated within a central aqueous cavity. Nanoliposomes have demonstrated the ability to deliver various substances such as small drugs, proteins, imaging agents, peptides, and nucleic acids. They have also been found to exhibit sustained release of encapsulated drugs, resulting in prolonged exposure to the target area and improved effectiveness. Importantly, nanoliposomes have been successfully utilized as both passive and active targeting delivery systems (72).

Nanoliposomes are smaller versions of liposomes, with nanoscale dimensions. These nanosystems offer advantages such as efficient penetration into targeted tissues through blood capillaries and membranes, easy uptake by cells, potent therapeutic activity, and sustained effects that can last for extended periods, even weeks, as compared to larger microsystems. Additionally, nanoliposomes have a prolonged circulation time in the body, enhancing their effectiveness as drug delivery systems (73).

Nanoparticles, including nanoliposomes, have the potential to enhance the effectiveness of bioactive agents by improving their solubility and bioavailability both in laboratory settings and in living organisms. Nanoliposomes specifically have shown promise in delivering and transporting substances like vitamin E and ascorbic acid to areas where oxidation occurs in food systems. They are also effective in encapsulating antioxidants. Other types of nanoparticles, such as those based on polymers, gold, and carbon nanotubes, should not be overlooked despite having fewer clinical trials conducted on them (74-76). Liposomes and nanoliposomes have largely the same thermodynamic,structural, and chemical properties. But nano-liposomes have the capacity to enhance solubility, bioavailability, and surface area in comparison to liposomes. Further, they support the specific targeting of encapsulated chemicals (77).

The attachment of ligands to nanoparticles is done to enhance the effectiveness of targeted therapies. Nanoliposomes are used as carriers for drugs because they can improve stability and bioavailability during in vivo treatments. These particles help prevent the drugs from binding to unwanted molecules, reducing side effects. Nanoliposomes offer several benefits, including biodegradability, biocompatibility, low toxicity, and the ability to be modified in size (78-80).

To prevent liposomes from being recognized and cleared by macrophages, a biocompatible polymer called polyethylene glycol (PEG) is now being used as a coating on liposomes. These modified liposomes are referred to as PEGylated liposomes. This approach increases the stability and duration of circulation for liposomes in the body. Additionally, liposomes can be further modified by attaching ligands that have the ability to recognize and bind to specific groups, thereby enhancing the accumulation of liposomes in targeted tissues (81,82). Polymeric nanoparticles have garnered interest for their ability to achieve controlled burst release. However, these systems are prone to aggregation and exhibit lower encapsulation efficiency compared to other options (83).

2.2.3. Niosomes

The rapid progress of nanotechnology in treating and diagnosing diseases has led to the emergence of nanomedicine. Different materials like polymers, nanogels, metals, metal oxides, liposomes, and niosomes can be utilized to create nanostructures. The downsizing of drug carriers to the nanoscale brings various benefits, such as enhancing the pharmacokinetics and distribution of therapeutic agents, minimizing toxicity by targeting drug aggregation in specific regions, facilitating drug transport between cells, and prolonging drug retention in biological systems to improve effectiveness.The main objective of developing vesicular structures is to achieve controlled drug release, modify distribution profiles, and target specific areas of the body. Vesicular systems have the capacity to carry both hydrophilic and lipophilic components and offer larger drug loading capacity and sufficient surface area for targeting. Niosomes, a unique type of vesicle developed from nonionic surfactants in

an aqueous phase, possess membrane permeability and the advantages of liposomes. The successful use of niosomes as drug carriers depends on their stability in biological fluids, circulation in the body, drug preservation, interaction with target areas, and intracellular delivery of their contents. Niosomes are preferred over other bilayer structures due to their chemical stability, low production cost, low toxicity, biodegradability, biocompatibility, and ease of storage and handling. Niosomes have been studied with various administration methods, including oral, transdermal, intramuscular, and intravenous routes. They can improve the absorption rate of certain drugs through cell membranes. Over the past decade, the development of niosomes has emerged as an effective tool in drug delivery, contributing to advancements in drug delivery systems (84).

A new approach in treating Covid-19 involves the use of nanomedicine and Niosomes as drug carriers. Niosomes are vesicles made from synthetic nonionic surfactants, sometimes with the inclusion of cholesterol or lipids. Similar to liposomes, they can transport lipophilic and amphiphilic drugs. Niosomes are biodegradable, non-ionic, biocompatible, nonimmunogenic, and offer structural flexibility. They have been extensively studied for controlled drug release and targeted delivery in the treatment of viral infections, cancer, and other microbial diseases. Niosomes have the capability to encapsulate both lipophilic and hydrophilic drugs and prolong the drug's circulation in the body (85).

A niosome is a non-ionic surfactant-based liposome. Niosomes are produced generally by cholesterol incorporation as an excipient. Niosomes have more penetrating capacity than emulsions. Although niosomes share a similar bilayer structure with liposomes, their composition of materials makes them more stable and provides additional advantages compared to liposomes. The size of niosomes is microscopic. The particle size varies from 10nm-100nm (86,87).

A typical niosome vesicle consists of a vesicle-forming amphiphile like a non-ionic surfactant (Span-60), which is stabilized by the addition of cholesterol and a small quantity of anionic surfactant, such as dicetyl phosphate, which aids in the

stabilization of the vesicle (88,89). The two main ingredients used for preparing niosomes are cholesterol and nonionic surfactants. Cholesterol is used to supply rigidity and proper shape, conformation to the niosomes preparations. The main function of surfactant is in the production of niosomes. The non-ionic surfactants like Spans,Tweens and Brijs are usually used for the preparing niosomes. The nonionic surfactants possess a hydrophilic head and a hydrophobic tail (89-91).

Niosomes, which are mainly composed of surfactants, possess a unique chemical structure characterized by both hydrophilic and lipophilic properties. Surfactants consist of a hydrophilic head and a lipophilic tail, resulting in two distinct solubility regions. The hydrophilic head contains anionic, cationic, and amphoteric molecules that dissolve easily in water. On the other hand, the lipophilic region can contain nonpolar groups such as fluorocarbons, alkanes, or aromatics. Surfactants are categorized as anionic, amphoteric, cationic, or nonionic based on the properties of their head group. Nonionic surfactants are commonly used in niosome preparation due to their compatibility, stability, and low toxicity compared to other surfactants (93). In the production of niosomes, various types of nonionic surfactants are used, such as alkyl esters, alkyl ether derivatives, and sorbitan fatty acid esters. Among them, sorbitan fatty acid esters (Spans) and polyoxyethylene sorbitan fatty acid esters (Tweens) are widely employed as nonionic surfactants. These surfactants are known for their safety and non-irritating properties. The gel transition temperature of Spans increases as the length of the acyl chain in the molecule increases. For example, Span 20 (sorbitan monolaurate) with a 9-carbon chain remains in a liquid state at room temperature. Span 40 with a 13-carbon chain undergoes gel transition at around 47°C, while Span 60 with a 15-carbon chain exhibits gel transition at approximately 58°C. Interestingly, as the carbon-chain length of the surfactant increases, the entrapment efficiency of niosomes improves (95).

HLB is a crucial parameter for selecting surfactants in niosome production, as it affects the size and drug-loading capacity of the vesicles. Surfactants with HLB values between 4 and 8 are suitable for vesicle formation. Those with HLB values higher than

6 have difficulty in forming vesicles, so cholesterol needs to be added when producing niosomes (96).

Additives are used in niosome formulations to enhance physical stability, alter biodistribution, and improve permeability. Cholesterol is the most significant additive, providing increased stability by raising the transition temperature of the vesicles. Cholesterol also affects various characteristics of niosomes, including hydrodynamic diameter, entrapment efficiency of drugs, membrane permeability, rehydration capability, rigidity, and toxicity. Cholesterol, a commonly used additive, prevents leakage, stabilizes bilayers, and slows down the permeation of solutes encapsulated in the aqueous core of the vesicles (97).

Entrapment efficiency is a crucial factor in utilizing niosomes for drug delivery. It depends on the preparation method, surfactant type, drug properties, and the presence of additives. Tween surfactants with long alkyl chains and high HLB values exhibit the highest entrapment efficiency for water-soluble drugs. Entrapment efficiency is quantified as the total amount of active component released from the niosomes, and it can be calculated using a specific equation.
(EE): = (%EE) (Amount of drug entrapped / total amount of drug) x 100

One of the frequent methods to find out the amount of entrapped drug in niosomes is, separating unentrapped drug (centrifugation, dialysis, or gel filtration); digesting noisome by way of using proper medium (methanol,isopropanol, etc.) and finally, examining the resultant solution by suitable assay method to evaluate the entrapped drug. The entrapment efficiency of niosomes is greatly affected by the pH of the hydration medium (98).

Niosomes, which are vesicular structures used as drug carriers, can be classified into different types based on their composition and characteristics. Multilamellar Vesicles (MLV) are niosomes composed of multiple lipid bilayers surrounding an aqueous compartment. They have a diameter ranging from 0.5 to 10 μm and are known for their mechanical stability and long-term storage capability. MLV niosomes are

ideal for delivering lipophilic compounds. Large Unilamellar Vesicles (LUV) are another type of niosome with a size range of 100 to 3000 nm. LUVs have a high ratio of aqueous phase to surfactant compartment, allowing for efficient encapsulation of bioactive materials using a reasonable amount of surfactant membrane. Small Unilamellar Vesicles (SUV) are typically derived from MLVs through methods like high-pressure extrusion, sonication, or high-pressure homogenization. They have a size range of 10 to 100 nm. SUVs, however, have three drawbacks: they are thermodynamically unstable, prone to aggregation, and generally have lower capacity for encapsulating hydrophilic drugs compared to other types of niosomes.

Proniosomes are dry formulations consisting of a water-soluble carrier coated with a thin film of nonionic surfactant, such as sorbitol, mannitol, maltodextrin, lactose monohydrate, glucose monohydrate, or sucrose stearate. They provide benefits like decreased physical instability, ease of handling as a powder, and the ability to be hydrated before use (101).

2.2.3.1. Niosome preparation

Specific additives, surfactants, and an aqueous solvent are required in order to produce niosomes. The formation of niosomes occurs when surfactant monomers aggregate into vesicles upon hydration, driven by the high interfacial tension between water and the lipophilic portion of the surfactant. The surfactant molecules align themselves in a way that the hydrophilic head groups face outward, while the lipophilic tails come together to form a bilayer structure. These opposing forces lead to the formation of a supramolecular assembly. Other essential components, such as cholesterol, are also included in the niosome preparation. Various methods have been developed for the production of niosomes.

2.2.3.2. Thin film hydration method

The thin film hydration method is a widely used and effective technique for preparing niosomes. In this method, surfactants, additives like cholesterol, and, if

needed, a lipophilic drug are dissolved in organic solvents. The solution is then mixed in a round-bottom flask under vacuum and at a specific temperature. The organic solvent is removed, resulting in the formation of a thin film on the flask's inner surface. Hydration is initiated by adding water or Phosphate-buffered saline (PBS) to the mixture at a temperature higher than the surfactant's phase transition temperature, particularly when incorporating a hydrophilic drug into the formulation. There are also Ether Injection Method, Bubble Method, Hand-Shakıng Method, Sonication Method, Heating Method, Reverse Phase Evaporation Method, Microfluidization Method, Enymatic Method, Trans-Membrane pH Gradient Method and Supercritical Carbon Dioxide Fluid Method.

2.2.3.3. Characterization

It is necessary to perform physicochemical characterization to ensure the quality of niosome products,. This involves evaluating various parameters including the morphology, bilayer composition, size, charge of the vesicles, stability, zeta potential, entrapment efficiency, and in vitro release. These factors must be carefully assessed to control the quality of the niosomes.

2.2.3.4. Morphology and size

Determining the size of niosomes is an important quality control test as it significantly affects their plasma pharmacokinetics and biodistribution. Niosomes are typically spherical, and their size can be measured using various techniques such as dynamic light scattering (DLS) or microscopy. A multifunctional zeta potential analyzer can be utilized to determine the size and polydispersity index (PdI) of niosomes. The repulsive forces between the bilayers and the entrapped drug play a crucial role in determining the final size of the niosomes. Zetasizer analysis also provides valuable information about the uniformity of the niosome product. A PdI value of less than 0.4 indicates a homogeneous sample. However, one limitation of DLS is that it does not provide information about the shape of the niosomes. Zeta potential is a critical factor that influences the behavior and characteristics of vesicles,

and it should be carefully measured during the niosome preparation process. The Hydrophilic-Lipophilic Balance (HLB) values of surfactants have a significant impact on the zeta potential (102-103).

Niosomes offer several advantages in drug delivery as mentioned below:

- They provide controlled and gradual drug release.
- Niosomes have superior stability and drug storage compared to liposomes.
- They enhance medication-taking behavior by protecting drugs, delaying clearance, and targeting specific areas.
- Niosomes are biodegradable, biocompatible, and non-immunogenic, resulting in low toxicity and high compatibility with biological systems.
- Various administration routes are possible, including oral and intravenous.
- Niosomes improve oral bioavailability and enhance drug permeability into the skin.
- They can encapsulate a wide range of drugs with different solubilities.
- Niosomes effectively deliver drugs to targeted organs.
- Niosomes are easily modified and flexible due to the functional groups on their hydrophilic heads.
- Surfactant storage and handling do not require special conditions.
- Water-based niosome suspensions offer better patient compliance compared to oil-based systems.
- The characteristics of niosomes, such as size and lamellarity, can be adjusted as needed.
- Niosomes can function as depots for controlled and sustained drug release.
- They provide protection to drugs from the biological environment, enhancing therapeutic performance (104-107).

The size of niosomes plays a crucial role in their tissue distribution. Large niosomes tend to accumulate in the lungs, while smaller ones can easily access the spleen through fenestrations in the liver. Niosomes and liposomes, due to their structural similarity, operate through similar mechanisms when interacting with cells. These mechanisms include intermembrane transfer, contact release, endocytosis,

fusion, and adsorption. In vivo, niosomes function similarly to liposomes in their interactions with cells (108,109).

2.2.3.5. Pharmaceutical applications and administration of niosomes

Niosomes find applications in various fields, but they are predominantly used in drug delivery. The choice of administration method significantly impacts the formulation design of niosomes. Niosomes can be utilized for ocular, pulmonary, and nasal delivery. Nasal delivery offers advantages such as faster and higher drug absorption compared to the gastrointestinal tract due to factors like the absence of enzymatic activity, reduced dilution, and neutral pH of nasal mucus (110).

Nasal drug delivery offers several advantages, including bypassing first-pass metabolism, enhancing bioavailability compared to oral and rectal administration, fast onset of action, and enabling systemic circulation for drugs with poor oral absorption or polar ingredients. Targeted drug delivery using niosomes can be achieved through interactions with the cells of the Reticulo Endothelial System (RES) facilitated by opsonins. These opsonins recognize niosomes, leading to clearance by RES macrophages, making niosomes useful for targeted drug delivery in cases where infectious organisms reside in RES organs. Research has shown that Tween 20 niosomes exhibit inherent selectivity to macrophages, further supporting their potential for targeted delivery (103). Second, the drug can be passed to the target and direct organs, such as liver and brain. Targeted and specific delivery of therapeutic molecules is crucial to avoid complications associated with non-targeted therapy. Ligands for different receptors can be coupled to the surface of niosomes using a spacer molecule or by direct attachment. This enables niosomes to specifically target receptors and facilitate the effective delivery of therapeutic substances.

The Figure 2.2.3. depicting the active targeting of receptors on malignant cell surfaces have also been provided (111).

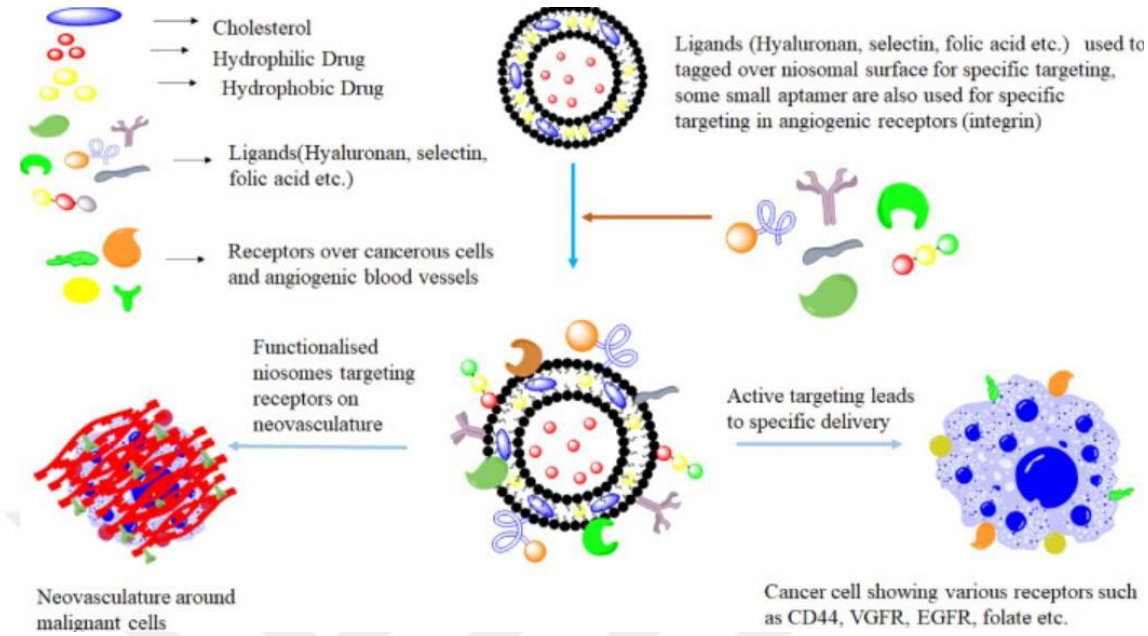

Figure 2.2.3.5. Niosomes with active targeting of various receptors expressed on and around malignant cell surface

The spike (S) protein of SARS-CoV plays a crucial role in binding to host cell receptors and promoting fusion between the viral envelope and host cell membranes. Previous research has identified significant amino acid variations in the S protein region. Researchers have hypothesized that interfering or competitively binding with these protein domains could hinder SARS-CoV infections by disrupting the function of the S protein. Synthetic peptides targeting specific regions of the S protein have been shown to inhibit viral infections by preventing virion-cell membrane fusion. These findings suggest the potential therapeutic value of these peptides in treating viral diseases. A recent study has demonstrated that a peptide targeting a specific region of the SARS-CoV S protein effectively inhibits virus infection. A figure presented in the text illustrates the effectiveness of synthetic peptides targeting different regions of the S protein in inhibiting SARS-CoV infection in a monkey kidney cell line (112-117).

2.2.3.6. Peptide conjugated niosomes

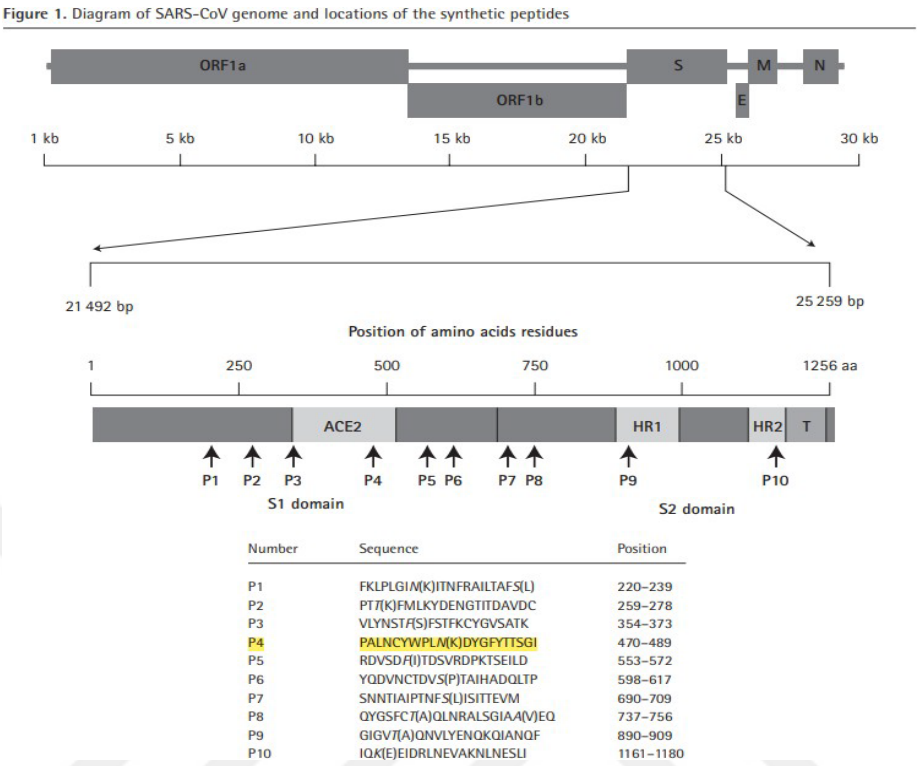

Figure 2.2.3.6. Diagram of SARS-SoV genome and location of the synthetic peptides

A set of ten 20-mer peptides, referred to as P1-P10, was designed to cover the 12 distinct variations of the S gene found in different genome sequences of human SARS-CoV and animal SARS-CoV-like virus isolates (112). The study found that these active peptides were effective in blocking the virus from entering cells, although they did not inhibit virus replication. Notably, peptides P3 and P4 contained specific variations (F360S and N479K) in the virus receptor binding region (ACE2) that differed between human and animal isolates. (118,119). The results indicated that the tested peptides were found to be inactive, suggesting that the two specific sites in question may not play an active role in the binding between the spike protein and ACE2 receptor. It is possible that these peptides are unable to compete with the S protein for ACE2 binding. Since these peptides occupy regions at the interface between S protein monomers, it is proposed that they could interfere with the function of the spike protein by competitively binding to the monomers. This binding would mimic the regions that become exposed after a conformational change induced by ACE2

binding. These regions may be involved in proteinase cleavage, co-receptor binding, and/or interaction with the virus-cell membrane. Consequently, these peptides may potentially compete with the spike protein for the interaction between the virus and the cell membrane.

2.3. Nanomedicine for Sars-CoV-2 Infections

2.3.1. SARS-CoV2 infections

COVID-19, a global health concern at present, poses a significant threat to the medical community. It originated in Wuhan, China and was first reported on December 31, 2019. The initial outbreak consisted of 27 pneumonia cases characterized by symptoms such as difficulty in breathing, fever, and lung damage. COVID-19 is a virus that originated from bats and exhibits symptoms including dry cough, persistent fever, chills, difficulty in breathing, muscle pain, fatigue, loss of taste or smell, and headache when it infects humans (120,121). While most of the cases are resolved with small symptoms, some patients have fatal complications, such as pulmonary edema, septic shock, and acute respiratory distress syndrome (ARDS) (122).

It is known that Coronaviruses have caused pneumonia epidemics in humans, such as SARS- CoV (related to SARS-CoV-2) and Middle East Respiratory Syndrome (MERS-CoV) This genome is nearly 80% similar to SARS-CoV that was the first coronavirus outbreak in China in 2002 (2), which killed many people. (123,124) As no particular action has been approved untill now, the only present means to avoid the transmission of SARS-CoV-2 are the use of N95 and surgical masks, hand hygiene and physical distancing (125).

SARS-CoV2, a member of the Coronaviridae family, is a β-coronavirus with a single-stranded positive RNA genome. Within this family, there are other viruses such as SARS-CoV and MERS-CoV, which share sequence similarity with SARS-CoV-2. Both SARS and MERS have posed significant public health risks. SARS-CoV-2, the causative agent of COVID-19, is classified within the β-coronavirus subfamily. It has

the ability to infect humans and can result in severe illness and even mortality. In terms of its structure and arrangement, SARS-CoV-2 shares similarities with other coronaviruses in terms of its structural proteins, which include the envelope, spike (S) glycoprotein, membrane, and the non-structural nucleocapsid protein. Additionally, the virus contains a positive RNA genome, ranging from 26.2 to 31.7 kilobases, that is enclosed within the ribonucleocapsid complex (RNP) and enveloped by an outer layer (127,128). The virus S glycoprotein of SARS-CoV-2 is responsible for host cell entry after interacting with the human receptor ACE2 (129,130–132). Numerous SARS-related coronaviruses have been found in their natural reservoir host, bats. (133–136)

A new coronavirus emerged in Wuhan, China, causing an outbreak of acute respiratory syndrome in humans. The virus is similar to a bat coronavirus at the genetic level and uses the same cell entry receptor as SARS-CoV. Previous coronaviruses, such as SARS and MERS, have led to significant global pandemics. The outbreak in Wuhan originated from a local seafood market and has resulted in thousands of confirmed infections and numerous deaths. Clinical symptoms of the infected individuals include dry cough, breathing difficulties, fever, headache, and pneumonia, which can progress to respiratory failure and death. The disease is transmitted through human-to-human contact and can range from asymptomatic or mild cases to moderate or severe disease, with the potential for fatal outcomes (137-142). Some seriously ill patients go through an immunological phenomenon that is known as cytokine storm, characterized by a proinflammatory cytokine response that results in lung injury (143).

In terms of clinical manifestations, 80% of individuals infected with COVID-19 experience mild or asymptomatic symptoms such as headaches, body pain, fever, loss of smell and taste, and diarrhea. The remaining 20% may develop moderate to severe symptoms, including difficulty breathing, secondary infections, pneumonia, renal or cardiac failures, and blood clotting abnormalities, which can potentially lead to death. The primary mode of virus transmission is through the air, although there is some evidence of transmission through contaminated surfaces and fomite droplets, albeit less frequently (142).

A significant research finding is the interaction between the spike protein of the virus and the angiotensin-converting enzyme 2 (ACE2) receptor in humans. Interestingly, ACE2 is more resistant to SARS-CoV-2 compared to SARS-CoV, which might explain the higher infectivity and transmissibility of the current coronavirus. ACE2 is considered a cellular receptor for SARS-CoV (129,144).

ACE2 is identified as a potential cell receptor for the entry of 2019-nCoV. Unlike other coronaviruses, such as SARS-CoV and MERS-CoV, 2019-nCoV does not use other known coronavirus receptors like APN and DPP4. ACE2 is an enzyme present on the cell membrane and is part of the renin-angiotensin system (RAS). It plays a crucial role in safeguarding the lungs by regulating processes like lung tissue proliferation, fibrosis, and inflammation, thus protecting against acute respiratory injuries. (145-146). The high affinity of SARS-CoV-2 to ACE-2 and the abundance of ACE-2 receptors in lung epithelium explain why the lungs are particularly vulnerable to COVID-19. Once the virus enters the lung tissue, it triggers an inflammatory response as part of the body's natural defense mechanism. However, this immune activation also leads to significant lung damage. COVID-19 stimulates the release of various proinflammatory mediators, including cytokines and chemokines, at a rapid rate. These molecules attract large numbers of monocytes and dendritic cells to the lungs, exacerbating the inflammatory response and causing severe and potentially fatal lung injury. This excessive immune response is known as a cytokine storm (147-151).

This means that managing upregulated inflammation, which is the main cause of COVID-19 deaths, would dramatically increase the survival of the patients and as a result, it would avoid fatal complications. Therefore, it is extremely attractive to discover the interference with the cytokine storm as a treatment method to overcome COVID-19. In a healthy person, the airway epithelium works as a barrier against the usual onset of bacteria,viruses, and different particles in order to prevent infection and tissue injury. SARS-CoV-2 mostly goes into the human body through the respiratory tract, and worsens the alveolar epithelium, airway epithelium and vascular endothelium (152,153). Ciliated airway epithelial cells are the main places of SARS-CoV-2 infection (154). Just like other coronaviruses, the SARS-CoV-2 infection arises

through, firstly, the binding of the viral S (spike) protein to the Angiotensin-converting enzyme 2 receptors (ACE2), extravagantly present on the surface of lung alveolar epithelial cells, this is followed by the cleavage of the spike protein by Transmembrane serine protease 2 (TMPRSS2) (155-158).

After filtering through the nasal mucosa, SARS-CoV-2 repeats and activates the repertory of inflammatory and immune responses that make up the symptoms and signs of COVID-19 infection (159). Following infection with SARS-CoV-2, the epithelium in the upper respiratory tract experiences compromised gas exchange and respiratory insufficiency. This triggers a cascade effect where the virus particles produced by the infected epithelial cells proceed to infect nearby cells, including endothelial cells, neighboring epithelial cells, and macrophages. These cells actively participate in the process of efferocytosis (160). Reinfection is the ability of SARS-CoV-2 to infect patients who are previously infected, it is an important problem with SARS-CoV-2, because it can help escape from vaccines and this can reduce the life quality of re-infected patients (161). Patients with severe or moderate symptoms are less susceptible to reinfection due to the presence of intermediate to long-term memory or duration of neutralizing antibodies (nAbs) lasting from 3 to 8 months.

On the other hand, individuals with mild symptoms or who are asymptomatic are more prone to reinfection because they exhibit a lower response from memory B and T cells and have a shorter duration of nAbs (162,163). Some of the SARS-CoV-2 variants that escape from nAbs/memory cells are a rising problem at present. There are several SARS-CoV-2 variants, however, four of them are more dangerous and transmissible than the original SARS-CoV-2 and they require more concern.These four variants are now Beta (former B.351 South African variant), Alpha (former B.117 British variant), Gamma (former P1 Brazilian variant), and Delta (former B.1.617.2 Indian variant) (164-168).

Because of the exponential increase in COVID-19 cases worldwide, it is urgently necessary to find out effective treatments to minimize the number of mortalities because of the disease. The rising evidence draws attention to cytokine storm as the

major culprit in COVID- 19 progression and the development of complications in a definite subset of patients, such as ARDS and multiorgan failure that would cause fatal outcomes in alot of individuals (126,169). The earliest clinical studies that are from Wuhan (170,171) proposed that patients having life-threatening COVID-19 showed clinical features which cause cytokine-release syndrome (CRS), macrophage activation syndrome (MAS) and acute respiratory distress syndrome (ARDS) (172).

The SARS-CoV-2 cytokine storm that is stimulated by macrophages and other natural immune cells, is determined by elevated levels of key cytokines such as IL-1β, TNF-α and IL-6 (129,173). The indication of these pro-inflammatory cytokines is very definitely discovered in COVID-19 pneumonia patients, together with other severity-related symptoms for example coagulation (143).

It is interesting that macrophages generally interact with ACE2-expressing cells available in the lung tissue and it cause destructive and defensive functions (174). The vascular endothelium is an important site of infection in COVID-19. Infection of endothelial cells occurs in the interstitial or luminal space, leading to the release of chemokines and cytokines. The infection with SARS-CoV-2 triggers a "cytokine storm" that impairs macrophage function and disrupts the clearance of apoptotic cells. Additionally, SARS-CoV-2-infected epithelial cells express inflammatory mediators (175-178).

In vitro analyses have indicated that type II alveolar cells, due to infection with coronavirus or influenza virus, release pro-inflammatory cytokine mediators (179). Increased release of chemokines due to SARS-CoV-2 infection in the lungs leads to elevated levels of pro-inflammatory cytokines. This can disrupt the clearance of apoptotic cells and contribute to various lung disorders and complications (180). Dysregulated immune response and macrophage activation syndrome have been observed in COVID-19 patients who are suffering from severe respiratory disorder (181). In addition to pulmonary fibrosis and failure, other complications such as hyper-coagulation or clot formation have been observed in COVID-19 patients (182–184).

2.3.2. Targeted drug delivery systems for Covid-19

In addition to traditional vaccine types like live attenuated vaccines, inactivated vaccines, and recombinant protein vaccines, nanoparticle vaccines offer a unique opportunity to advance vaccine science and provide effective solutions for the current pandemic and future challenges. Over 26 nanoparticle-based vaccine candidates have entered human clinical trials. These vaccines utilize different formats such as lipid nanoparticles (LNPs), micelles, virus-like particles (VLPs), protein nanoparticles, and other technologies. Nanoparticle vaccines can be categorized into two groups: those that encapsulate vaccine antigens or nucleic acid cargos within their core, and those that present vaccine antigens on their surface. Antigen-encapsulating nanoparticle vaccines ensure the preservation and controlled release of the cargo after immunization, while nanoparticles displaying vaccine antigens can effectively stimulate antigen-presenting cells (APCs) and promote strong immunogenicity through B cell receptor (BCR) cross-linking (185,186).

Lipid nanoparticles (LNPs) are employed to deliver DNA and RNA that encode vaccine antigens. Encapsulation within LNPs works to protect mRNA cargo from quick degradation by RNases, and also to advance cellular delivery of mRNA which is difficult because of size and charge limitations (187). A key ingredient of LNPs is an ionizable lipid, that is charged positively at low pH to admit encapsulation of negatively-charged mRNA, while it is neutral at physiological pH (188). Both lipid particles and mRNA hold strong immunostimulatory characteristics (28,29), contradicting the requirement for formulation with adjuvants additionally (189,190). Both the Moderna and BioNTech/Pfizer mRNA-LNP vaccines employ mRNA carrying modified nucleosides, that are suitable to limit the immunogenicity of mRNA, admitting higher vaccine doses and improving translational capacity (191).

The CureVac mRNA-LNP holding nucleosides that were lacking modification needed lower doses to be delivered in clinical trial, and showed only 47% efficiency against variants circulating at present (192).

Polymers (e.g. PLGA), chitosan, or polyethylenimine (PEI)) have been extensively employed in the past to make nanoparticle vaccines for other coronaviruses (e.g. SARS-CoV, MERSCoV, or hCoV) (193). Chitosan,that is a natural polysaccharide, was used to encapsulate the SARS-CoV-2 RBD proteins (194).

VLPs imitate morphological and molecular characteristics of native viral virions, while they are lacking genetic material making them non-replicating and non-infectious. (195). Micelles are amphiphilic structures that are self-assembled and that can deliver SARS-CoV-2 proteins, an example being the vaccine presently in late-stage phase 3 clinical trial (196).

Protein-based nanoparticles have been developed for delivering subunit protein vaccines targeting SARS-CoV-2, specifically the S (spike) protein and RBD (receptor-binding domain). One example is a self-assembling nanoparticle called S ferritin nanoparticle (SpFN) at phase 1 in clinical trials (197).

Liposomes, on the other hand, are nanostructures made up of amphipathic phospholipids. They consist of one or multiple lipid bilayers that form a membrane enclosing an aqueous core. Unlike LNPs (lipid nanoparticles), liposomes have been utilized to deliver SARS-CoV-2 vaccine antigens (e.g RBD-liposomal vaccine in a preclinical trial) (198).

The high degree of efficiency provided by nanoparticle COVID-19 vaccines that are now approved has saved several lives and it improved the science of vaccinology considerably. Present COVID-19 vaccine advancement is not fair universally with selected high- and middle-income countries that are approaching high vaccine coverage while vaccine roll-out has hardly started in several low-income countries (199).

mRNA-LNP vaccines are more expensive than conventional vaccines. Moreover mRNA-LNP and protein nanoparticle vaccines need specialized production facilities and highly skilled labor forces,that is a great problem in various resource-limited

environments (200). A further disadvantage of mRNA vaccines is the common need for ultra-cold chain storage, that makes the logistics of vaccine production, storage and distribution complicated (201). The fast and extensive use of new classes of nanoparticle vaccines has increased safety considerations, with proof of highly infrequent but severe anaphylaxis and myocarditis after vaccinations with mRNA-LNP (202).

2.3.3. Inflammation and cytokine storm in SARSs-CoV-2 infection

Increased systemic inflammation is related with worse results in COVID-19. Uncontrolled inflammation gives rise to disease severity in COVID-19 (203,204). Increased levels of inflammatory chemokines and cytokines have been observed. This excessive inflammatory response, often referred to as a cytokine storm, bears similarities to the immune reactions observed in patients infected with other severe coronaviruses such as SARS-CoV and Middle East respiratory syndrome coronavirus (205-211).

A study aimed to evaluate the role of cytokines in predicting patient outcomes and disease severity after COVID-19 hospitalization. The results showed that each cytokine measured upon admission could independently predict overall survival, even after accounting for demographic factors and comorbidities. Cytokines were found to be valuable for risk classification and survival prediction, independent of commonly used laboratory and clinical severity metrics. Early measurement of cytokines can serve as safe predictors of patient outcomes and may help guide treatment decisions. Patients who have moderate disease with high IL-6 levels may be trated with cytokine blockade, because the dexamethasone treatment could be attributed to its ability to decrease IL-6 levels. These findings highlight the importance of serum cytokine levels in determining treatment strategies and identifying individuals at risk of severe complications and death (212).

‘Cytokine storm’ is the uncontrolled and excessive production of soluble inflammatory markers and it is a critical reason for ARDS in COVID-19 patients (213).

ARDS (acute respiratory distress syndrome) is the leading cause of death in COVID-19 patients and is characterized by immune cell infiltration in the lungs and low oxygen levels. In ARDS, the inflammation damages the alveolar-capillary membranes, leading to increased lung permeability and the leakage of fluid containing high levels of proteins into the air sacs. A recent study on SARS-CoV-2 by Huang et al. (2020) reported elevated levels of pro-inflammatory cytokines and chemokines in infected patients (214-216).

There are various researches describing the systemic inflammatory response in COVID-19 and they have similarly linked cytokine elevations developing into severe disease. Furthermore, COVID-19 cause endothelial damage and microthrombosis (217). In fact, some patients with severe COVID-19 demonstrate catastrophic microvascular damage with complement activation (218).

Cytokine storm syndrome (CSS) refers to a group of clinical symptoms caused by an overactive immune system. Recent studies have shown that there is a positive feedback loop between the release of cytokines and cell death pathways. Certain cytokines, as well as damage-associated molecular patterns (DAMPs) and pathogen-associated molecular patterns (PAMPs), can trigger inflammatory cell death, leading to the release of more cytokines. Many of the clinical features of CSS, such as enlarged liver and spleen, fever, low blood cell counts, progressive liver failure with clotting problems, and high levels of ferritin, can be explained by the effects of common proinflammatory cytokines (219,220).

Corticosteroids, for instance dexamethasone and glucocorticoids, serve as immunomodulatory and anti-inflammatory agents by way of hindering the synthesis of proinflammatory cytokines and prompting lymphocyte cell death (221). Regarding COVID-19, dexamethasone was indicated to be effective only in patients who required mechanical ventilation or supplemental oxygen in the randomised open-label Phase II/III Recovery study in patients hospitalised with COVID-19 (222).

The cytokine storm, which involves the excessive activation of the immune system and subsequent attack on the body's cells, can lead to multi-organ failure, acute respiratory distress syndrome (ARDS), and death in severe cases of infection. Like other severe respiratory, corticosteroids can be used in the treatment of severe pneumonia caused by coronaviruses. Systemic corticosteroid therapy is recommended for 3-5 days in severe COVID-19 cases accompanied by pneumonia. A recommended dose of methylprednisolone is less than 2-3 mg/kg as an additional treatment for COVID-19. The potential role of corticosteroids in inhibiting the inflammatory pathway in critical conditions needs to be carefully monitored due to the risks of adverse effects and secondary infections. (223-225). Pathogenesis of COVID-19 includes pro-inflammatory cytokine production by macrophages in lung alveoli (226). The use of corticosteroids is for suppressing the host inflammatory reactions in the lungs, which may cause acute lung damage and ARDS (227).

Dexamethasone, which is a synthetic glucocorticoid, has been used previously to treat various conditions such as allergies, arthritis, asthma, and autoimmune diseases. It works by blocking two inflammation pathways: immune cell migration and vasodilation. When dexamethasone enters host cells and binds to glucocorticoid receptors in the cytoplasm, it triggers a series of immune cell responses that suppress pro-inflammatory cytokines.

The disease is known to affect the blood vessels, as severe cases of the disease show signs of blood clotting and systemic inflammation, suggesting the involvement of the endothelium in the development of the disease. Additionally, COVID-19 patients have shown elevated levels of endothelial injury markers, which are associated with the severity of the disease (228-232).

The vascular endothelium is liable for keeping the homeostasis in the organism. It participates in fibrinolysis and coagulation, controls constriction and relaxation of vessels and it is also necessary to adjust immune responses (233). In certain pathological situations, endothelial cells undergo an activated state characterized by increased procoagulant and proinflammatory activity. This phenomenon, observed in

conditions such as sepsis and COVID-19, demonstrates that systemic inflammation is a potent trigger for endothelial activation (234,235). Both diseases exhibit a high mortality rate in their more severe forms (236) and they are identified by intense activation of immune mediators ("cytokine storm") (231) and antifibrinolytic and prothrombotic state (238).

2.3.4. Drugs for Sars-CoV-2 therapy

Presently, health care professionals depend on strategies that are known to prevent other infections, such as dexamethasone (239), anti-coagulation drugs, oxygen therapy, and intensive care unit interventions such as mechanical respiration and tracheostomy (240). Vaccines are another necessary tool to decrease the effect of the pandemic. Nevertheless, vaccinating billions of people defines a production and logistics problem, especially in developing and underdeveloped countries, having the less economic power to buy vaccine doses (241-242). Additionally, anti-science and anti-vaccine movements make up a serious risk for the success of vaccination campaigns, like the denialist positions that some leaders and their followers confirm (243).

At the beginning of the pandemic, the main strategies included using accessible medicines to handle or even avoid infection. This strategy had a misdirecting success at the beginning, because some chemical compounds that are tested in vitro and in vivo demonstrated proof of early treatment and prophylaxis , such as the novel and promising usage of clofazimine and molnupiravir, in addition to compounds that have already used for similar applications, such as hydroxychloroquine, chloroquine, azithromycin and ivermectin (239,245–252).

Chloroquine (CQ) has been used for prophylaxis and treatment of malaria for a long time (253). Besides their antimalarial activity, they have a strong anti-inflammatory activity that may prevent the cytokine storm in patients that are infected with SARS-CoV2. This will decrease the production and release of different pro-

inflammatory cytokines (254), that are the main mediators of the cytokine storm syndrome.

The false sense of protection is another risk of using ivermectin, which causes people to avoid actions of prevention from contamination. In the mean time, the usage of azithromycin can cause microbial resistance and, finally, sepsis (255). Additionally, it is found out that these medicines offer no clinical benefits in randomized researches (256).

With these results, the most useful treatment for severe COVID-19 may continue to be corticosteroids. Various researches have indicated that corticosteroid treatment can decrease mortality in severe COVID-19, especially in the RECOVERY Trial. Here it is seen that dexamethasone up to 10 days reduced 28-day mortality significantly, with the most evident responses in those patients receiving oxygen without invasive ventilation (rate ratio 0.82) or requiring mechanical ventilation (age-adjusted rate ratio 0.65) (257).

Many researches approved the whole benefit of corticosteroids in severe COVID-19 and corticosteroid treatment is commonly advised at the moment for children and adults hospitalized with severe COVID-19 infection (258-260).

2.3.5. Corticosteroids

Corticosteroids are effective in reducing inflammation associated with various conditions. As a result, corticosteroid treatment leads to a decrease in the levels of inflammatory mediators involved in the cytokine storm. The use of dexamethasone in severe COVID-19 cases has garnered significant attention due to promising findings. In a large randomized, controlled trial conducted in the United Kingdom, initial results favored the use of dexamethasone. The trial included hospitalized COVID-19 patients, with 2,104 patients receiving 6 mg dexamethasone (oral or intravenous) once daily for up to 10 days, and 4,321 patients receiving standard care. After 28 days, dexamethasone showed significant benefits in patients requiring respiratory support.

It reduced mortality in patients on invasive mechanical ventilation and receiving oxygen support without invasive mechanical ventilation. Furthermore, patients in the dexamethasone group had shorter hospital stays and a higher likelihood of being discharged within 28 days compared to those receiving standard care (261,262).

Controlling inflammation with dexamethasone presents a significant opportunity to improve treatment outcomes for COVID-19 patients in the later stages of the disease. The effectiveness of corticosteroid administration largely relies on factors such as the patient's clinical condition, the timing of administration, and the dosage given. Considering these details is crucial for optimizing the use of corticosteroids, including dexamethasone, in COVID-19 treatment. Additionally, the widespread availability and affordability of dexamethasone, coupled with its long duration of action, which allows for once-daily dosing, provide an advantage in its use (263).

Despite the superior effectiveness of corticosteroids compared to non-steroidal anti-inflammatory drugs, their limited water solubility poses significant challenges for their use. Corticosteroids have poor water solubility, which greatly restricts their application. The limited administration volume makes it difficult to load an adequate amount of the drug while maintaining solubility. Additionally, solutions offer a more consistent drug dosage, but it is challenging to develop consistent water-soluble formulations for poorly water-soluble corticosteroids, including viscous solutions and hydrogels (264-266). For the present, suspension,prodrugs and nanosystems are the principal strategies to develop the water solubility of ophthalmic corticosteroids. Developing the water solubility of drugs is a significant subject in the pharmaceutical industry (267,268). Despite corticosteroids are more effective than non-steroidal anti-inflammatory drugs, poor water solubility, seriously limits the usage of corticosteroids. (269). Nanosystems enhance the solubility of corticosteroids via several mechanisms, including particle size reduction (268,270,271).

COVID-19 is described by cytokine storm or cytokine release syndrome (CRS) that is related with the excessive production of proinflammatory cytokines. The high morbidity and mortality related with SARS-COV-2 infection can be associated with

the autoimmune destruction of the lungs and it is mediated by the release of a storm of pro- inflammatory cytokines (272). At present, there are very few or no treatment options to avoid COVID-19 infection (273,274).

Anti-inflammatory drugs such as corticosteroids can be used to decrease the lung damage induced by the cytokine storm in patients with COVID-19 (275). During the last decade, corticosteroids (CS) have appeared as steroidal medicine to decrease inflammation in different disorders, including systemic lupus erythematosus, rheumatoid arthritis, asthma, and certain cancers by imitating anti-inflammatory hormones that are produced by the body (276-278). Dexamethasone was recorded on the world health organization (WHO) and it is currently available in most of the countries at acceptable cost and off-patent (279). During the fight against corona infection, the immune system of the body is initiated and it activates inflammation as the body's immune response. Nevertheless, the immune system leads to a cytokine storm, fetal reactions, and it begins to attack the body's cells. Coronavirus additionally stimulates coagulopathy, respiratory failure, and multi-organ failure (280). Dexamethasone, a synthetic corticosteroid, exhibits broad immunosuppressive effects and has a longer duration of action compared to cortisone. Corticosteroids like dexamethasone possess anti-inflammatory properties by reducing the transcription of various chemokines, pro-inflammatory cytokines, and adhesion molecules. In the context of COVID-19, dexamethasone can be beneficial as it suppresses the production of cytokines and mitigates their detrimental effects, making it a potential intervention against the cytokine storm associated with COVID-19. Studies have demonstrated that short-term dexamethasone treatment can alleviate the severity of inflammation by preventing the occurrence of a severe cytokine storm or hyperinflammatory phase in COVID-19 patients with pneumonia (272,281-285).

2.3.5.1. Dexamethasone

The World Health Organization declared general guidelines to overcome SARS-COV-2 disease (COVID-19). COVID-19 is either asymptomatic or it involves a high risk of acute respiratory distress syndrome (ARDS), cytokine storm syndrome, shock,

devastating pneumonia and death (286,287). According to the initial clinical trial results from the United Kingdom (UK), on June 16, 2020 WHO declared that dexamethasone can be lifesaving for patients who have critically COVID-19 disease.

The useful effects of dexamethasone treatment cannot be generalized and they are limited to severly ill COVID-19 patients who have developed into a stage requiring respiratory support (288). As a result, we can suppose that immunomodulatory effects of glucocorticoids are useful only in the later hyperinflammatory phase of the disease. As a more reliable approach, intravenous dexamethasone can be administered controlledly (272).

Dexamethasone is a cheap and easily available drug that can be acquired without a prescription in some countries. Therefore, there is an increased possibility of self-medication and drug shortage after the social media reports about its useful effects.
The Randomized Evaluation of COVID-19 Therapy (RECOVERY) conducted a trial which aims to compare the therapeutic efficacy of various drugs, including lopinavir-ritonavir, dexamethasone, hydroxychloroquine, azithromycin, or tocilizumab, in hospitalized COVID-19 patients. The trial shows that these drugs decrease the mortality rate in patients with COVID-19.

Dexamethasone was found to be effective in reducing the mortality rate of COVID-19 patients. The trial administered a daily dose of 6 mg of dexamethasone for ten days, to evaluate its clinical effectiveness compared to standard care alone in 4321 patients. It supports the use of dexamethasone in COVID-19 patients with low oxygen levels. However, it is important to note that these results should not be generalized to patients with milder forms of the disease (288-290).
Early evidence has shown that dexamethasone reduces mortality risk in ventilated patients and those on oxygen therapy for extended periods. The use of dexamethasone did not result in significant side effects but was ineffective in mild cases. However, the Oxford RECOVERY Trial has limitations regarding potential adverse effects, secondary outcome results, and the effectiveness of dexamethasone in patients with comorbidities. Current guidelines recommend restricting corticosteroid administration

to severe cases associated with cytokine storm. The World Health Organization (WHO) issued guidelines endorsing the use of dexamethasone and other corticosteroids for COVID-19 treatment, particularly in critical and severe patients. While dexamethasone is effective, it carries the risk of severe side effects such as hormonal imbalance, weight gain, anxiety, fluid retention, and sleep disturbances. Blurred vision, hemorrhage, and eye disorders are rare risks. Additionally, a low dose of dexamethasone is necessary for COVID-19 patients at risk of developing restricted ARDS. Optimizing the dexamethasone use might obtain therapeutic improvement in COVID-19 when it is used in the right patient, at the right time and at the right dose (291-294).

3. MATERIALS AND METHODS

3.2. Materials

Span 60, Poly-ethylene glycol distearate (PEG) (Mwt: 50-190 kDa), Tween 80 (for synthesis), PEG Dicholesterol was acquired from Sigma to create niosomes. An acetate buffer with a pH of 5.5 was prepared using acetone, acetic acid from Merck, and distilled water. Phosphate saline buffer tablets from Biomatik Corporation were dissolved in distilled water for drug release profile experiments. HATU, diethyl ether, and anhydrous sodium sulfate from Merck were also obtained. Fischer Science provided Spectrum™ Spectra/Por™ 6, pre-wetted Standard RC Dialysis Tubing with a 1kD MWCO, for dialysis. Phosphate-buffered saline (PBS) buffer was prepared with certain amount of distilled water and 1 PBS tablet which were purchased from Thermo Fisher Scientific Inc. Dexamethasone was purchased Sigma Aldrich to use as drug in niosome. HATU, DIPA, Et3N, DMF and Oleic acid were purchased from Sigma for the conjugation of peptide with the peptide. P4 peptide was synthesized with Alanine, Asparagine, Aspartate, Cysteine, Glycine, Isoleucine, Leucine, Lysine, Phenylalanine, Proline, Serine, Threonine, Tryptophan and Tyrosine purchased from Sigma. Sephadex beads and sephadex column were purchased from Sigma for the size exclusion chromatography. Ultracentrifugation tube (3.5 K) purchased from Sigma for the purification of the drug-loaded niosomes.

3.3. Preparation of Niosomes

3.3.1. Optimization studies for niosome formulations

Optimization of Thin Film Method:

In thin film method technique, an organic solvent is added into round bottom flask. All lipids, surfactants and drugs are solved in an organic solvent (like ether, chloroform, benzene etc. Chloroform is usually preferred as an organic solvent.

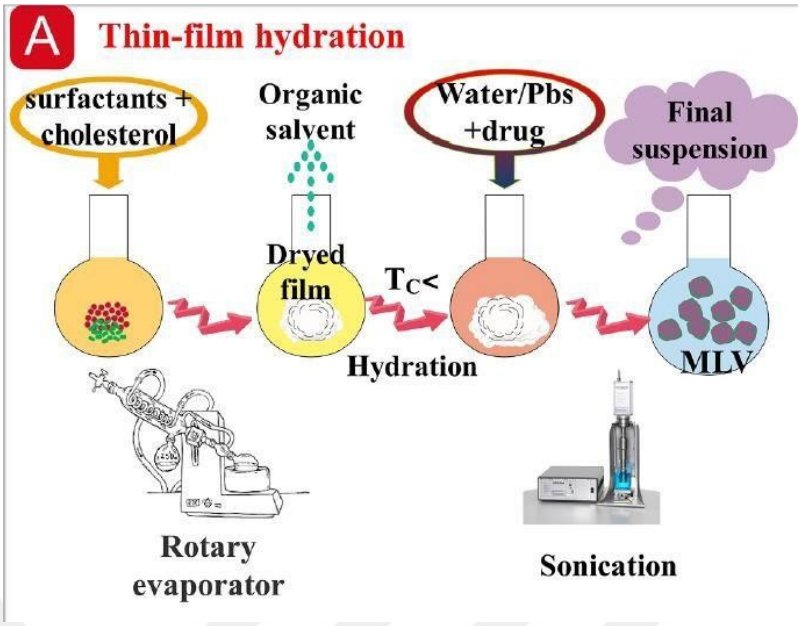

Figure 3.2.1. General scheme for Thin-Film Method

Certain amounts of surfactants (Tween 80) and Cholesterol were added and they were dissolved in certain amount of chloroform at round bottom flasks. After mixing, the organic solvent was evaporated under decreased pressure in vacuum rotary evaporator; thin layers were formed on the inner surface after evaporation. According to this procedure, thin film formation was tried at different ratio of materials and these experiments enabled the optimization of the thin film method.

At first, 3 different formulations at small and big sized round bottom flasks (50mL and 100 mL) were tried to find the optimum ratio of surfactant and cholesterol. Certain amounts of cholesterol and Tween 80 as a surfactant at different ratios were dissolved with certain amounts of chloroform as an organic solvent.

Formulation A included Cholesterol and Tween 80 at 1:0,25 ratio and this formulation was prepared at 50 mL and 100 mL round bottom flasks. Formulation B included Cholesterol and Tween 80 at 1:0,5 ratio and this formulation was prepared at 50 mL and 100 mL round bottom flasks. Formulation C included Cholesterol and Tween 80 at 1:1 ratio and this formulation was prepared at 50 mL round bottom flask.

Prepared solutions were transferred into 50 mL and 100 mL round bottom flasks. Then, solutions were mixed in round-bottom flasks and put into the rotatory evaporator to remove the organic solvent (chloroform). Then, thin film layers were formed on the wall of round bottom flasks.

Round bottom flasks were put into the desiccator and left under vacuum at room temperature for one night. Certain amounts of PBS (doubled amount of the total amount of materials) were used to hydrate and lift thin film layers. Hydrated thin film layers formed niosomes after sonication for 20 min at 25 °C in the sonicator and they were vortexed for 2 min. They were put into the room at +4 °C overnight.

After incubation of niosomes at +4°C, they were sonicated for 20 min. After vortex, size of niosomes was measured by DLS before filter. Size reduction with different filters (the filter with 0,45 μm sized syringe filter, the filter with 0,22 μm sized syringe filter) was made. Firstly, the filter (0,45 μm) was used and DLS analysis was made to measure the size. Then, the filtration process continued with filter (0,22 μm). After filtration for 1,5,10 and 20 times, the size values were measured by DLS. According to the DLS results, filtration for 5 times was selected the best to continue other experiments.

Dialysis and Sephadex were tried to eliminate non-assembled materials or very small niosomes. After Dialysis and Sephadex, DLS results were taken. Sephadex was selected to eliminate undesired niosomes.

Another experiment included Span 60 instead of Tween 80 as a surfactant. Thin film formation with Span 60 (13.5 mg, 0,01034 mmole, 12,8 mL) and Cholesterol (1 mg, 0,00258 mmole) at 1:0,25 ratio was made. The same process was used for the formation of thin film layer, hydration, incubation and size analysis.

Briefly, after hydration with certain amounts of PBS and incubation at +4 °C room, the particle size and size distribution of niosomes were determined by dynamic light scattering (DLS) technique.

The analysis of size distribution was conducted at a temperature of 25 °C, using deionized water as the dispersant. A volume of 80 µL from the niosome solutions was transferred to the vial of the dynamic light scattering (DLS) instrument using a pipette. The results were reported as the average diameter of the niosomal suspension, represented by the z-value mean. The Polydispersity Index (PdI) was utilized to assess the extent of size distribution.

Sephadex was tried to eliminate non-assembled materials. However, the experiment was cancelled because the sephadex column was blocked. Another day, sephadex was prepared and the experiment was repeated. Resultants of sephadex column were measured in respect to the size of niosomes.

Optimization of Niosome Preparation Conditions:

New formulations which include Span 60, Tween 80 and Cholesterol at different ratios were created to prepare niosomes while cholesterol ratio. Calculations were made as shown as table below. The period of the preparation of niosomes is 3 days.
In total, 4 formulations were prepared to find the optimum ratio. AA-06-01 included Tween 80 (0,01034 mmol, 13,5 mg, 12,8 mL) and Cholesterol (0,00586 mmol,1 mg) at 1:0,25 ratio. AA-06-02 included Span 60 (0,00258 mmol,1,11 mg),Tween 80 (0,01034 mmol,13,5 mg, 12,8 mL) and Cholesterol (0,00258 mmol,1 mg) at 0,25:0,75:0,25 ratio. AA-06-03 included Span 60 (0,00258 mmol,2,23 mg),Tween 80 (0,00775 mmol, 6,78 mg, 6,4 mL) and Cholesterol (0,00258 mmol,1 mg) at 0,5:0,5:0,25 ratio. AA-06-04 included Span 60 (0,00775 mmol,3,34 mg),Tween 80 (0,00258 mmol, 3,39 mg, 3,2 mL) and Cholesterol (0,00258 mmol,1 mg) at 0,75:0,25:0,25 ratio. AA-06-05 included Span 60 (0,00775 mmol,3,34 mg) and Cholesterol (0,00258 mmol, 1 mg) at 0,75:0,25 ratio. For all formulations, the same procedure was performed to prepare the niosomes. Certain amounts of Span 60, Tween 80 and Cholesterol and 10 mL chloroform ($CHCl_3$) were mixed in round bottom flasks and thin film layers were created after evaporation of the chloroform by rotatory evaporator.

Round bottom flasks were incubated in the desiccator overnight. Thin film layers prepared at different ratios in 4 separated round bottom flasks were hydrated with 27 mL PBS for AA-06-01, 24,62 mL PBS for AA-06-02, 20,02 mL PBS for AA-06-03,15,46 mL PBS for AA- 06-04 and 10,9 mL PBS for AA-06-05.

Table 3.2.1. Content of formulations with different ratios of Span 60, Tween 80 and Cholesterol

Code	Span 60:Tween 80: Cholesterol	Amount (mg)	PBS (mL)
AA-06- 01	0: 1: 0,25	0: 13,5: 1	27,00
AA-06- 02	0,25: 0,75: 0,25	1,11: 10,2: 1	24,62
AA-06- 03	0,5: 0,5: 0,25	2,23: 6,78: 1	20,02
AA-06- 04	0,75: 0,25: 0,25	3,34: 3,39: 1	15,46
AA-06- 05	1: 0: 0,25	4,45: - : 1	10,90

All samples were filtered with 0,45µm sized syringe filter and filtered with 0,22µm sized syringe filter for 1,5 and 10 times. According to DLS results, the ratio of surfactants was determined.

Optimization of Mitochondria-Targeted Niosome Preparation Conditions:

TPP was used to enhance drug targeting and delivery of niosomes to the mitochondria. After TPP was conjugated to Tween 80, ratios and amounts of materials were calculated accordingly to prepare and characterize the niosomes. Calculations were indicated as below.

Table 3.2.2. Ratios for the formulations for Mitochondria-Targeted Niosomes

No	Span 60	Tween 80/(TPP-Tween 80)	Cholesterol
1	0,75	0,25:0 (10:0)	0,25
2	0,75	0,225:0,025 (%10) (9:1)	0,25
3	0,75	0,20:0,05 (%20) (8:2)	0,25
4	0,75	0,15:0,10 (%40) (6:4)	0,25

Amounts used in the formulation were as below:

While 3,34 mg Span 60 and 1 mg Cholesterol were used for the thin film formation, Tween 80/TPP- Tween 80 ratio was different for these formulations. For the first formulation; 3,39 mg Tween 80 and 3,86 mL PBS instead of 15,46 mL PBS were used. For 2. formulation; 3,05 mg Tween 80, 0,11 mg TPP/Tween 80 and 3,75 mL PBS instead of 15 mL PBS were used. For 3. formulation, 2,71 mg Tween 80, 0,22 mg TPP/Tween 80 and 3,63 mL PBS instead of 14,54 mL PBS were used. For 4. formulation, 2,03 mg Tween 80, 0,44 mg TPP/Tween 80 and 3,4 mL PBS instead of 13,62 mL PBS were used. All formulations were prepared with different ratios of Tween 80 and TPP/Tween 80 in the separated round bottom flasks. Thin film layers were created via rotatory evaporator. After samples stayed the desiccator overnight, they were hydrated with certain amounts of PBS and left incubated at+4 °C room for one night. After incubation, samples were sonicated at 25°C for 30 minutes and then, they were put on the vortex for 1 minute. Firstly, all samples were filtered with 0,45 µm sized syringe filter and filtered with 0,22 µm sized syringe filter for 1, 5 and 10 times. Then, size analysis was made with DLS. The particle size and size distribution of niosomes were determined based on dynamic light scattering (DLS) technique.

The size distribution analysis was performed at 25 °C using distilled water. 80 µl of niosome solutions was taken via pipette and put into the vial of DLS instrument.

Results were presented as an average diameter of the niosomal suspension (z-value mean). The Polydispersity Index (PdI) was used as a measure of the size distribution. The optimized formulation was analyzed for zeta potential value to determine the stability of the formulation. Zeta Potential of vesicles was measured by using ZetaSizer. The analysis was carried out by using double distilled water as dispersion medium at the temperature of 25 °C.

The other experiment included Span 60: Cholesterol at 1:0,25 ratio, Span 60: Tween 80: Cholesterol at 0,75:0,25:0,25 ratio, Span 60: PEG Distearate: Cholesterol at 0,75:0,25:0,25 ratio and Span 60:PEG Distearate at 0,75:0,125 ratio.

Mwt of PEG Distearate is 930 $g.mol^{-1}$.

Amounts used in the formulation were as below:

1) 4,45 mg Span 60,1 mg Cholesterol and 10.9 mL PBS
2) 3,34 mg Span 60,3,39 mg Tween 80, 1 mg Cholesterol and 15,46 mL PBS
3) 3,34 mg Span 60,2,40 mg PEG Distearate, 1 mg Cholesterol and 13,48 mL PBS
4) 3,34 mg Span 60,1,20 mg PEG Distearate and 9,08 mL PBS

All formulations were prepared with the same method of the niosome preparation as mentioned above.10 mL chloroform was used for each formulation to make thin film in100 mL rbf. After thin film formation with rotary evaporator, samples were put into the desiccator overnight. Then, the hydration step was completed with certain amounts of PBS. After homogenization of niosome samples with sonication for 30 minutes and vortex for 1 minute, the filtration step was completed with the filter with 0,45 µm sized syringe filter and filters with 0,22 µm sized syringe filter for 1,5 and 10 times.

3.3.2. Purification strategies

Sephadex column chromatography

Sephadex column chromatography was used to eliminate unnecessary particles from the niosome solution by using molecular size fractions. 3 grams of Sephadex G25 beads, was mixed with 15 mL PBS, pH 7.4, and left to swollen in the beaker in order to prepare the sephadex column. Then, the prepared sephadex gel was introduced into the microfilters to give columns clearly 6 cm. long after washing with more PBS and settling. Then, 3 mL of PBS was carefully pipetted on to the top of the columns and the level of the top of the PBS was marked on the outside of the microfilters, so that it was possible subsequently to add 3 mL of the PBS directly to the columns from a polythene wash bottle. Exactly 1 mL of the niosome solution was pipetted onto the column and allowed to enter it; 1 mL of eluate was discarded and collected into many different bottles at same amounts. They were accepted as resultant and kept for the size measurement of niosome with DLS analysis.

In total, 2 sephadex columns at different lengths were prepared. First one was called as short sephadex approximately 15 cm, because it has short distance. 1,5 g sephadex and 20 mL 1xPBS were mixed and they were swollen. Niosome samples stayed at -20 °C were taken. After thawing and sonication for homogenization, size of niosomes at the first sample was measured with DLS. After filtration of the resultant for one time, the size was measured with DLS. The same amount of sample was put into the column and same amount of solute was collected into the separated bottles. Approximately,15 solutes were collected from short column sephadex.

6 grams sephadex and 40 mL 1xPBS were mixed and swollen to prepare long sephadex column (approximately 60 cm). Same procedure was used for the long sephadex. 1 mL of samples was pipetted on to the column and solutes were collected into many different bottles at same amounts. In this way, the length of sephadex column was determined to purify niosomes samples better and take the best results.

3.3.3. Characterization methods

The particle size values and size distribution of prepared niosomes were determined using DLS instrument (Waytt QUELS). The size distribution analysis was performed at 25 °C using deionized water as dispersant. 80 µL of niosome solutions was taken via pipette and put into the vial of DLS instrument. The average diameter of the niosomal suspension (referred to as the z-value mean) was reported as the outcome of the study. The Polydispersity Index (PdI), which indicates the size distribution, was assessed using the dynamic light scattering (DLS) technique.

The optimized formulation was analyzed for zeta potential value to determine the stability of the formulation. Zeta Potential of vesicles was measured by using ZetaSizer. The analysis was carried out by using double distilled water as dispersion medium at the temperature of 25 °C (11, 14). The z- average diameter of sonicated vesicles was determined by DLS technique using a ZetaSizer, Nano ZS 90. For the measurement, 100 µl of the formulation was diluted with an appropriate volume of PBS, pH 7.4 and the size of vesicle, polydispersity index (PdI), and zeta potential were determined.

3.3. Preparation of drug-loaded niosomes

2 formulations were prepared as drug-loaded niosomes. The first formulation included Span 60, Tween 80 and Cholesterol at 0,75: 0,25: 0,25 ratio. 3,34 mg, Span 60, 3,39 mg Tween 80 and 1 mg Cholesterol were used for the thin film formation. They were dissolved in10 mL chloroform. Second formulation included the same ingredients as the first formulation. In addition, a drug (dexamethasone (0,773 mg)) was added into this second formulation. The percentage of the drug used was %10 of the total amount of the basic formulation.

Thin films were formed with these formulations as mentioned above. 10 mL chloroform was used for each formulation. After hydration with PBS and incubation at +4°C room steps were followed, the filtration was applied by filters with 0,45 µm

and 0,22 µm for 1,5 and 10 times. Then, DLS results were taken to examine size of free niosomes and drug loaded niosomes. 15,46 mL PBS used for the hydration of Free NP and 17 mL PBS used for the hydration of Dex-NP.

In another experiment, Drug loaded niosomes were prepared with the formulation including PEG Distearate. 4 formulations were created with same ratios of materials. The first formulation included Span 60: Tween 80: Cholesterol at 0,75:0,25:0,25 ratio. The second formulation included same ingredients with the first formulation and 0,86 mg Dexamethasone. The third formulation included Span 60: PEG Distearate: Cholesterol at 0,75:0,25:0,25 ratio. The fourth formulation included same ingredients with the third formulation and 0,75 mg Dexamethasone.

Amounts used in the formulation were as below:

The first formulation includes 3,34 mg Span 60,3,38 mg Tween 80,1 mg Cholesterol and 15,44 mL PBS. The second formulation includes 3,34 mg Span 60, 3,38 mg Tween 80 and 1 mg Cholesterol, 0,86 mg dexamethasone and 17,16 mL PBS. The third formulation includes 3,34 mg Span 60, 2,4 mg PEG Distearate,1 mg Cholesterol and 13,48 mL PBS. The fourth formulation includes 3,34 mg Span 60, 2,4 mg PEG Distearate and 1 mg Cholesterol, 0,75 mg dexamethasone and 15 mL PBS. The percentage of the drug used was %10 of the all amount of the basic formulation. The same method was applied to prepare niosomes.

Thin films were formed with these formulations as mentioned above. 10 mL chloroform was used for each formulation. After hydration with certain amounts of PBS and incubation at +4 °C room steps were followed. The filtration was applied by filters with 0,45 µm and 0,22 µm for 1, 5 and 10 times. Then, size of free niosomes and drug loaded niosomes were examined after DLS results.

Also, 100 µl from each formulation was diluted with an suitable volume of PBS (pH 7.4) and the size of vesicles, polydispersity index, and zeta potential were determined by Anton-Paar DLS instrument. According to these results, the other

experiment was made with dexamethasone at different ratios. Drug loaded niosomes were prepared with the formulation including PEG Distearate. The basic formulation included Span 60: PEG Distearate: Cholesterol at 0,75:0,25:0,25 ratio. In total, 2 formulations were prepared with %5 and %10 dexamethasone.

The same method was applied for the preparation of niosomes. 3,34 mg Span 60, 2,4 mg PEG Distearate, 1 mg Cholesterol and 10 mL chloroform were mixed. Then, 0,375 mg dexamethasone added for the first formulation (%5 Dex by weight) and 1,5 mg dexamethasone added for the second formulation (%10 Dex by weight). After hydration with certain amounts of PBS and incubation at +4 °C room steps were followed, The filtration was applied by filters with 0,45 µm and 0,22 µm for 1, 5 and 10 times. Then, the size of drug loaded noisomes was measured with DLS instrument.

3.3.1. Purification strategies

Analytical ultra-centrifugation (AUC) was a great tool to characterize the particle size distribution and relative amount of free and encapsulated drug of niosomes. In addition to assessing the distribution of particle sizes, the absorption spectroscopy technique known as AUC (area under the curve) can also offer insights into the ratio of free drug to encapsulated drug, especially when the trapped molecule exhibits a distinct absorption band in the UV-Vis region.

The Ultra-centrifuge tubes were pre-wetted by deionized water. The cut-off value of the ultracentrifuge tube is 3,5 kDa. The tube was centrifuged with the deionized water for 20 minutes. Samples prepared with dexamethasone (5, 10 and %20 by weight) were taken from -80 °C room. The initial volume of samples was 2 mL. At first, the sample prepared with %10 dexamethasone was put into the empty ultracentrifuge tube and it was centrifuged with 6000 rpm nearly 30 minutes until 2,5 mL of sample stayed in the tube. The liquid above the filter was drawn and put back with the pipette to move the solution. Then, a small amount of deionized water was put into the tube to make centrifugation again so that the remain of the free drug above the filter pass the filter. When the solution above the filter stayed at 2,5 mL, it was

taken via the pipette and put into the vial. Then, it was completed to 3 mL solution with deionized water. Therefore, drug loaded niosomes were collected and free drug was discarded. To prepare the ultracentrifuge tube for the other formulation, the tube was cleared with deionized water and the centrifugation was done with clear deionized water for 20-30 minutes. Other samples (%5 and %20 dexamethasone) were centrifuged with same method. At the end, the ultracentrifuge tube was cleared and deionized water was put into the tube to keep the filter from drying. Then the sizes of 3 niosome formulation collected from ultracentrifuge tubes were measured with DLS instrument.

3.3.2. Characterization methods

The particle size, PdI value, and zeta potential of niosomes were measured as explained in the section 3.2.3.

The Morphological analysis of the prepared niosomal formulation was carried out by Scanning electron microscope (SEM) and Transmission Electron Microscopy (TEM). SEM and TEM are the most widely used techniques used in characterization of nanomaterials and nanostructures. TEM image analysis demonstrated the presence of individual niosomes in a spherical shape and confirmed the noisome formation though TEM results were compatible with the data obtained by DLS analysis. A drop of the sample was placed onto a carbon-coated grid and allowed to dry to a thin film. The grid was allowed to air dry thoroughly and then examined using a transmission electron microscope (12) with an accelerating voltage of 80 kV.

3.3.3. Determination of drug content

50 µL of solutions were taken from these samples with dexamethasone (5, 10 and %20 by weight) and they were put into the HPLC vials after mixing with 50 µL of acetone. Then, these 3 HPLC vials were put into the orbital shaker for 20 minutes. Acetone was used to burst niosomes which included dexamethasone. So, the amount of drug inside niosomes could be measured with LC-MS/MS.

After the ultrafiltration by centrifugation step, niosome formulations were separated from the free drug molecules in the solution and the drug loaded only in the niosomes were measured by LC-MS/MS instrument with the calibration curve specifically prepared for Dexamethasone.

Entrapment efficiency (EF) = (Loaded amount of drug/Total amount of drug used) ×100

3.3.4. Drug release studies

Drug release experiments were carried out for these suture samples. While performing the stability test on these sutures, 100 µL samples were taken from the buffer receptor solutions in which the suture pieces were incubated at different time intervals (0,1,2, 4, 6, 8, 12, 24, 48, 72 and 96 hours). These collected samples were analyzed in 6420 TripleQuad LC/MS (Agilent Technologies) for the amount of free peptide and drug molecules in them.

First, two separate methods specific to this peptide and dexamethasone were created in the LC-MSMS device. Then, two different standard curves were created with peptide and dexamethasone solutions prepared at different concentrations (2000, 1000, 500, 200, 100, 50,25 ppb) using pure peptide molecules and pure dexamethasone, and release samples were analyzed using these curves. Therefore, depending on time, how much peptide and what is removed from the suture surface simultaneously information about the release profiles related to the release of dexamethasone has been obtained.

3.4. Synthesis of P4 Peptide

3.4.1. Structural details for peptide P4

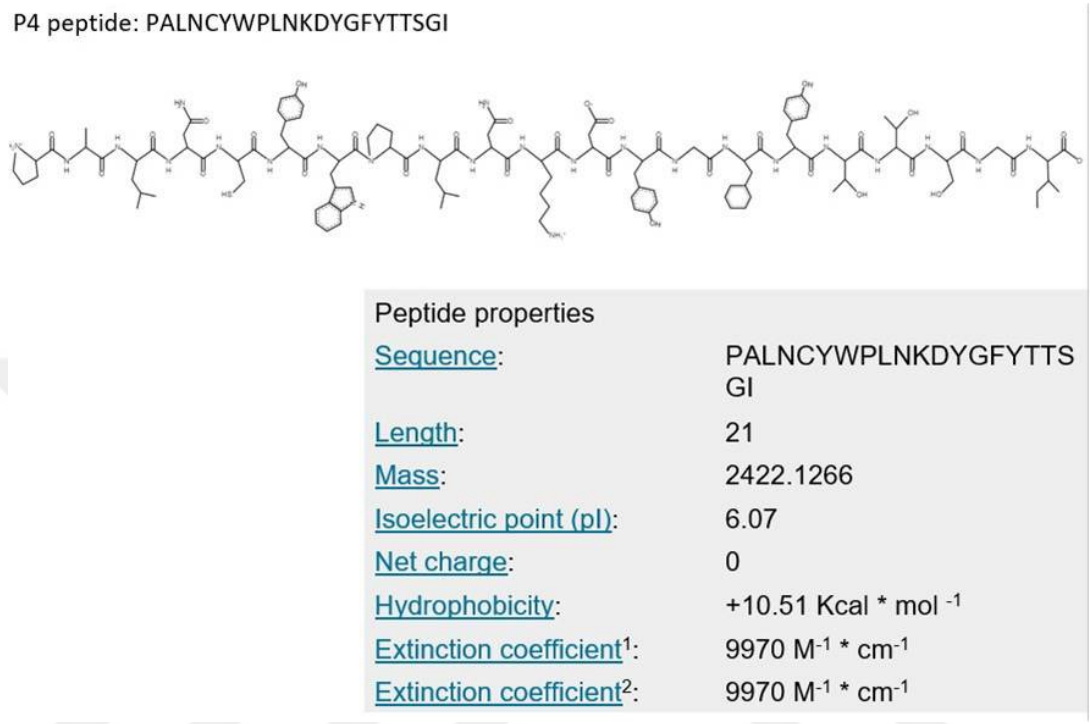

Figure 3.4.1. Structural details of P4 peptide

3.4.2. Solid phase peptide synthesis

Peptide sequence (PALNCYWPLNKDYGFYTTSGI) for P4 peptide was synthesized with selected amino acids on CEM Liberty Blue TM. Amino acids used for the synthesis of the peptide and their amounts were indicated below.

Table 3.4.2. The content and their amount for peptide synthesis

Amino acids	Mass(g)
Alanine	0.19
Asparagine	0.72
Aspartate	0.25

Table 3.4.2. The content and their amount for peptide synthesis (cont.)

Cysteine	0.36
Glycine	0.36
Isoleucine	0.22
Leucine	0.43
Lysine	0.29
Phenylalanine	0.24
Proline	0.41
Serine	0.24
Threonine	0.48
Tryptophan	0.32
Tyrosine	0.83
	Volume(mL)
DMF	537
Piperidine	110
DIC	26
Oxyma	13

P4 peptide was synthesized with the Liberty BlueTM Automated Microwave Peptide Synthesizer (CEM). The synthesis scale was set as 0,5 mmole prior to peptide synthesis, 0,071 g Rink Amide Protide resin was weighed and become distended in 10 mL N, N-dimethylformamide (DMF) at 30 minutes mark. All amino acids used in this peptide synthesis were dissolved in certain amounts of DMF. N, N'-Diisopropylcarbodiimide (DIC) was used as activator and Oxyma was used as activator base. 26 mL of DIC and 13 mL of Oxyma were used. Deprotection cocktail was prepared with 110 mL Piperidine and 537 mL DMF.

At the end of the peptide synthesize, resin has to be cleaved from the peptide. The device that was used to cleave resin from peptide is called RazorTM Peptide Cleavage System (CEM). The cocktail used to facilitate the action of this device consisted of 4.75 mL of trifluoroacetic acid (TFA), 125 µL of triisopropylsilane (TIS), and 125 µL of double distilled water (ddH_2O). The peptide cleavage process took place at a temperature of 38°C for a duration of 30 minutes. The resulting cleaved peptide was precipitated overnight in cold diethyl ether and subsequently subjected to centrifugation at 6000 rpm for 30 minutes. Following centrifugation, the diethyl ether was carefully removed, and the peptide pellet was dried using a vacuum. The dried peptide pellet was then stored at a temperature of +4°C.

3.4.3. Characterization methods

P4 peptide was prepared in 50% acetonitrile (ACN) to have a concentration as 0,5 mg/mL and sonicated to be dissolved homogeneously. P4 peptide was analyzed to check its purification and characterization with LC/MS (6420 Triple Quad -Agilent Technologies) system. Firstly, 10 µL of samples were directly injected to mass detector to be analyzed in scan mod between 50 to 2200 mass (m) range for 1 minute.

3.5. Synthesis of Lipid-Peptide Conjugate

Peptide was conjugated with oleic acid. Chemicals used for the conjugation of the peptide with oleic acid are P4 peptide, Oleic Acid, HATU, DIPA, Et3N and DMF.

Table 3.5. Content for Synthesis of Lipid-Peptide Conjugate

Chemicals	**eq**	**Mwt (g/mol)**	**n(mmol)**	**m (µg)**	**V(µL)**	**d (g/m3)**
P4	1	2422,1267	0,02064	50		
Oleic Acid	1,2	282,47	0,02477	6,99	7,86	0,890
HATU	1,5	380,23	0,03096	11,8		

Table 3.5. Content for Synthesis of Lipid-Peptide Conjugate (cont.)

DIPA	1,5	101,19	0,0396	3,13	4,3	0,722
Et_3N	0,5	101,19	0,01032	1,33	1,84	0,726
DMF					5 mL	

The manual conjugation of oleic acid to the peptide was carried out using a 5 mL syringe (0.05 mmol scale) equipped with a Teflon frit and stopcock. HATU was dissolved in DMF for 30 minutes. The quantities of reagents used were calculated based on the original substitution of HATU. In anhydrous DMF (5 mL) at room temperature, a solution of HATU (0.0396 mmol, 11.8 μg, 1.5 eq) and DIPA in anhydrous DMF (5 mL) were added to oleic acid. The mixture was stirred for an additional 48 hours, after which the solvent was evaporated. The resulting crude peptide conjugate mixture was precipitated by adding cold diethyl ether (-20 °C, 50 mL), isolated through centrifugation, and washed with diethyl ether (5 mL, repeated three times). The dry pellet was dissolved in deionized water and the resulting solution was lyophilized for further characterization.

3.5.1. Purification strategies

The conjugate's purity was assessed using analytical reverse-phase HPLC on a C18 Atlantis column (100 Å, 5 μm, 4.6 × 250 mm). The crude peptide conjugate was dissolved in a mixture of water and methanol (95:5). For the HPLC analysis, mobile phase A consisted of 0.05% formic acid in water, while mobile phase B consisted of 0.05% formic acid in methanol. A gradient of 5 – 85 – 5% B was applied over 65 minutes, with a flow rate of 1 mL/min for analytical purposes or 4 mL/min for semi-preparative purposes.

3.5.2. Characterization methods

The chemical structure of prepared peptide-polymer conjugate was evaluated by proton NMR spectroscopy, which was performed in $CDCl_3$. Bruker 400 Hz instrument was used and ~5mg conjugate was dissolved in CDCl3 and the analysis was run at 128 scan. The spectrum obtained was processed via MestReNova software.

Also, mass analysis was performed by using LC-MS/MS instrument, which was run by 50%ACN and 50%H2O as mobile phase, added with 0.05% formic acid, through C18 stationary column. 20 µL of the polymer-peptide solution was injected into the column by an autosampler and Triple-Quad property of mass spectrometry was provided the mass of fragments coming from both peptide and polymer components of the resultant conjugate.

3.6. Preparation of Targeted and Drug-Loaded Niosomes

3.6.1. Optimization studies

Drug-loaded niosome formulations were prepared with Span 60, PEG-Distearate and Cholesterol with the ratio of 0,75:0,25:0,25, two of which included polymer-peptide conjugate (Peptid-OA) in their compositions. First and second formulations were prepared without peptide-containing conjugate. The first formulation includes 3,34 mg Span 60, 2,4 mg PEG-Distearate and 1 mg Cholesterol. The second formulation includes same ingredients and 0,75 mg dexamethasone. The third formulation includes 3,34 mg Span 60, 2,4 mg PEG-Distearate,1 mg Cholesterol and 0,34 mg Peptid-OA. The fourth formulation includes 3,34 mg Span 60, 2,4 mg PEG-Distearate,1 mg Cholesterol,0,75mg dexamethasone and 0,34 mg Peptid-OA.

Thin film layers were prepared for 4 formulations according to thin film method mentioned at section 3.2.1. The thin film layers were hydrated with certain amounts of PBS and then, they were put into the sonicator for 20 minutes. 13,48 mL PBS for N1 and 14.98 mL PBS for N2, 14,15 mL PBS for N3, 15.66 mL PBS for N4 were used to

hydrate thin film layers. After incubation overnight at +4°C room, they were sonicated for 30 minutes.

3.6.2. Purification strategies

After sonication, one-half of second formulation were kept for ultra-filtration by centrifugation and one-half of solutions of N1 and N2 formulations were filtered for 1, 5 and 10 times. After filtration step, size of niosomes were measured with DLS for two formulations. The separated solution of second formulation was put into the ultracentrifugation tube. The solution was ultracentrifuged and the solution which left above the ultracentrifugation filter was taken into the vial in order to measure the amount of niosomes that consist of dexamethasone.

3.6.3. Characterization methods

The size, PdI value and zeta potential of drug-loaded niosomes were measured by using characterization methods as mentioned at Section 3.2.3. The Morphological analysis of the prepared niosomal formulation was carried out by SEM and TEM at Section 3.3.2.

3.6.4. Determination of peptide amount

NanoDrop instrument is based on an innovative sample retention system that uses the surface tension to hold and measure micro-volume samples between two optical pedestals without the use of cuvettes or capillaries. The NanoDrop spectrophotometer provides rapidly and easily measure 0.5-2 μL droplets of proteins. It is a full spectrum spectrophotometer for measuring the absorbance of proteins. 2 μL of samples (N1, N2, N3 and N4) were loaded on the optical pedestal surface. The average of 4 results for each sample was taken and according to the formulation, the peptide amount was calculated for N2 and N4 niosomes.

3.6.5. Determination of drug content

50 µL of ultracentrifuged solution was placed in the HPLC vial and added with 50 µL acetone to burst the niosomes. Then, the HPLC vials were incubated in the orbital shaker for 20 minutes. So, the amount of drug inside niosomes could be released out and measured with LC-MS/MS instrument.

3.4.1. Drug release studies

The drug release studies for prepared noisome formulations as N1-4 were investigated for their drug release profiles at both neutral and acidic environment based on the procedures explained at Section 3.3.4.

3.7. *in Vitro* Cell Culture Studies

3.7.1. Cells

Cytotoxicity of prepared noisome formulations and their drug loaded and/or targeted versions were assessed by CCK-8 viability assay against human skin fibroblast cell lines (CCD-1070Sk (ATCC® CRL-2091™). Fibroblasts were maintained according to the recommendations of ATCC, using minimum essential medium (Eagle) with 2 mM L- glutamine and Earle's BSS adjusted to contain 1.5 g/L sodium bicarbonate, 0.1 mM non-essential amino acids, and 1.0 mM sodium pyruvate, 90%, fetal bovine serum, 10%. Cells were incubated at 37 °C in a humidified atmosphere of 5% CO_2 and kept in logarithmic phase of growth throughout all experiments.

3.7.2. Cytotoxicity experiments

Cytotoxicity of polymer coated cells and its peptide and drug loaded versions were assessed by CCK-8 viability assay against skin fibroblasts. Cells ($1x10^4$ cells/well) were seeded in a 96-well plate as a quadruplet in 100 µL appropriate culture medium

and incubated at 37°C, 5% CO_2 overnight for cells to adhere completely. Test compounds (Niosomes free of drugs, niosomes with dexamethasone and dexamethasone samples) were sterilized by UV light of the biosafety cabinet for almost 30 minutes. Cells were treated with these test compounds and incubated at 37°C and under 5%CO_2 for 24 hours. After removal of test compounds, the left adherent cells at the bottom of the wells were washed with 100 µL PBS twice. The number of viable cells was determined by CCK-8 cell viability assay by adding 10 µL CCK-8 reagent in 100 µL fresh medium into wells and at the end of 1 hour incubation, absorbance values at 450 µm were measured via a microplate reader. For the 3rd day of experiment, 10 µL of WST-8 reagent was put into each well and was incubated at 37 °C, 5% CO_2 for 4h. Then, the results were measured by the microplate reader at 460 µm. Relative cytotoxicity values were calculated in an excel document with respect to the value obtained for non-treated cell-containing control.

4. RESULTS

4.1. Preparation of Niosomes

Table 4.1.1. Determination of Cholesterol in noisome formulations

Formulations	Ratio of Tween 80	Ratio of Cholesterol	Volume of rbf
A	1	0,25	(50ml)/(100ml)
B	1	0,5	(50ml)/(100ml)
C	1	1	

Details for Formulation A

Table 4.1.2. Effect of filtration to the size of niosomes

A*		0,45µmx1f	0,22µmx1f	0,22µmx5f	0,22µmx10f
**Size(nm)	2865	73	81,1	42,9	56,1
PDI (%)	30	26,8	18,4	16,9	28,6

* Formulation A was prepared with a ratio of 1:0,25 as Tween 80: Cholesterol
**Size value represents Radius of niosomes prepared in 100 mL rbf.

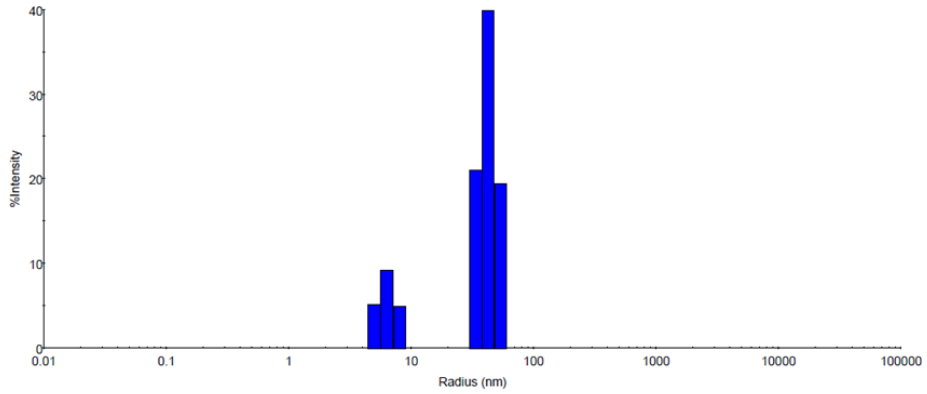

Figure 4.1.1 Size distribution of niosomes with the ratio of Tween 80 to cholesterol as1:0,25 after filtration (0,22µm x5)

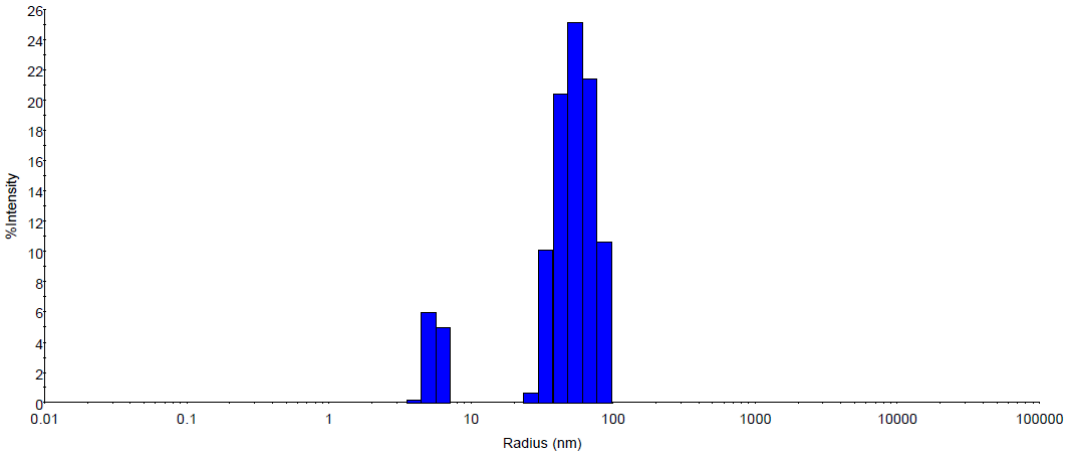

Figure 4.1.2. Size distribution of niosomes with the ratio of Tween 80 to cholesterol as 1:0,25 after filtration (0,22µmx10)

According to the obtained results, "formulation with the ratio of 1:0,25 as Tween 80: Cholesterol & prepared in 100 ml rbf" was selected to go further in experiments.

Details for Formulation B

Table 4.1.3. Effect of filtration to the Size of niosomes for formulation

*B	(100 mL rbf)	(100 mL rbf) 0,45µm x1f	(50 mL rbf) 0,45µm x1f	(50mL rbf) 0,22µmx1f	(50mL rbf) 0,22µm x5f	(50mL rbf) 0,22µm x10f	(50mL rbf) 0,22µm x15f
**Size (nm)	2795,7	74	58,4(%44,7) 588,1(%51)	66,2	59,6	67	76,7
PDI (%)	17,2	42,3	39,8-65	31,8	11,9	41,2	44,9

* Formulation B was prepared with a ratio of 1:0,5 as Tween 80: Cholesterol.
**Size is indicated by the radius. The niosomes were prepared in 50 mL and 100 mL-rbf.Intensity percentages of peaks detected in size distribution histograms were given in parenthesis.

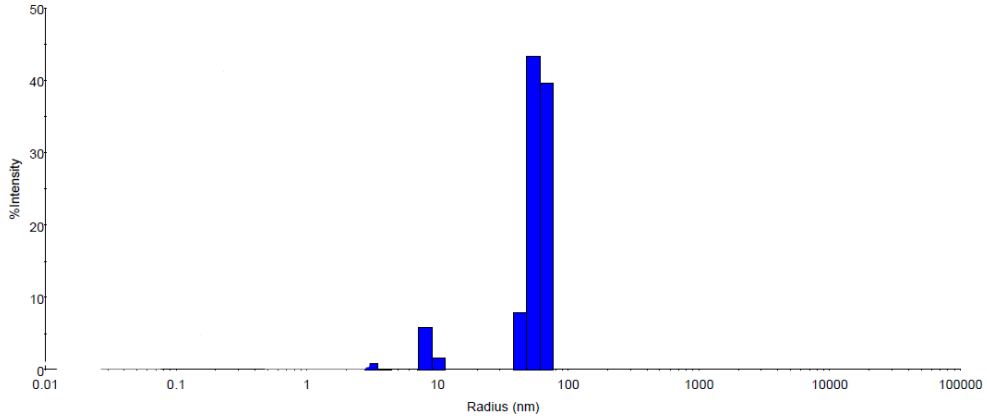

Figure 4.1.3. Size distribution of niosomes with the ratio of Tween 80 to cholesterol as 1:0,5 prepared at 50 ml rbf after filtration (10x0,22 µm)

Table 4.1.4. DLS results as radius and PDI values for the niosomes with the ratio of Tween80 to cholesterol as 1:0,5

B	After sonication	1x0,45µm	1x0,22µm	5x0,22µm	10x0,22µm	15x0,22µm
*Size (nm)	332,3 (%85) 64,1 (%12,6)	64,8 (%83,1) 7,2 (%16,9)	61,6 (%47,1) 15,2 (%32,1)	48,0 (%72,3) 7,4 (%27,7)	45,2 (%68,4) 7,7 (%31,6)	47,5 (%73,2) 8,0 (%26,8)
**PDI (%)	35,7	44,0	24,8	45,6	47,1	50,5

* The size is indicated by the radius. The niosomes were prepared in 100 mL-rbf, Intensity percentages of peaks detected in size distribution histograms were given in parenthesis,
**PDI values were represented respectfully.

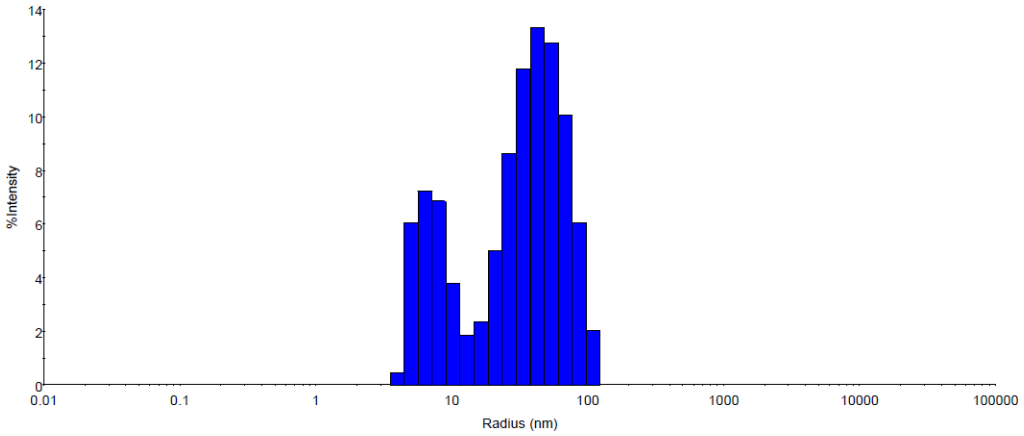

Figure 4.1.4. Size distribution of niosomes with the ratio of Tween 80 to cholesterol as1:0,5 prepared at 50 ml rbf after filtration (6x0,22µm)

Details for Formulation C

Table 4.1.5. DLS results as radius and PDI values for the niosomes with the ratio of Tween80 to cholesterol as 1:1

*C	After sonication	0,45µm x 1f	0,22µm x 1f	0,22µm x5f	0,22µm x10f	0,22µm x15f
**Size(nm)	2774	111	79,8(%79)	58 (%65)- 5,7 (%32)	5,7 (%35) 49 (%64,3)	5,9 (%33,6) 58,6 (%66,4)
***PDI(%)	13,9	53,8	34,6	26	28,8 49	33- 57

* Formulation C was prepared with a ratio of 1:1 as Tween 80: Cholesterol
The size is indicated by the radius. The niosomes were prepared in 100 mL-rbf, Intensitypercentages of peaks detected in size distribution histograms were given in parenthesis,
**PDI values were represented respectfully.

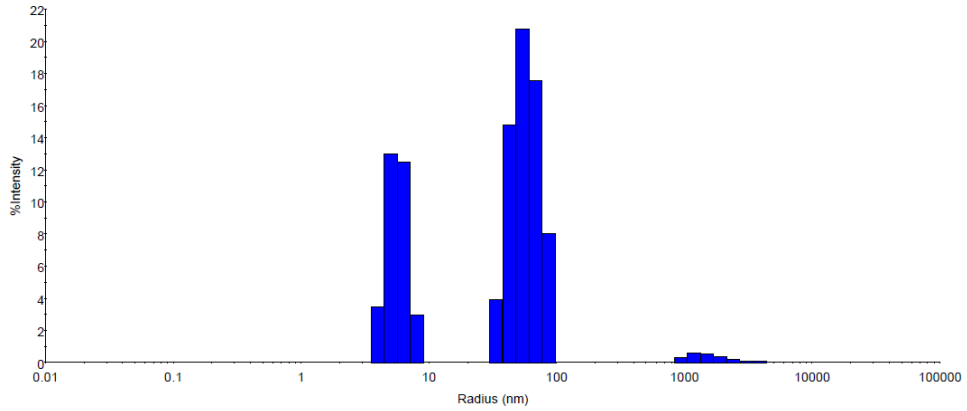

Figure 4.1.5. Size distribution of niosomes with the ratio of Tween 80 to cholesterol as1:1 after filtration (5x0,22 µm)

According to the obtained results, the ratio of Tween 80 to cholesterol as1:0,25 with 100 ml rbf was selected and filtering for 5 times provided the best results for size and PdI values.

Purification strategies of niosomes dialysis

Table 4.1.6. DLS results as radius and PDI values for the niosomes with the ratio of Tween80 to cholesterol as 1:0,25 after dialysis.

A	0,22µmx1f	0,22µmx5f
*Size (nm)	161,9 (%51,4) 1133,6 (%25,4) 40,5 (%17,9)	44,3(%85,3) 5,2(%14,7)
**PDI (%)	21,9 22,7	45,9 16,6

*The size is indicated by the radius. The niosomes were prepared in 100 mL-rbf, Intensity percentages of peaks detected in size distribution histograms were given in parenthesis.
**PDI values were represented respectfully.

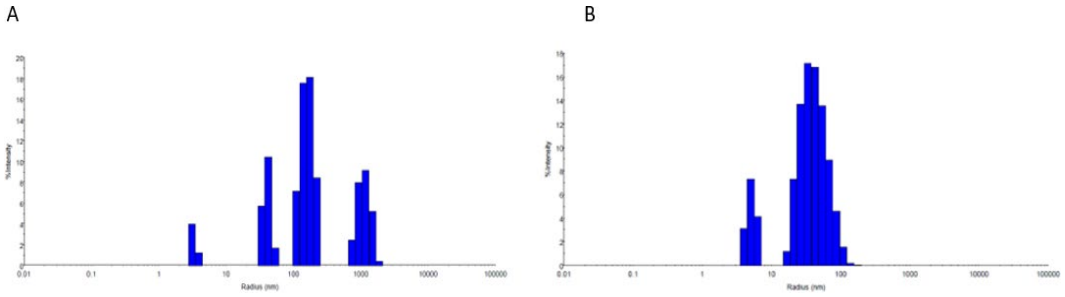

Figure 4.1.6. Size distribution of niosomes with the ratio of Tween 80 to cholesterol as 1:0,25. (A) after dialysis and filtration (1x0,22µm),(B) after dialysis and filtration (6x0,22µm)

Purification by sephadex column chromatography

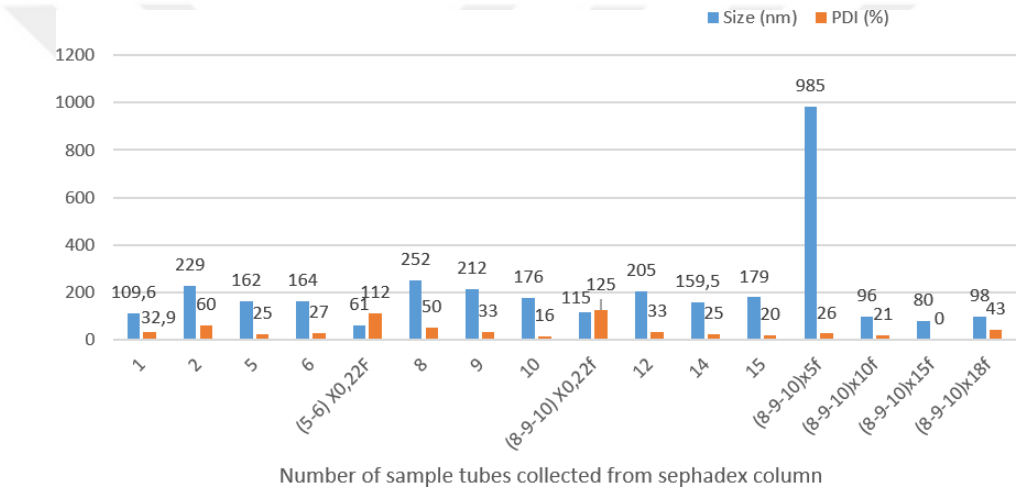

Figure 4.1.7. DLS and Pdi results of niosomes with the ratio of Tween 80 to cholesterol as1:0.25 after purification through sephadex column chromatography.

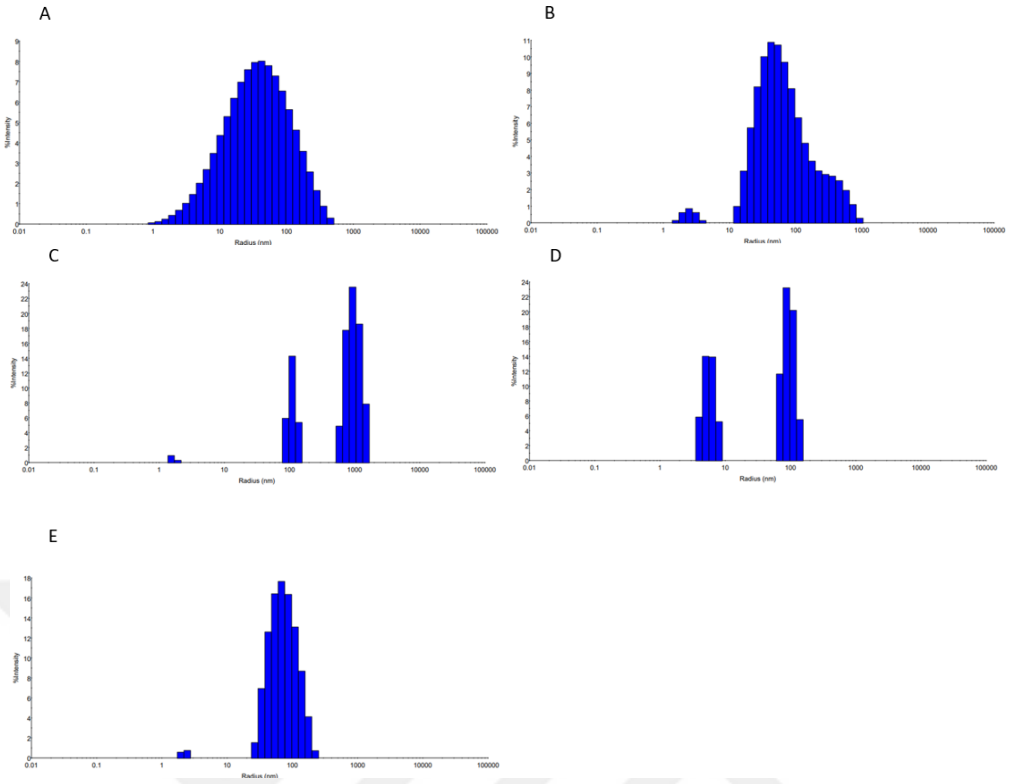

Figure 4.1.8. Size distribution of niosomes with the ratio of Tween 80 to cholesterol as1:0.25 after sephadex of certain combined samples. A-(5-6) x0,22f B-(8-9-10) x0,22f C-Combination of (5-6-8-9-10) x5f D- Combination of (5-6-8-9-10) x10f E-Combination of (5-6-8-9-10) x15f

Table 4.1.7. DLS results as radius and PDI values for the niosomes prepared with the ratio of Span60 to Cholesterol as 1:0,25

No	(Span 60: Cholesterol) 1:0,25	*Size (nm)	**PDI (%)
1	0,22µmx1f	390 (%68)	26
2	0,22µmx5f	128 (%79)	29
4	0,22µmx10f	155 (%56,5)	14

*The Size is indicated by the radius. The niosomes were prepared in 100 mL-rbf. Intensity percentages of peaks detected in size distribution histograms were given in parenthesis.
**PDI values were represented respectfully.

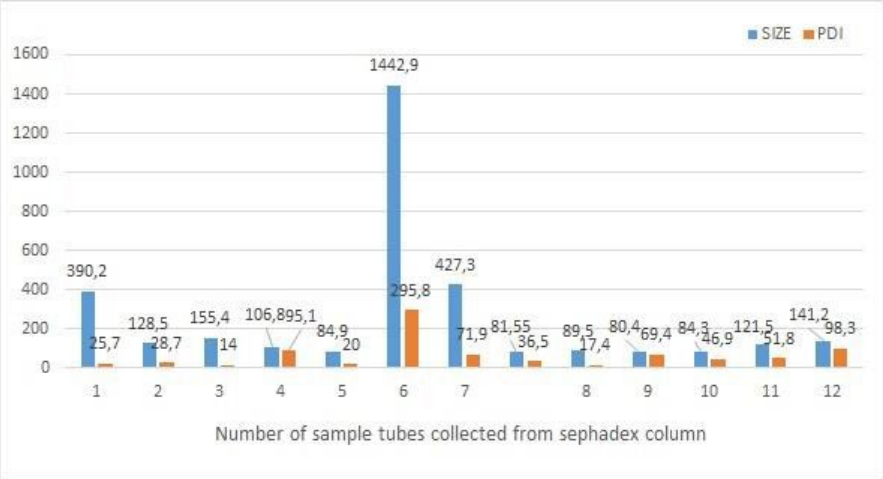

Figure 4.1.9. DLS and PDI results of niosomes with the ratio of Span 60 to cholesterol as1:0.25 after purification through sephadex column chromatography

Preparation of niosomes

Table 4.1.8. Composition details for niosomes

Code	Span 60: Tween 80: Cholesterol	Amount (mg)	PBS (mL)
AA-06-01	0:1:0,5	0:13,5:1	27
AA-06-02	0,25: 0,75: 0,25	1,11:10,2:1	24,62
AA-06-03	0,5:0,5:0,25	2,23:6,78:1	20,02
AA-06-04	0,75: 0,25: 0,25	3,34:3,39:1	15,46
AA-06-05	1:0:0,25	4,45:-:1	10,9

Table 4.1.9. DLS results as radius and PDI values for the niosomes with the ratio of Span 60: Tween 80: Cholesterol as0:1:0,5 after filtration (1x0,45µm,0,22µmx1f, 0,22µmx5f)

AA-06-01	0,45µmx1f	0,22µmx1f	0,22µmx5f
*Size (nm)	534,8(%20,6) 115,3(%63,9)	77,3(%81,9)	66,2(%71,4) 7,9(%10)
**PDI (%)	19,8 27,4	54,1 26,8	40,2 29,1

*The Size is indicated by the radius. The niosomes were prepared in 100 mL-rbf.

Intensity percentages of peaks detected in Size distribution histograms were given in parenthesis.
**PDI values were represented respectfully.

Table 4.1.10. DLS results as radius and PDI values for the niosomes with the ratio of Span 60: Tween 80: Cholesterol as 0,25 :0,75: 0,25 after filtration (1x0,45µm,0,22µmx1f,0,22µmx5f)

AA-06-02	0,45µmx1f	0,22µmx1f	0,22µmx5f
Size (nm)	722,9(%76,9)	73,7(%86,2) 8,7(19,4)	93,8
PDI (%)	17,5	15,7	35

Table 4.1.11. DLS results as radius and PDI values for the niosomes with the ratio of Span60: Tween 80: Cholesterol as 0,5:0,5:0,25 after filtration (1x0,45µm, 0,22µmx1f, 0,22µmx5f)

AA-06-03	0,45µmx1f	0,22µmx1f	0,22µmx5f
*Size (nm)	716,1(%51,4) 118,7(%45,4)	82,6	88,6
**PDI (%)	17,2 11,4	33,4	27,3

*The Size is indicated by the radius. The niosomes were prepared in 100 mL-rbf, Intensitypercentages of peaks detected in Size distribution histograms were given in parenthesis.
**PDI values were represented respectfully.

Table 4.1.12. DLS results as radius and PDI values for the niosomes with the ratio of Span 60: Tween 80: Cholesterol as 0,75 :0,25: 0,25 after filtration (1x0,45µm,0,22µmx1f,0,22µmx5f)

AA-06-04	0,45µmx1f	0,22µmx1f	0,22µmx5f
*Size (nm)	5903,1(%15) 328,6(%61,4) 75,7(%21,4)	66,5(%96,7)	83,4(%97,3)
**PDI (%)	62,7 41,5 23,7	53,1 22,3	49,8 32,7

*The size is indicated by the radius. The niosomes were prepared in 100 mL-rbf, Intensitypercentages of peaks detected in Size distribution histograms were given in parenthesis.
**PDI values were represented respectfully.

Table 4.1.13. DLS results as radius and PDI values for the niosomes with the ratio of Span60: Tween 80: Cholesterol as 1:0:0,25 after filtration (1x0,45µm,0,22µmx1f, 0,22µmx5f)

AA-06-05	0,45µmx1f	0,22µmx1f	0,22µmx5f
*Size (nm)	806,2(%19,3) 149,3(%68,3) 34,7(%12,4)	295,3(%53,9) 70(%46,1)	1.9
** PDI (%)	17,1 21,4 9,3	9,1 7,6	95.1

*The size is indicated by the radius. The niosomes were prepared in 100 mL-rbf, Intensitypercentages of peaks detected in size distribution histograms were given in parenthesis,
**PDI values were represented respectfully.

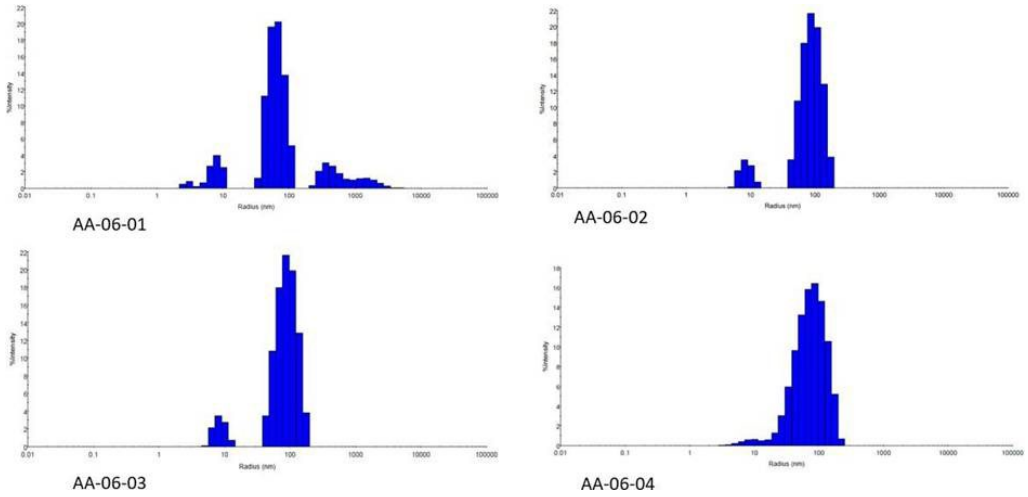

Figure 4.1.10. Size distribution of niosomes with the certain ratios of AA-06- 01-Tween 80 and Cholesterol as 1: 0,25 AA-06- 02- Span 60, Tween 80 and Cholesterol as 0,25: 0,75: 0,25 AA-06- 03- Span 60, Tween 80 and Cholesterol as 0,5: 0,5: 0,25 AA-06- 04- Span 60, Tween 80 and Cholesterol as 0,75: 0,25: 0,25 AA-06- 04“0,75:0,25:0,25 (Span 60: Tween 80: Cholesterol)” was selected as the best according to the obtained size and PdI values.

Purification strategies of niosomes

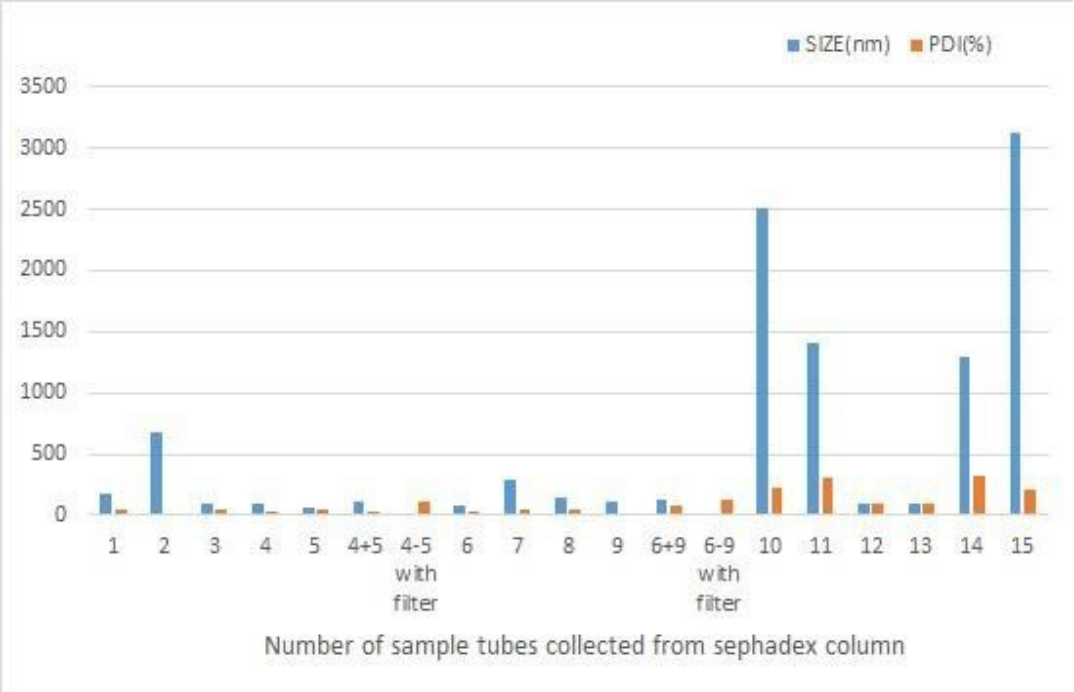

Figure 4.1.11. DLS results as radius and PDI values niosomes with the ratio of Span 60,Tween 80 and Cholesterol (0,75:0,25:0,25) after sephadex.

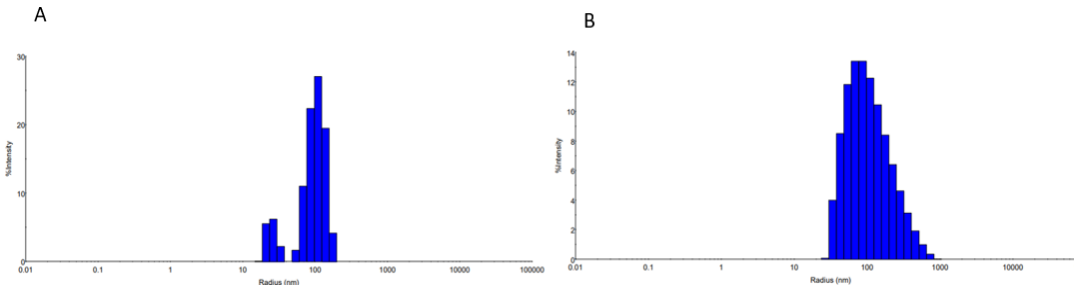

Figure 4.1.12. Size distribution of niosomes with the ratio of Span 60, Tween 80 and Cholesterol (0,75:0,25:0,25) after sephadex of certain combined samples. A-Combination of 4-5 without filter B-Combination of 6-9 without filter

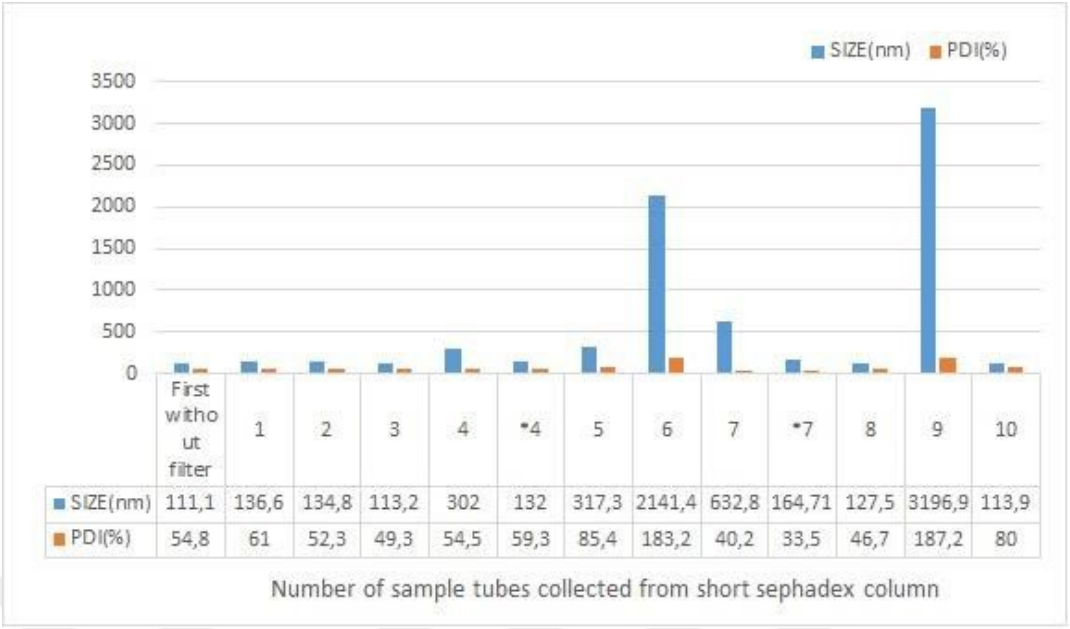

	First without filter	1	2	3	4	*4	5	6	7	*7	8	9	10
SIZE(nm)	111,1	136,6	134,8	113,2	302	132	317,3	2141,4	632,8	164,71	127,5	3196,9	113,9
PDI(%)	54,8	61	52,3	49,3	54,5	59,3	85,4	183,2	40,2	33,5	46,7	187,2	80

Figure 4.1.13. DLS results as size and Pdi of niosomes with the ratio of Span 60, Tween 80and Cholesterol (0,75:0,25:0,25) after purification through shorter sephadex column

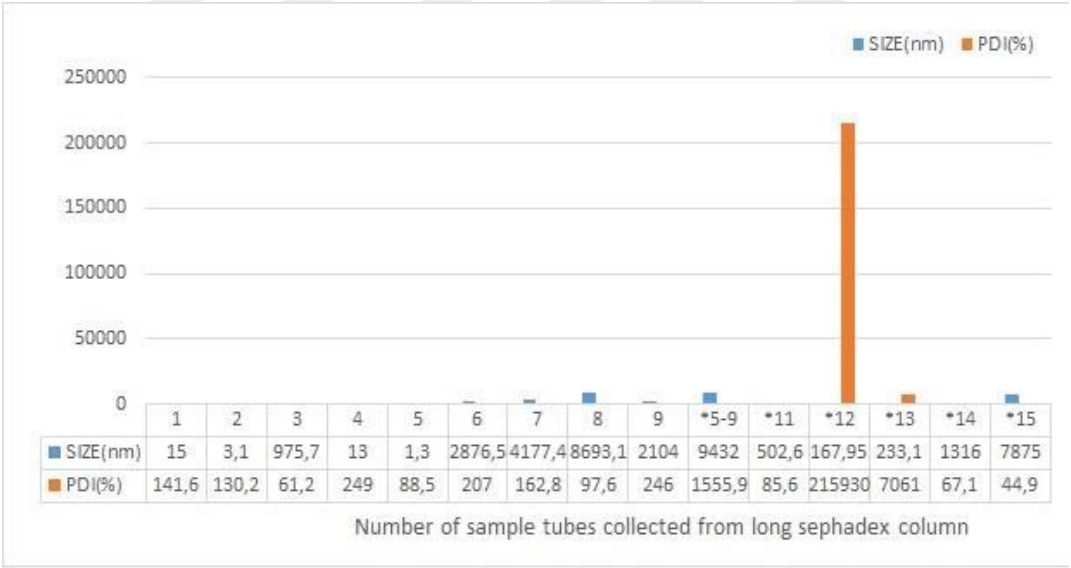

	1	2	3	4	5	6	7	8	9	*5-9	*11	*12	*13	*14	*15
SIZE(nm)	15	3,1	975,7	13	1,3	2876,5	4177,4	8693,1	2104	9432	502,6	167,95	233,1	1316	7875
PDI(%)	141,6	130,2	61,2	249	88,5	207	162,8	97,6	246	1555,9	85,6	215930	7061	67,1	44,9

Figure 4.1.14. DLS results as of niosomes with the ratio of Span 60, Tween 80 and Cholesterol (0,75:0,25:0,25) after purification through longer sephadex column

Characterization of mitochondria targeted niosomes

Table 4.1.14. Composition details for Mitochondria Targeted Niosomes

	Span 60	Tween 80/TPP-Tween 80	Cholesterol
1	0,75	0,25:0 10:0	0,25
2	0,75	0,225:0,025(%10) (9:1)	0,25
3	0,75	0,20:0,05(%20) (8:2)	0,25
4	0,75	0,15:0,10(%40) 6:4	0,25
Amounts(mg)	3,34 mg		1 mg

Table 4.1.15. DLS results as radius and PDI values for the niosomes with the ratio of Span60: Tween 80/TPP-Tween 80: Cholesterol as 0,75: (0,25:0): 0,25 after filtration (1x0,45µm, 0,22µmx1f, 0,22µmx5f, 0,22µmx10f)

1	0,22µmx1f	0,22µmx5f	0,22µmx10f
Size (nm)	72,3 (%93,9) 18,2 (%5,1)	69,5 (%96,4) 7,5 (%3,6)	64,9 (%98,4) 2,8 (%1,6)
PDI (%)	29,5 19,2 8,2	39,4 18,6	40 11,9

Table 4.1.16. DLS results as radius and PDI values for the niosomes with the ratio of Span60: Tween 80/TPP-Tween 80: Cholesterol as 0,75: (0,225:0,025): 0,25 after filtration (1x0,45µm, 0,22µmx1f, 0,22µmx5f, 0,22µmx10f)

2	0,22µmx1f	0,22µmx5f	0,22µmx10f
Size (nm)	85,2	84,8	56,3
PDI (%)	57,5	46,3	31,2

Table 4.1.17. DLS results as radius and PDI values for the niosomes with the ratio of Span 60: Tween 80/TPP-Tween 80: Cholesterol as 0,75: (0,20:0,05): 0,25 after filtration (1x0,45µm, 0,22µmx1f, 0,22µmx5f, 0,22µmx10f)

3	0,22µmx1f	0,22µmx5f	0,22µmx10f
Size (nm)	87,7 (%97,6) 8,7 (%2,4)	70,7 (%94) 9,6 (%6)	56,3 (%97,1) 5,3 (%2,9)
PDI (%)	54,1 29,4	37,4 19,3	40,6 15,8

Table 4.1.18. DLS results as radius and PDI values for the niosomes with the ratio of Span 60: Tween 80/TPP-Tween 80: Cholesterol as 0,75: (0,15:0,10): 0,25 after filtration (1x0,45µm, 0,22µmx1f, 0,22µmx5f, 0,22µmx10f)

4	0,22µmx1f	0,22µmx5f	0,22µmx10f
Size (nm)	81,4(%98,5)	72,9(%98)	53,2(%97,7)
PDI (%)	54,7	53	38,8

Table 4.1.19. Zeta potential of formulations were measured by Lite Sizer 500

Formulations	Mean zeta potential (mV)
1	-8,1 ± 2,7
2	-0,5 ± 1,7
3	-0,9 ± 1,5
4	-1,9 ± 1,8

Table 4.1.20. Composition ratios for niosomes prepared with Tween 80 and PEG Distearate

1	Span 60	Cholesterol	-
	1	0,25	-
2	Span 60	Tween 80	Cholesterol
	0,75	0,25	0,25
3	Span 60	PEG Distearate	Cholesterol
	0,75	0,25	0,25
4	Span 60	PEG Distearate	-
	0,75	0,125	-

Table 4.1.21. DLS results as radius and PDI values for the niosomes with the ratio of Span 60: Cholesterol as1:0,25 after sonication and filtration (1x0,45µm,0,22µm x1f,0,22µmx5f)

1	After sonication	0,22µmx1f	0,22µmx5f
Size (nm)	100 (%80,9) 0,9 (%19,1)	56,5 (%68,1) 1,3 (%31,9)	1
PDI (%)	114 81,8	64,8 84,4	24

Table 4.1.22. DLS results as radius and PDI values for the niosomes with the ratio of Span 60: Tween 80: Cholesterol as 0,75: 0,25: 0,25 after sonication and filtration (1x0,45µm,0,22µmx1f,0,22µmx5f)

2	After sonication	0,22µmx1f	0,22µmx5f
Size (nm)	59	68,9	55,7
PDI (%)	51,4	64	48,6

Table 4.1.23. DLS results as radius and PDI values for the niosomes with the ratio of Span60: PEG Distearate: Cholesterol as 0,75: 0,25: 0,25 after sonication, filtration (1x0,45µm,0,22µmx1f,0,22µmx5f) and homogenization

3	After sonication	0,22µmx1f	0,22µmx5f	0,22µm X5f after homogenizer	repeat
*Size (nm)	48,1 (%46,7) 1,2 (%59,9)	42,3 (%40,9) 1 (%59,1)	44,2 (%64,3) 0,6 (%35,7)	99,3 (%77,4) 1081,7 (%16,8) 26 (%5,8)	82,3 (%57,7) 0,9 (%42,3)
**PDI (%)	33,1 59,9	3,3 15,1	26,1 58,2 86,1	24,1 22,9 12	9,6 7,3

*The Size is indicated by the radius. The niosomes were prepared in 100 mL-rbf. Intensity percentages of peaks detected in Size distribution histograms were given in parenthesis.
**PDI values were represented respectfully.

Table 4.1.24. DLS results as radius and PDI values for the niosomes with the ratio of Span 60: PEG Distearate as 0,75:0,125 after sonication, filtration (1x0,45µm,0,22µmx1f,0,22µmx5f) and homogenization

4	0,22µmx1f	0,22µmx5f
*Size (nm)	60,6	102,8 (%55,9) 518,3 (%44,1)
**PDI (%)	22,2 33	30,3 29,5

*The size is indicated by the radius. The niosomes were prepared in 100 mL-rbf. Intensitypercentages of peaks detected in size distribution histograms were given in parenthesis.
**PDI values were represented respectfully.

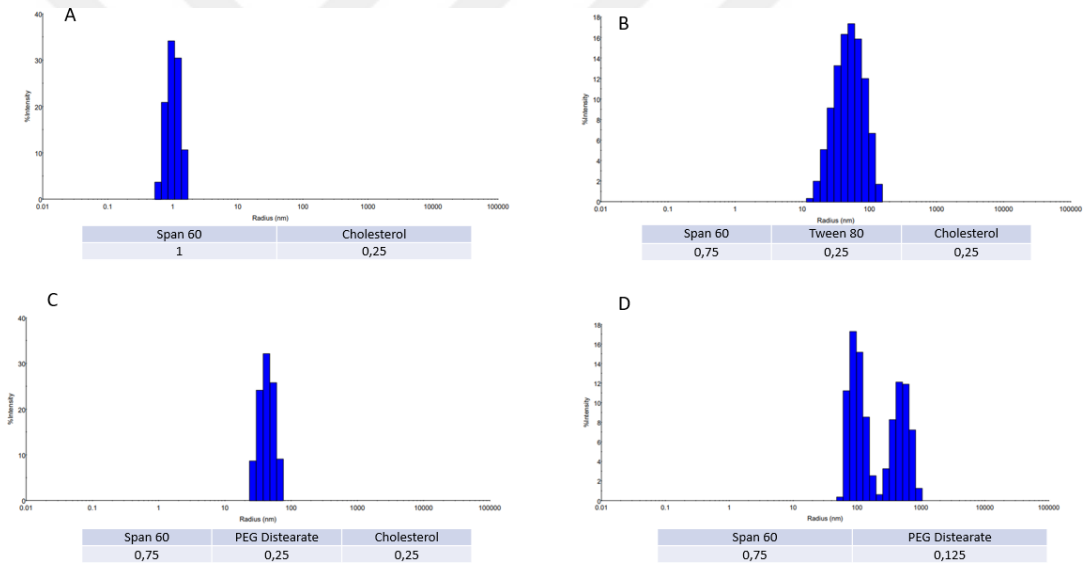

Figure 4.1.15. Size distribution of niosomes with the certain ratios, as follows:
A-Span 60:Cholesterol as 1: 0,25 after sonication and filtration (1x0,45µm, 0,22µmx1f, 0,22µmx5f) B-Span60:Tween80:Cholesterol as 0,75:0,25:0,25 after sonication and filtration (1x0,45µm, 0,22µmx1f, 0,22µmx5f) C-Span60:PEG-Distearate:Cholesterol as 0,75: 0,25: 0,25 after sonication, filtration (1x0,45µm, 0,22µmx1f, 0,22µmx5f) and homogenization D-Span 60:PEG-Distearate as 0,75: 0,125 after sonication, filtration (1x0,45µm, 0,22µmx1f, 0,22µmx5f) and homogenization

4.2. Preparation of Drug-Loaded Niosomes

Table 4.2.1. Composition details for drug loaded niosomes with a 10% drug loading ratio

Content	Span 60	Tween 80	Cholesterol	Dexametasone
Ratio	0,75	0,25	0,25	%10 of the total amount
Amount of Components	3,34 mg	3,39 mg	1 mg	0,773 mg*

Table 4.2.2. DLS results as radius and PDI values for the free NP with the ratio of Span 60:Tween 80: Cholesterol as 0,75: 0,25:0,25 after sonication, homogenization, filtration (1x0,45µm, 0,22µmx1f, 0,22µmx5f, 0,22µmx10f)

FreeNP	After sonication	After homogenizer	0,22µmx1f	0,22µm x 5f	0,22µm x 10f
*Size (nm)	731,3 (%46,4) 131,4 (%46,4)	199 (%89,3)	101,7	124,4	121
**PDI (%)	29,1	36,4	33,1	36,1	45,4

*The Size is indicated by the radius. The niosomes were prepared in 100 mL-rbf. Intensitypercentages of peaks detected in size distribution histograms were given in parenthesis.
**PDI values were represented respectfully.

Table 4.2.3. DLS results as radius and PDI values for the Dex-NP with the ratio of Span 60:Tween 80: Cholesterol as 0,75: 0,25:0,25 and %10 Dex after sonication, homogenization and filtration (1x0,45µm, 0,22µmx1f, 0,22µmx5f, 0,22µmx10f)

Dex-NP	After sonication	0,22µmx1f	0,22µmx5f	0,22µmx10f
* Size (nm)	967,6	51,9	83,5	72,3
PDI (%)	74,1	8,2	41,9	16,4

*The size is indicated by the radius. The niosomes were prepared in 100 mL-rbf. Intensitypercentages of peaks detected in size distribution histograms were given in parenthesis.

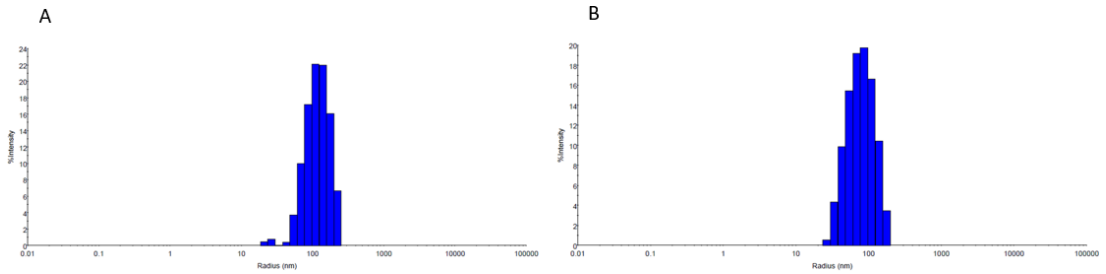

Figure 4.2.1. Size distribution of the free NP and Dex-NPs with the ratio of Span 60:Tween 80: Cholesterol as 0,75:0,25:0,25 and %10 Dex. (A) Free NPx5f & (B) Dex-NPx5f

Table 4.2.4. Composition details for free and drug loaded niosomes prepared with Tween 80 and PEG Distearate

1	Span 60	Tween 80	Cholesterol	
	0,75	0,25	0,25	
2	Span 60	Tween 80	Cholesterol	Amount of Dex
	0,75	0,25	0,25	0,86 mg
3	Span 60	PEG Distearate	Cholesterol	
	0,75	0,25	0,25	
4	Span 60	PEG Distearate	Cholesterol	Amount of Dex
	0,75	0,25	0,25	0,75 mg

Table 4.2.5. DLS results as radius and PDI values for the niosomes with the ratio of Span 60: Tween 80: Cholesterol as 0,75:0,25:0,25

1	0,22µmx1f	0,22µmx5f
Size (nm)	55,3	71,5
PDI (%)	48,5	55,7

Table 4.2.6. DLS results as radius and PDI values for the Dex-NP with the ratio of Span 60:Tween 80: Cholesterol as 0,75:0,25:0,25 and %10 dexamethasone

2	0,22µmx1f	0,22µmx5f
Size (nm)	63	65,8
PDI (%)	49,4 23,2	55,4 36,6

Table 4.2.7. DLS results as radius and PDI values for the niosomes with the ratio of Span60: PEG Distearate: Cholesterol as 0,75:0,25:0,25

3	0,22µmx1f	0,22µm x5f
Size (nm)	113,2	101,9
PDI (%)	17,5 10,7	12,5

Table 4.2.8. DLS results as radius and PDI values for the Dex-NP with the ratio of Span 60: PEG Distearate: Cholesterol as 0,75:0,25:0,25 and %10 Dexamethasone

4	0,22µmx1f	0,22µm x5f
Size (nm)	99,5	110,7
PDI (%)	26,1 34,7	41,5

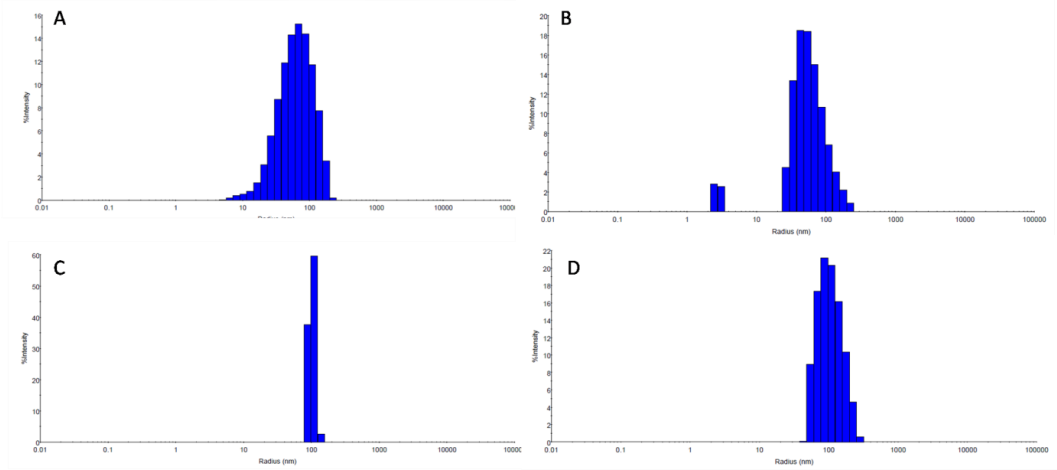

Figure 4.2.2. Size distribution of the free NP and Dex-NPs with the ratio of (A) Span 60:Tween 80: Cholesterol (0,75:0,25:0,25) after filter for 5 times , (B) Span 60: Tween 80: Cholesterol (0,75:0,25:0,25)+ Dexamethasone after filter for 5 times, (C) Span 60: PEG Distearate: Cholesterol (0,75:0,25:0,25) after filter for 5 times (D) PEG Distearate: Cholesterol (0,75:0,25:0,25)+ Dexamethasone after filter for 5 times

Table 4.2.9. DLS results as radius and PDI values for the niosomes with the ratio of (A) Span 60:Tween 80:Cholesterol (0,75:0,25:0,25) after filter for 5 times, (B) Span 60: Tween 80: Cholesterol (0,75:0,25:0,25)+ Dexamethasone after filter for 5 times, (C) Span 60: PEG Distearate: Cholesterol (0,75:0,25:0,25) after filter for 5 times (D) PEG Distearate: Cholesterol (0,75:0,25:0,25)+ Dexamethasone after filter for 5 times

	Size(nm) (Radius)	PDI (%)
1x5f	136,55	27,0
2x5f	104,46	23,4
3x5f	186,34	36,1
4x5f	200,2	24,4

According to DLS results, formulation 4 gives better results than 3, and 2 is better than 1. It shows that dexamethasone decreases niosomes Size, 3 is better than 1. So, PEG-Distearate has an improved effect on particle size. As a result, Formulation 4 was selected as the best formulation to go for further experimental procedures with.

Table 4.2.10. Equivalent values for the preparation for PEG distearate-based niosomes formulated withdifferent drug contents

No	Span 60	PEG Distearate	Cholesterol	Loading Percentage of Dex	Amount of Dex
1	0,75	0,25	0,25	%5	0,375 mg
2	0,75	0,25	0,25	%20	1,5 mg

Table 4.2.11. DLS Results of drug-loaded niosomes with %5 and %20 Dexamethasone

%5 Dex	0,22µmx1f	0,22µmx5f
Size (nm)	91,8	81,2
PDI (%)	33	10,3
%20 Dex	0,22µmx1f	0,22µmx5f
Size (nm)	123,9	120
PDI (%)	23,6	29,7

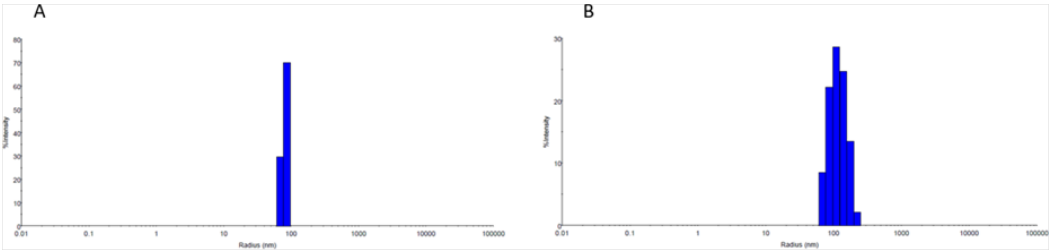

Figure 4.2.3. Size distribution of drug-loaded niosomes with the ratio of Span 60: PEG Distearate: Cholesterol (0,75:0,25:0,25), %5 and %20 dexamethasone after filtration (5x0,22µm) (A) %5Dex, (B) %20Dex

Table 4.2.12. Zeta potential of free niosomes and drug-loaded niosomes (%10dex)

Drug-loaded niosomes	Zeta potential (mV)
%0 Dex-Nio	-13,9 ± 1,9
%10 Dex-Nio	-12,1 ± 1,5

Table 4.2.13. Zeta potential values for drug-loaded niosomes (%5 and %20 Dex)

Formulations	Zeta Potential (mV)
%5 Dex	-12,8 ± 5,0
%20 Dex	-7,4 ± 1,7

Purification of drug-loaded niosomes

DLS results after ultrafiltration by centrifugation process

Table 4.2.14. DLS results as radius and PDI values for the niosomes with the ratio of Span 60: PEG Distearate: Cholesterol (0,75:0,25:0,25), %5, %10 and %20 Dexamethasone after filtration (0,22µmx5f) and ultrafiltration by centrifugation.

No	Dexamethasone Content	*Size(nm)	**PDI(%)
1	%5	117,7 (%80,6) 9335,7(%19,4)	42,9 81,5
2	%10	101,9	27,3
3	%20	122,9	12,7

*The size is indicated by the radius. The niosomes were prepared in 100 mL-rbf. Intensity percentages of peaks detected in size distribution histograms were given in

parenthesis.
**PDI values were represented respectfully.

Table 4.2.15. DLS results as radius and PDI values for the niosomes with the ratio of Span 60: PEG Distearate: Cholesterol as 0,75:0,25:0,25 with dexamethasone after filtration (0,22µmx1f,0,22µmx5f)

N1	0,22µmx1f	0,22µmx5f
Size (nm)	90,0	90,0
PDI (%)	8,8	17,1

N2	0,22µmx1f	0,22µmx5f	Repeat	0,22µm x5f (another sample)
Size (nm)	88,2	1663,7	1277	1,5
PDI (%)	9,8	282,5	315	22,1

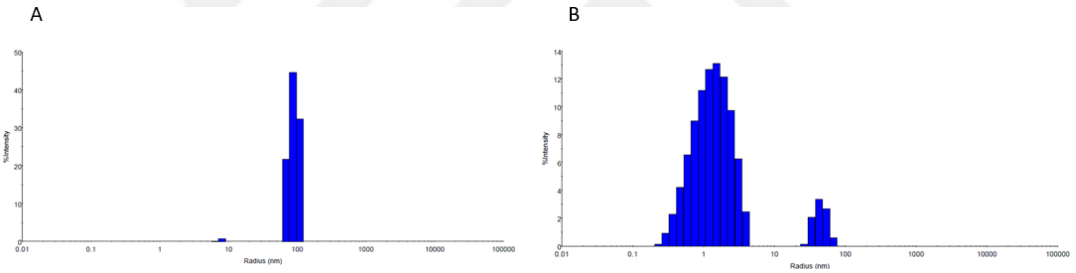

Figure 4.2.4. Size distribution of the free NP and Dex-NPs with the ratio of A-Span 60: PEG Distearate: Cholesterol (0,75:0,25:0,25) and B-Span 60: PEG Distearate: Cholesterol (0,75:0,25:0,25) and dexamethasone

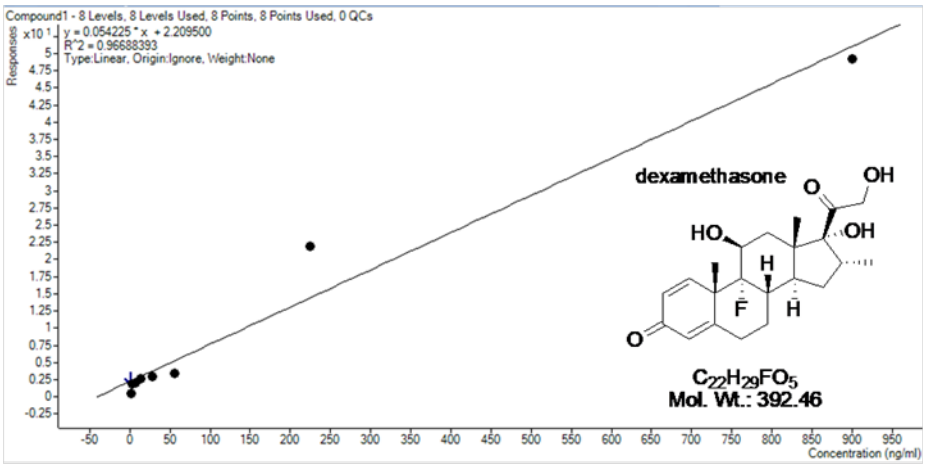

Figure 4.2.5. Calibration Curve for Dexamethasone from LC-MS/MS

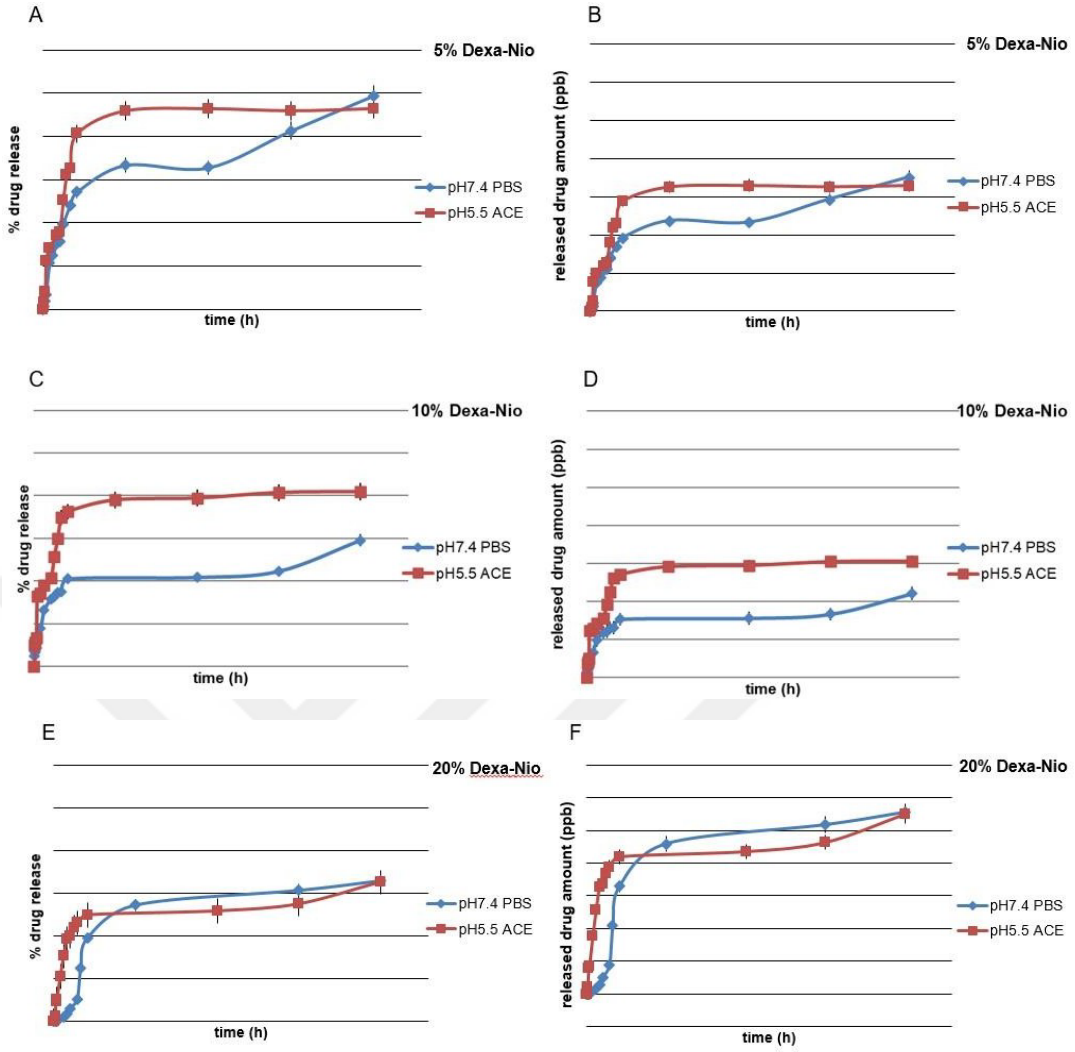

Figure 4.2.6. Drug release profiles for drug-loaded niosomes with %5, %10 and % 20 of dexamethasone.

4.3. Synthesis of P4 Peptide

Purification and characterization of peptide-lipid conjugate

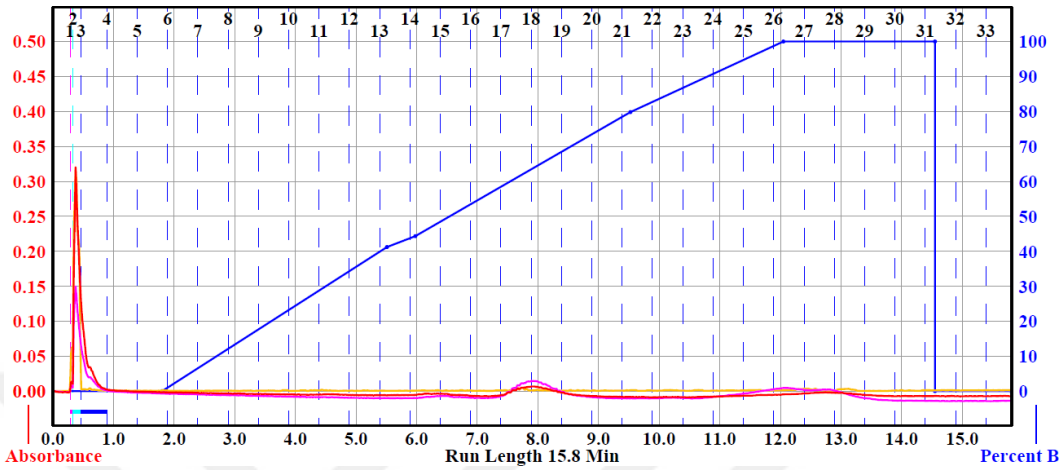

Figure 4.3.1. Prep-HPLC chromatogram for the purification of P4 peptide

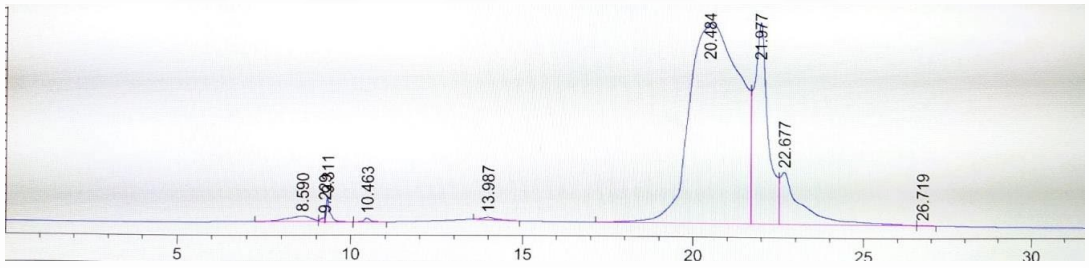

Figure 4.3.2. HPLC chromatogram for P4 peptide

The purity of P4 peptide is %96.

4.4. Synthesis of Lipid-Peptide Conjugate

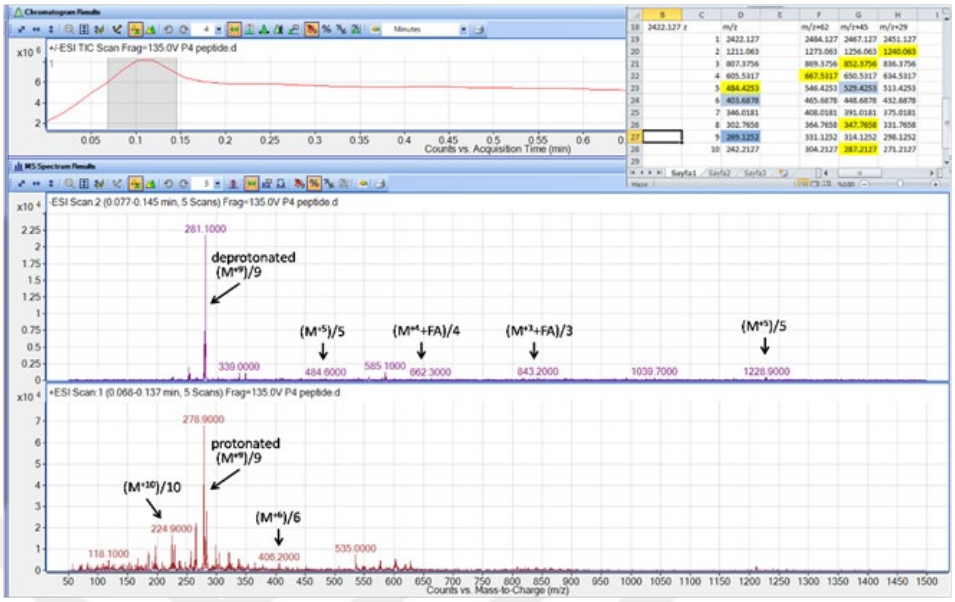

Figure 4.4.1. LC-MS/MS spectrum of P4 peptide

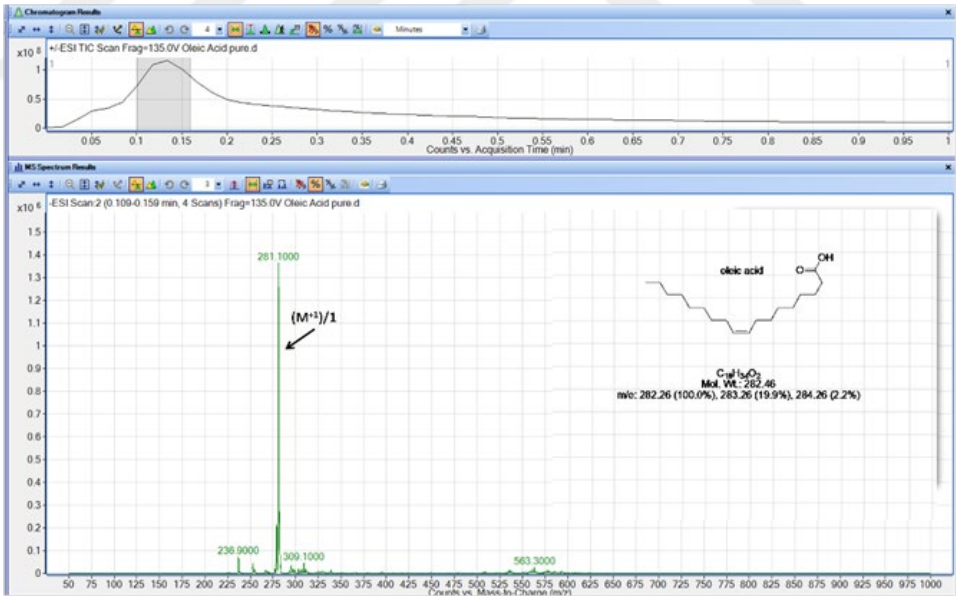

Figure 4.4.2. LC-MS/MS spectrum of Oleic Acid (OA)

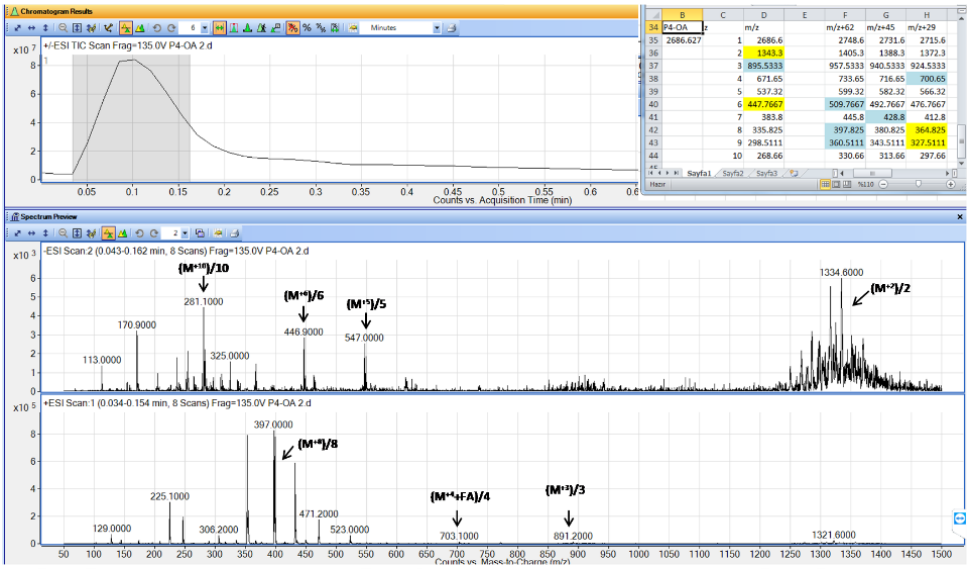

Figure 4.4.3. LC-MS/MS spectrum of P4-OA Conjugate

Figure 4.4.4. Comparison for LC-MS/MS spectra of P4 peptide, Oleic Acid (OA) and P4-OA Conjugate

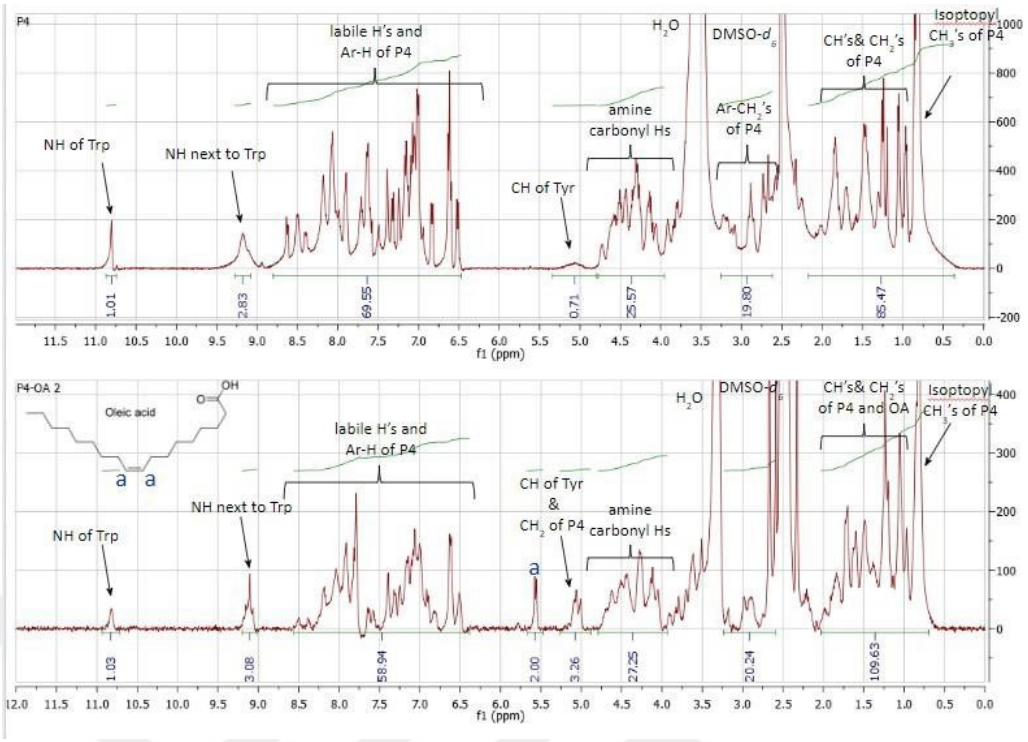

Figure 4.4.5. ^{1}H NMR spectra for P4 peptide itself (above) and P4 peptide-oleic acid conjugate(below) with assigned peaks and comparative integration values

4.5. Preparation of Targeted and Drug Loaded Niosomes

Table 4.5.1. Preparation details of targeted and drug-loaded niosomes

Content	Span 60	PEG Distearate	Cholesterol	Drug	Peptid-OA
No	0,75	0,25	0,25	%10	%15
N1	3,34 mg	2,4 mg	1 mg	-	-
N2	3,34 mg	2,4 mg	1 mg	0,75 mg	-
N3	3,34 mg	2,4 mg	1 mg	-	0,34 mg
N4	3,34 mg	2,4 mg	1 mg	0,75 mg	0,34 mg

DLS results after ultra-filtration by centrifugation process:

Table 4.5.2. Repeated DLS results as radius and PDI values for the niosomes with the ratioof Span 60: PEG Distearate: Cholesterol as 0,75:0,25:0,25 with dexamethasone after filtration (0,22µmx1f, 0,22µmx5f)

N1	0,22µmx1f			0,22µmx5f
Size (nm)	103,9			154,3
PDI (%)	29,1			135,1
N2	0,22µmx 1f	0,22 µmx5f	After Sonication	After ultra-filtration by centrifugation process
Size (nm)	95,6	97,0	141,9	90,6
PDI (%)	34,4	31,0	52,4	85,4

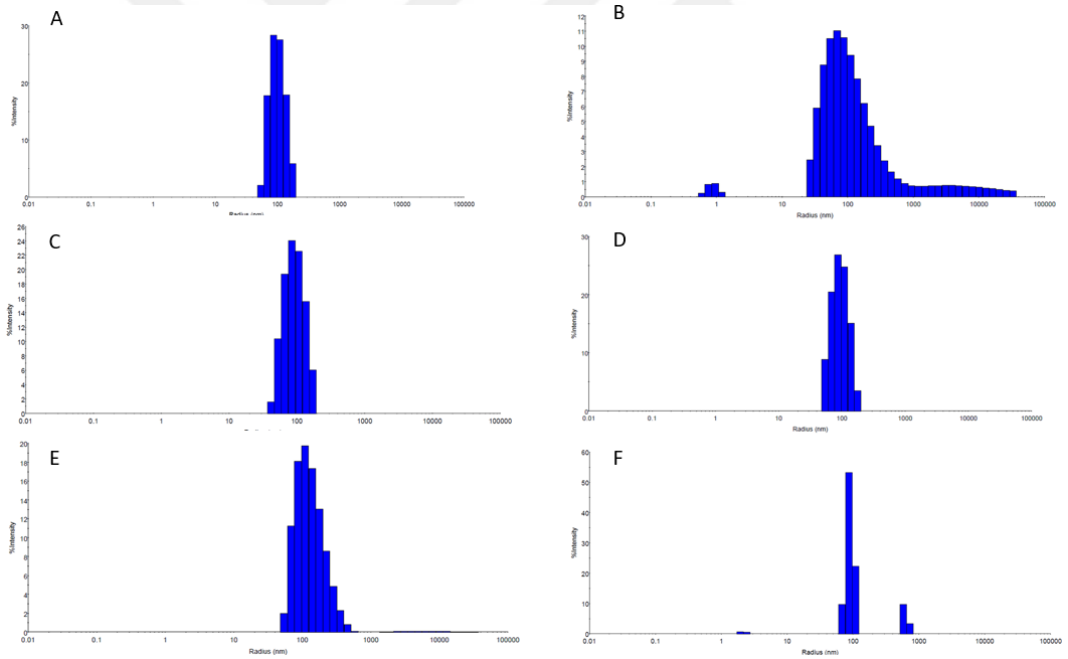

Figure 4.5.1. Size distribution of the free NP and Dex-NPs with the ratio of A-Span 60: PEG Distearate: Cholesterol (0,75:0,25:0,25) after filter (0,22µmx1f) B-Span 60: PEG Distearate: Cholesterol (0,75:0,25:0,25) after filter (0,22µmx5f) C-Span 60: PEG Distearate: Cholesterol (0,75:0,25:0,25) + dexamethasone after filter(0,22µmx1f) D-Span 60: PEG Distearate: Cholesterol (0,75:0,25:0,25) + dexamethasone after filter (0,22µmx5f) E-Span 60: PEG Distearate: Cholesterol (0,75:0,25:0,25) + dexamethasone aftersonication F-Span 60: PEG Distearate: Cholesterol (0,75:0,25:0,25) + dexamethasone after ultra- filtration by centrifugation process.

Table 4.5.3. DLS results as radius and PDI values for the niosomes with the ratio of Span60: PEG Distearate: Cholesterol as 0,75:0,25:0,25 with the peptide-OA after filtration (0,22µmx1f, 0,22µmx5f), sonication and ultra-filtration by centrifugation process

N3	0,22µmx1f	0,22µmx5f	Sonication	Ultracentrifugation
*Size (nm)	111,7	1,6(%85,2)	71,3	99,1(%78,0)
**PDI (%)	35,4	68,3	9,5	31,5

*The size is indicated by the radius. The niosomes were prepared in 100 mL-rbf. Intensitypercentages of peaks detected in size distribution histograms were given in parenthesis. **PDI values were represented respectfully.

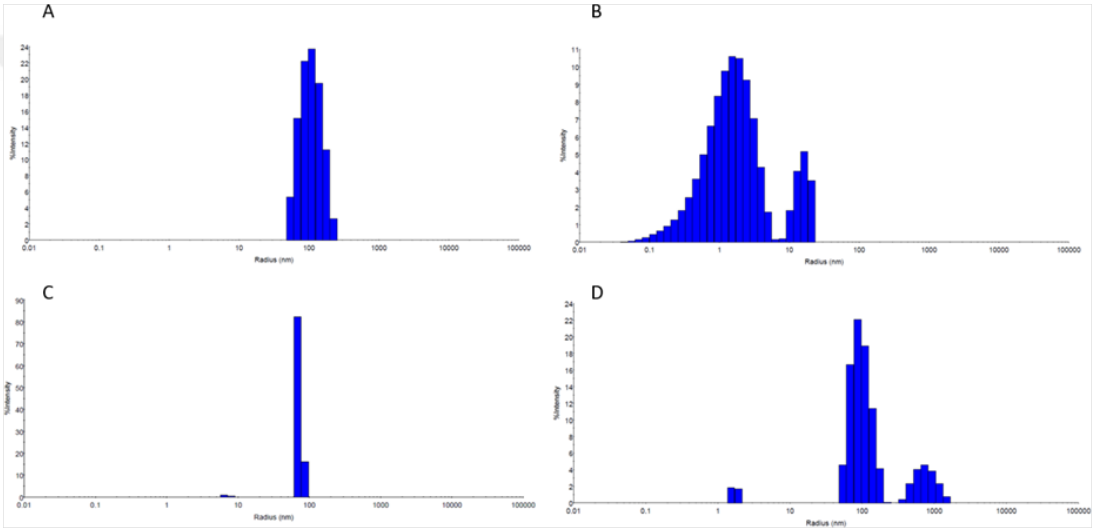

Figure 4.5.2. Size distribution of the NPs conjugated with the peptide-OA with the ratio of A-Span 60: PEG Distearate: Cholesterol (0,75:0,25:0,25) + peptide after filter (0,22µmx1f) B-Span 60: PEG Distearate: Cholesterol (0,75:0,25:0,25) + peptide after filter (0,22µmx5f) C-Span 60: PEG Distearate: Cholesterol (0,75:0,25:0,25) + peptide after sonication D-Span 60: PEG Distearate: Cholesterol (0,75:0,25:0,25) + peptide after ultra-filtration bycentrifugation process

Table 4.5.4. Size and PDI values for the niosomes with the ratio of Span 60: PEG Distearate: Cholesterol as 0,75:0,25:0,25 with dexamethasone and peptide-OA after filtration(0,22µmx1f,0,22µmx5f)

N4	0,22µmx1f	0,22µm x5f	Sonication	Ultracentrifugation
*Size (nm)	100	120,5	392,1	523,8
PDI (%)	14,4	49,47	109,1	33,8

*Size values are represented as radius.

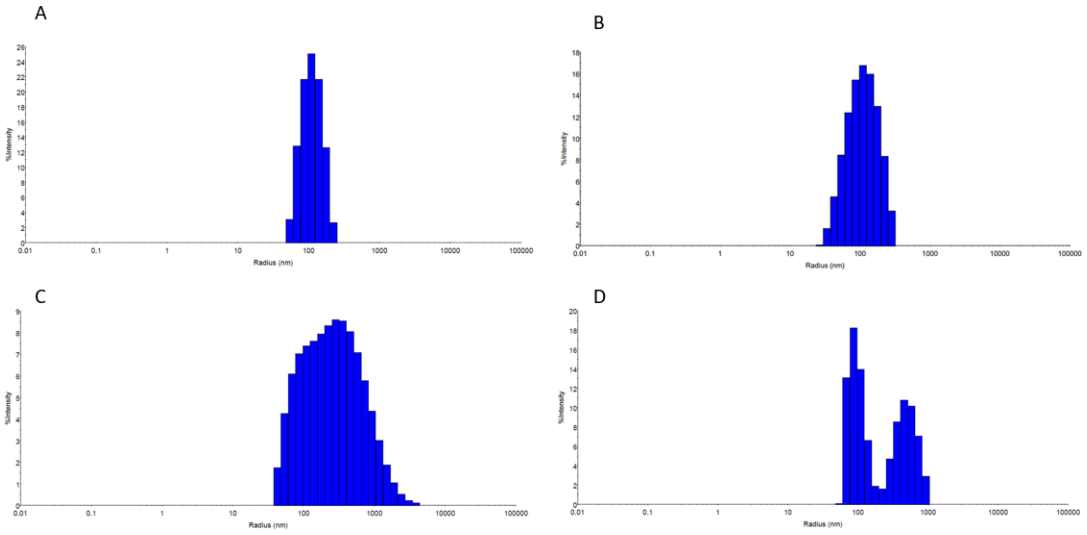

Figure 4.5.3. Size distribution of the Dex-NPs conjugated with the peptide-OA with the ratios: A-Span60: PEG Distearate: Cholesterol (0,75:0,25:0,25) +peptide + dexamethasone after filtration (0,22µmx1f) B-Span60: PEG Distearate: Cholesterol (0,75:0,25:0,25) +peptide + dexamethasone after filtration (0,22µmx5f) C-Span 60: PEG Distearate: Cholesterol (0,75:0,25:0,25) +peptide + dexamethasone after sonication D-Span60: PEG Distearate: Cholesterol (0,75:0,25:0,25) +peptide + dexamethasone after ultracentrifugation

Calculation of drug content and encapsulation efficiency

Table.4.5.5 Drug Content and Encapsulation Efficiency

	N2	N4
Loaded drug amount (µg)	457,75	446,76
Drug encapsulation efficiency (%)	61,03	59,57

Determination of Peptide Amount

Table 4.5.6. Nanodrop results of niosome formulations

Formulation Codes	Formulation Content	Peptide content (mg/mL)
N1	Span 60, PEG-Distearate and Cholesterol	0
N2	Span 60, PEG-Distearate, Cholesterol and Dexamethasone	0
N3	Span 60, PEG-Distearate,Cholesterol and Peptide	0,02
N4	Span 60, PEG-Distearate, Cholesterol, Dexamethasone and Peptide	0,1

According to obtained results, peptide amounts for N3 and N4 niosomes were calculated as 0,02 and 0,1 mg/mL, respectively.

Table 4.5.7. Zeta potential values of N1, N2, N3 and N4

Code	Drug	Peptide	Zeta Potential (mV)
N1	-	-	-1,45 ± 4,89
N2	+	-	-21,1 ± 6,24
N3	-	+	-4,76 ± 4,16
N4	+	+	-24,7 ± 4,26

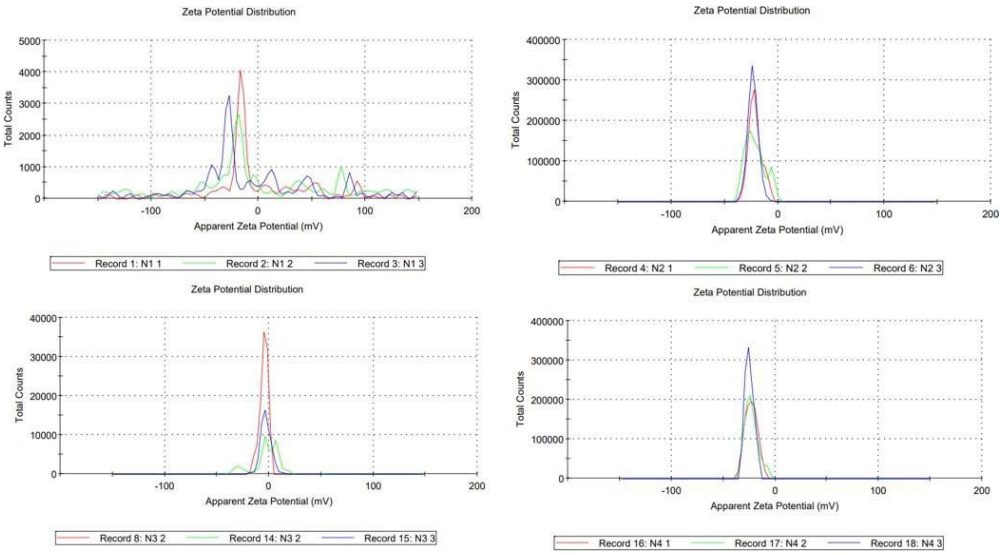

Figure 4.5.4. Zeta potential graphs of N1, N2, N3 and N4

Morphological evaluations of niosome formulations

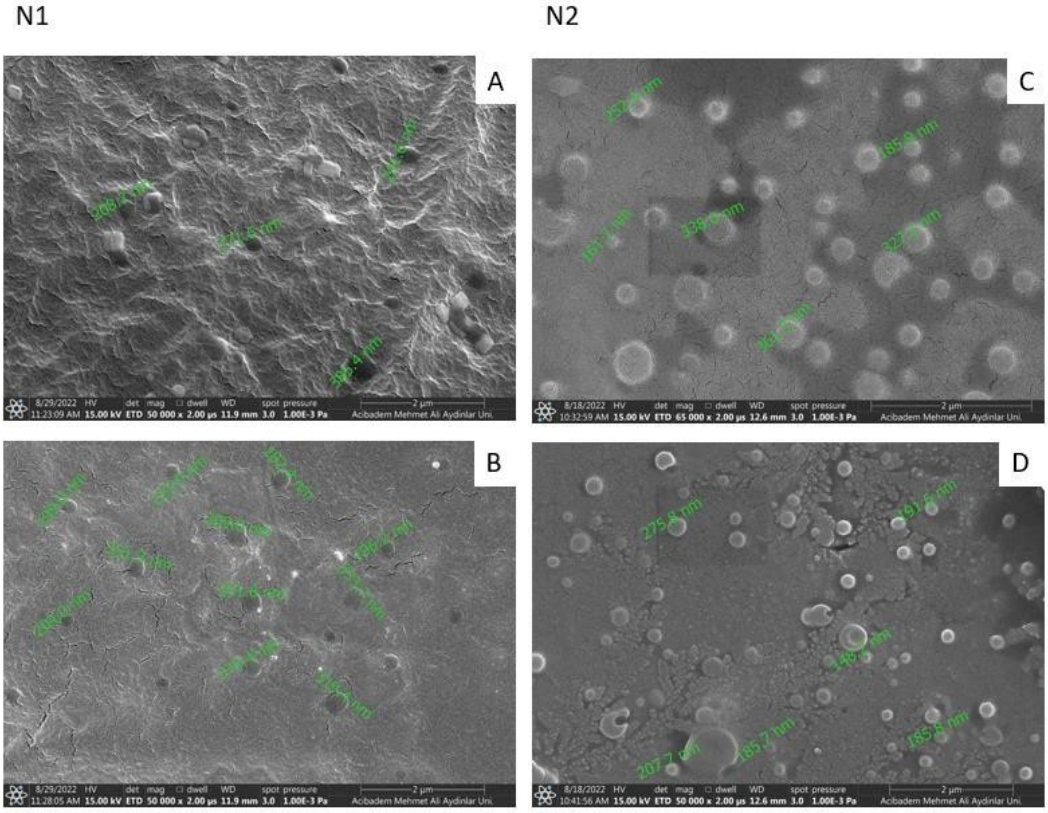

Figure 4.5.5. SEM images of empty (N1) (A, B) and drug-loaded (N2) (C, D) niosomes.Scale bars are 2µm for A, B, C and D

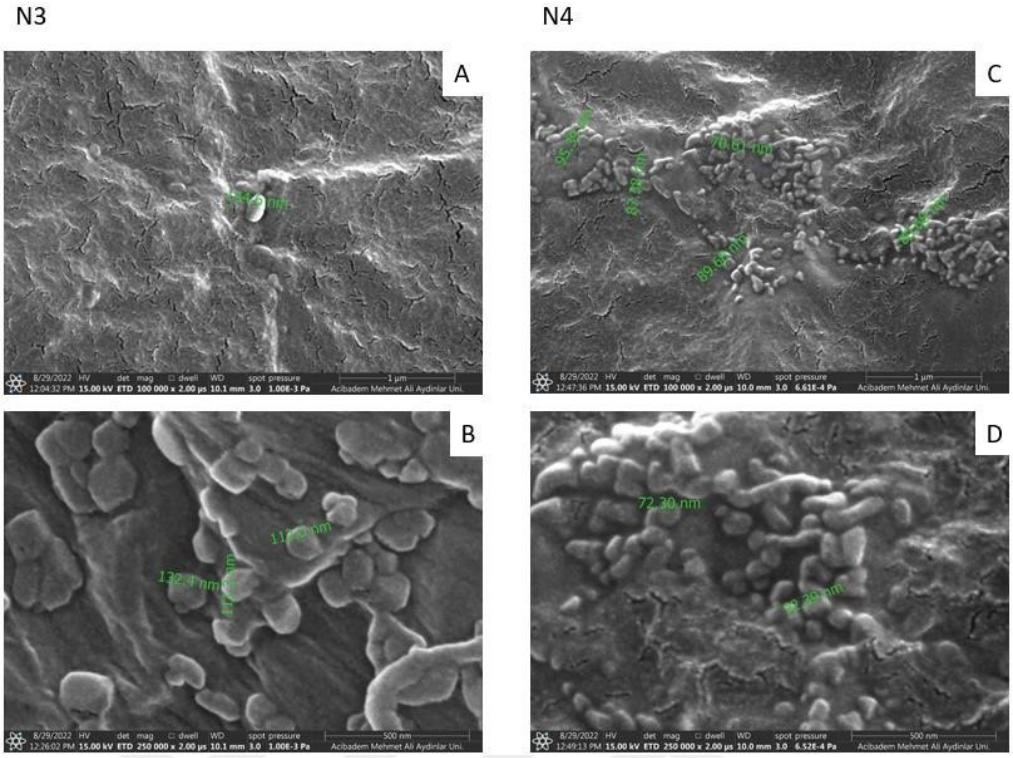

Figure 4.5.6. SEM images of peptide-OA niosomes (N3) (A, B) and drug-loaded conjugated niosomes with peptide-OA (N4) (C, D).Scale bars are 1 μm for A and C, 500 nm for B and D.

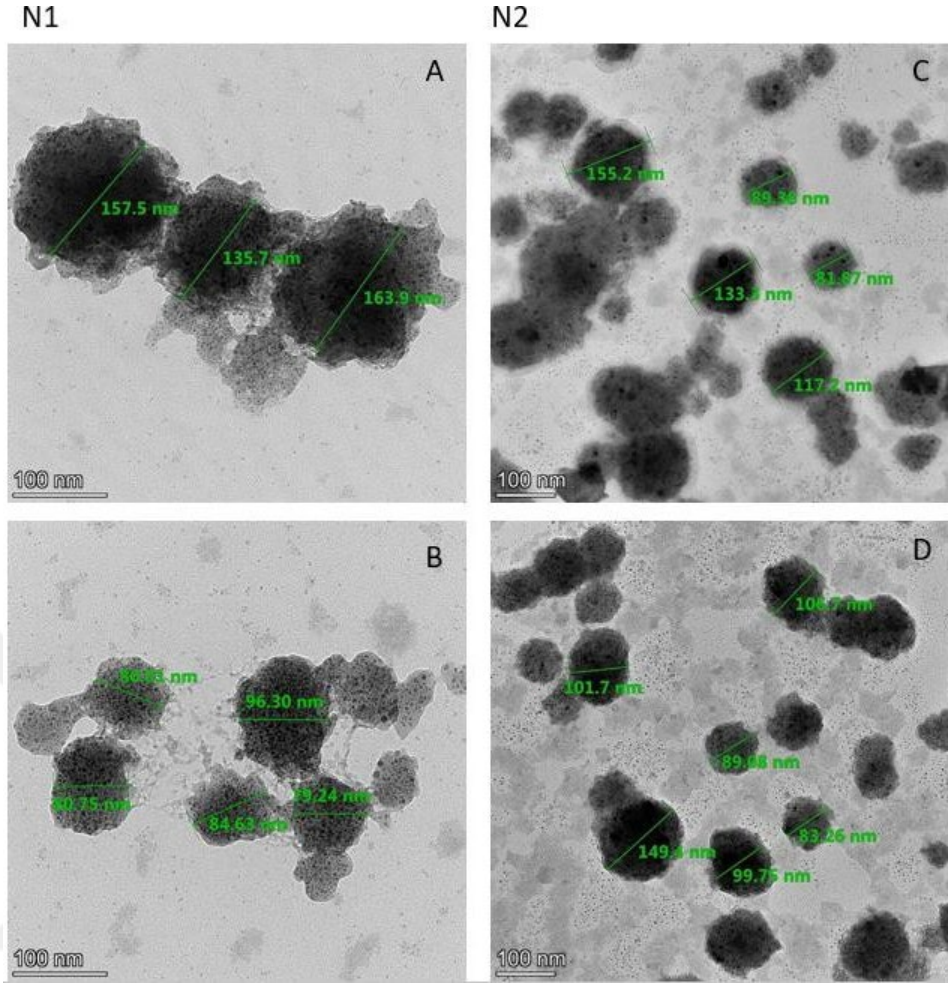

Figure 4.5.7. TEM images of empty (N1) (A, B) and drug-loaded (N2) (C, D) niosomes. Scale barsare 100 nm for A, B, C and D

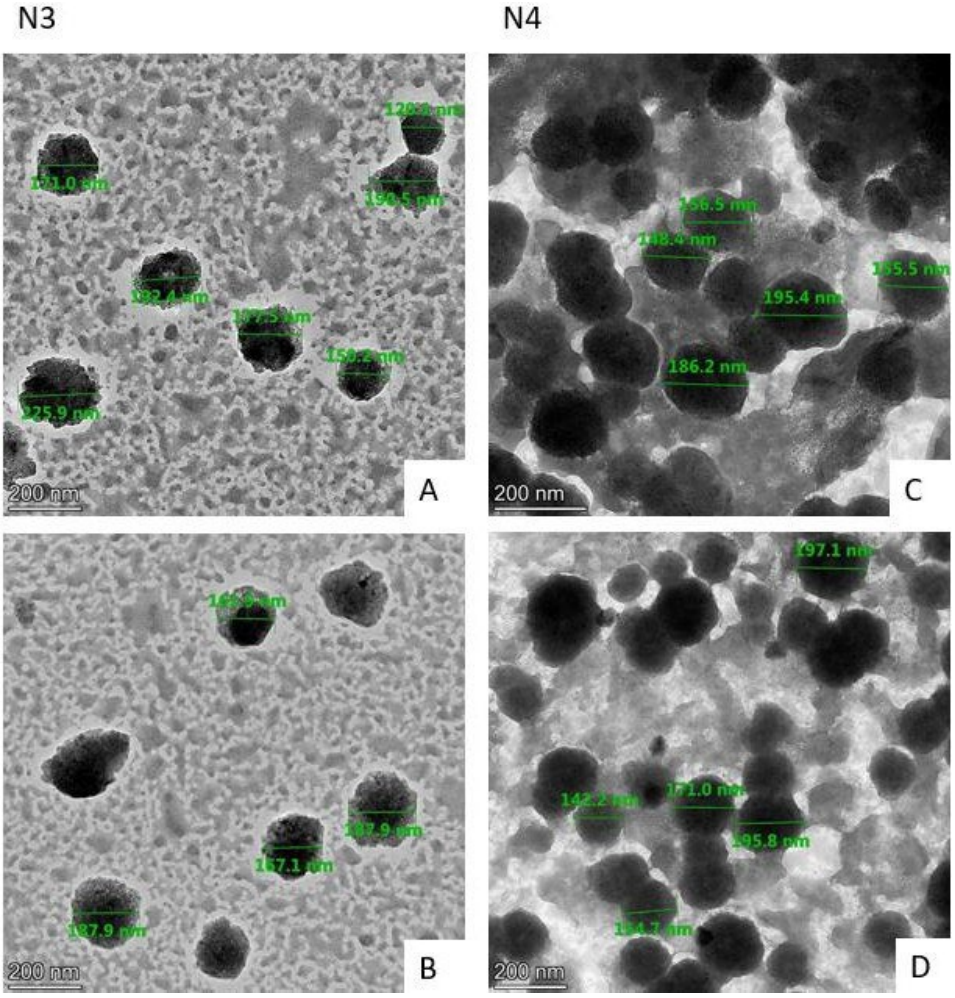

Figure 4.5.8. TEM images of conjugated niosomes with peptide-OA (N3) (A, B) and drug-loadedconjugated niosomes with peptide-OA (N4) (C, D). Scale bars are 200 nm for A, B, C and D

4.6. *in Vitro* Cell Culture Studies

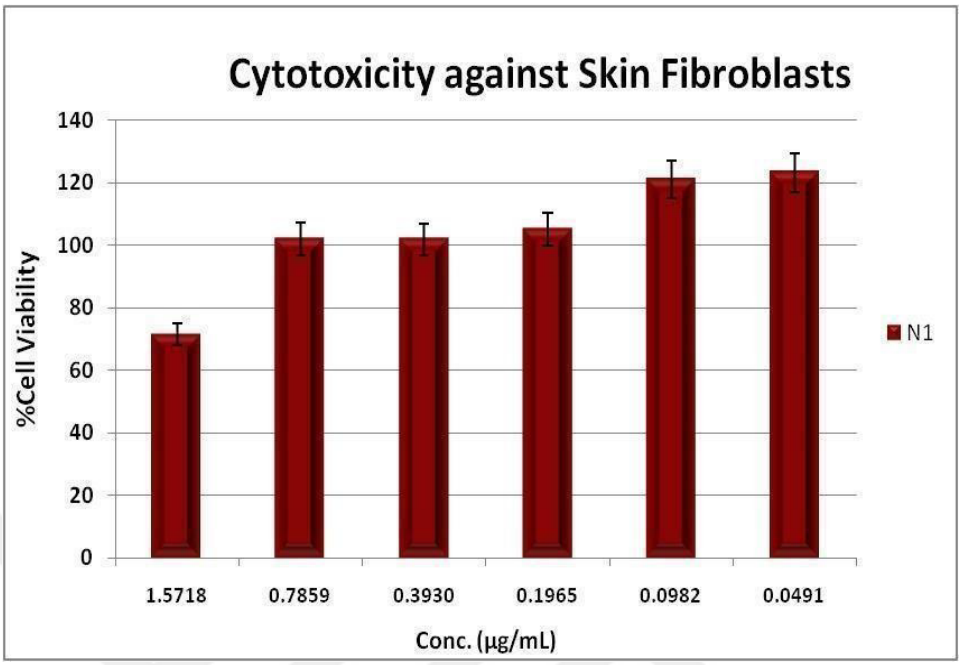

Figure 4.6.1. Cytotoxicity profile of N1, empty noisome as the carrier

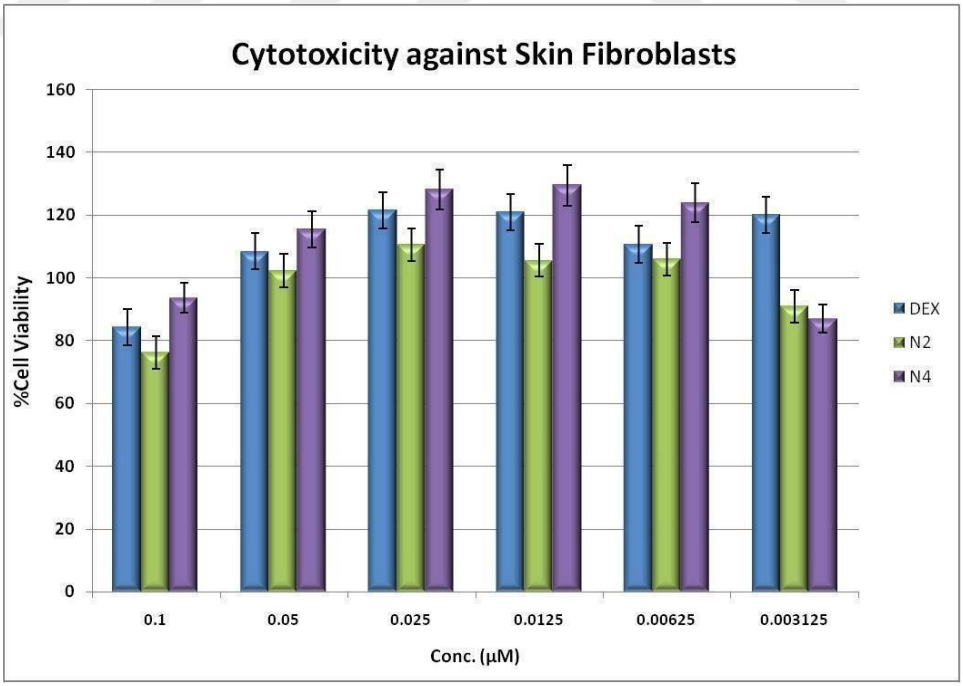

Figure 4.6.2. Cytotoxicity profile of drug-loaded noisomes N2 (non-targeted) and N4 (targeted) and Dexamethasone (as free drug)

5. DISCUSSION

Within the scope of the research project, a new drug delivery system was prepared that has the potential of an active pharmaceutical ingredient to treat some viral diseases. For this purpose, drug-loaded niosomes were prepared with an anti-inflammatory drug called dexamethasone which is used in various inflammation-based diseases including viral ones like SARS-CoV2. Since it has been shown that dexamethasone decreases the severity of this disease and shortens the duration of this viral disease in the body, it appears as a potential therapeutic agent for the development of effective therapies for Covid-19 based viral infections. Here, the noisome formulations were designed to target ACE2 receptor over-expressing cells, which have the high potential for Covid-19. Targeted niosomes were obtained by chemical conjugation of a peptide with ACE-2 receptor specific amino acid sequence. Therefore, it has become specific for cells prone to virus infection and increases the treatment efficiency.

Firstly, the thin film hydration method (TFH method) was applied using different volumes of round bottom flask (rbf) with different inner surface area and ratio of surfactants. Based on the obtained results for size of niosomes, the volume of rbf and ratio of surfactants were optimized. The thin film layer was prepared with 3 different ratios of cholesterol (0,25;0,5 and 1) and Tween 80 as the surfactant at 50 ml and 100 ml rbf as indicated in Table 4.1.1.

DLS which is known as photon correlation spectroscopy, is rapid and non-destructive, and only a small amount of sample is required. It can be used to measure particles in the size range of 3–3000 nm. So, the DLS method was used for the size measurement during the characterization of niosomes. The polydispersity index (PDI) is an indication of the distribution of noisome size, with PDI value of less than 0.5 indicating a monodispersed sample. When obtained DLS results as size and PDI value were evaluated, it was seen that the increased cholesterol at formulations decreased the size of niosomes, and it was decided that among formulations A, B, and C, the formulation with the least cholesterol ratio resulted in the smaller size. Then, 100 ml

rbf provided smoother thin film layer, and the ratio of cholesterol as 0,25 in 100 ml rbf provided more suitable Size and PDI values according to DLS results shown in Table 4.1.2.

When the literature was considered, it can be clearly seen that TFH method provides stable unimodal dispersions of niosomes with similar particle sizes and low PDI values. The role of cholesterol in increasing the compatibility and in controlling both the stability and the size of their particles was confirmed. During the formation of niosomes, an excess of cholesterol provides regions of bilayers with increased rigidity, which makes it difficult to roll into small niosomes. Also presence of cholesterol both improves the physical stability of particles and reduces the permeability of drugs encapsulated in the niosomes, providing highly efficient drug entrapment (8). Addition of extra cholesterol might result in a decrease in the drug encapsulation efficiency (11).

The number of niosome filtration was investigated to get the best result in the size and PDI value of niosomes by filtering the niosomes 1, 5, 10, and 15 times. It has been seen that filtering niosomes solution provided smaller niosomes size but it did not make a significant change after 5 times (5X) filtration. Therefore, the ratio of 'Tween80 to cholesterol' as 1:0,25 in 100 ml rbf was selected, and 5X-filtration was selected with the best results as size (smaller) and PDI (lower).

Various purification strategies were applied to eliminate low Mwt molecules or very smaller size particles for the prepared niosome solution (formulation A). In articles related to niosome preparation, either dialysis or high-speed centrifugation approaches were often used to remove unwanted substances or impurities during the preparation process of drug carriers. Dialysis-based and Sephadex Chromatography based purification strategies were applied in this thesis to eliminate unwanted impurities. According to DLS results stated in Table 4.1.6 and shown in Figure 4.1.6, dialysis-based strategy was not successful to eliminate small particles. Next, sephadex-based chromatography technique was applied for this purpose. According to DLS results stated in Figure 4.1.7 and Figure 4.1.8, Sephadex-based purification was

evaluated as a better separation technique rather than dialysis for removing low Mwt impurities. Niosome solution was applied to the top of the prepared column and mobile phase was left to flow through it continuously. Collected sample tubes were analyzed for their Size, and similar ones were combined. The Size result of mixed sample tubes with number 5 and 6 was seen to be good. Mixed sample tubes with number 8-9-10 gave better results for noisome Size after filtration with a syringe-filter for 10 times.

Another surfactant as Span 60 was used instead of Tween 80 to see the best surfactant for the formulation of niosome. Sorbitan monostearate (Span 60) is a non-ionic surfactant that is widely used to prepare niosomes because it provides improved physical stability due to its high phase transition temperature (5), (6), (7). In Table 4.1.7, DLS results as Size and PDI after 1, 5 and 10 times filtration were presented. It is seen that niosome size was decreased with Span 60: Cholesterol at 1:0,25 ratio after filtering 5 times and the PDI value was decreased after every filtration until 10th one, but the best result was selected after 5 times filtration because of resultant heterogenous Size distribution. On the other hand, for Span 60: Tween 80 based niosomes, it was shown in Figure 4.1.9 that #5 sample tubes gave better results.

In literature, it has been reported that drug-loaded niosomes prepared with Tween 80 provided smaller particle Sizes, compared to those prepared with Span 80. As expected, in this study, Tween 80 niosomes exhibited higher particle Size on day 0 than Tween 20 niosomes, due to longer hydrocarbon chains within Tween 80, resulting in the formation of larger vesicles (22). According to another study, Span 60, Tween 80, and Cholesterole are used for the formation of stable niosomes with a radius of about 200 nm, which provides high compatibility and stability compared to binary monolayers.

In the “Preparation of Niosomes” section, Niosomes were prepared with Span 60, Tween 80, and Cholesterol at 5 formulations which were shown in Table 4.1.8. Among 5 formulations, N4 (Span60:Tween80:Cholesterol as 0,75:0,25:0,25) provided better DLS and PDI results shown in Table 4.1.12. When Figure 4.1.10 was evaluated, the

homogeneity of niosomes was seen at N4. Therefore, N4 was selected by considering to better DLS results and more uniform Size distribution.

In the “Purification Strategies” section, Sephadex results were taken for N4. When Figure 4.1.11 was evaluated, mixing 4-5 and 6-9 sample tubes without filter provided the best results for the size and PDI. Also, the short Sephadex column and long Sephadex column were tried and compared in order to understand the effect of the length of the Sephadex column. DLS results as size and PDI of short and long Sephadex were shown in Figure 4.1.13 and Figure 4.1.14. Considering to DLS and PDI results, these short and long Sephadex columns were not found as suitable for purification.

Regarding the characterization of mitochondria-targeted niosomes, Span 60, Tween80/TPP-Tween 80, and Cholesterol were formulated with different ratios of Tween80/TPP-Tween 80 shown in Table 4.1.14. When DLS results were analyzed, DLS results indicated in Table 4.1.15 were the best although DLS results of formulation no 1, 2, 3 and 4 for Mitochondria Targeted Niosomes were similar. It can be concluded that Tween 80 was sufficient to provide a suitable range of size and PDI values.

The zeta potential of the formulations was measured to identify the surface charge of the particles, as a further indication of vesicular stability. The higher the negative or positive value of zeta potential gives the higher the stability of the system, because charged particles tend to repel each other and therefore reduce the probability of vesicles aggregating, thereby increasing system stability (32). Loading of drugs to niosome structures has been found to cause changes in zeta potentials (33). Zeta potential values of the formulations in this thesis were measured with LiteSizer 500 and Formulation 1 was selected because of the higher charged value and then, higher stability according to zeta potential values which were indicated in Table 4.1.19.

PEG Distearate was used to see the effect of lipid components on noisome stability instead of Span 60 and Tween 80. So, 4 formulations which include Span 60,

Cholesterol, PEG Distearate, and Tween 80 were prepared and compared each other. In Table 4.1.20, composition details of new formulations that include Span 60, Cholesterol, Tween 80, and PEG-distearate were presented.

4 formulations were prepared and the contribution of PEG-distearate and Tween 80 were examined. When Table 4.1.21 was evalauted, DLS results did not give homogenous size results after filtering 5 times. When Table 4.1.23 was compared with table 4.1.21, PEG Distearate decreased PDI and provided a similar size of niosomes with Tween 80 after filtering 5 times. PEG Distearate alone could not decrease the size of niosomes at desired level regarding Table 4.1.24. and the effect of cholesterol was seen that the usage of cholesterol provides smaller size and PDI results. When Figure 4.1.15 was examined, it is seen that Formulation 3 (Part C of Figure 4.1.15) gave a more uniform graphic at size distribution.

At 4.2. section, Drug-Loaded Niosomes were prepared with %10 Dexamethasone of the total amount. The first formulation (Span 60, Tween 80, and Cholesterol) and the second formulation (Span 60, PEG Distearate, and Cholesterol) were prepared alone and with %10 dexamethasone. When DLS results as radius and Pdi values in Table 4.2.2 and Table 4.2.3 were compared, dexamethasone decreased the Size of niosomes and It did not make a meaningful change at PDI value. Moreover, filtering became beneficial for niosomes after especially filtering 1 time. Moreover, the Size distribution figure of Dex-NP(Figure 4.2.1-Part B) was more uniform and better than the figure of free-NP (Figure 4.2.1-Part A)

In Table 4.2.4, 4 formulations were prepared with Span 60, Tween 80, and Cholesterol alone and together with Dex; Span 60, PEG-distearate, and Cholesterol alone and together with Dex. Composition details of free and drug-loaded niosomes prepared with Tween 80 and PEG distearate were indicated. Considering the obtained results as radius and PDI values in Table 4.2.7 and Table 4.2.8, dexamethasone seems to have no significant change in the size of niosomes prepared with PEG-distearate but drug loading was seen to increase the PDI value. When formulations with Tween 80 and PEG-distearate were compared, it was seen that Tween 80 provided a smaller

niosome size than that with PEG-distearate. It is very well know that almost all lengths of PEG chains are readily soluble in aqueous media. The advantage of these compounds is their solubility in water and their capability to solubilize other substances in preparations.

In Figure 4.2.2, the Size distribution of empty NP and Dex-NPs were presented and Part C provided the best Size distribution as being more uniform. When noisome-based particles were loaded with dexamethasone, the Size distribution graphic (Part D) was seen to be better than Part B. For DLS results obtained from another instrument (Anton-Paar), Table 4.2.9 reveals that the addition of dexamethasone into the formulation seems to decrease the PDI value and the size together with Tween 80. However, dexamethasone increased the size of niosomes prepared by using PEG-distearate and decreased the PDI value. So, it can be concluded that the drug loading into nisoomes provided better PDI values.

As a result, Formulation 4 is better than Formulation 3 while Formulation 2 is better than Formulation 1, based on Size and PDI values of obtained niosomes. It is understood that dexamethasone-loading has contributed to a decrease in the size of niosomes. Also, Formulation 3 is better than formulation 1. So, PEG-Distearate is useful to include into the noisome formulation content and the Formulation 4 was selected as the best formulation.

In another experiment, PEG distearate-based niosomes were formulated with different ratios of dexamethasone, and the effect of the percentage of dexamethasone (%5 and %20) was examined. At table 4.2.11, the Size and PDI values were rised by increasing the amount of loaded dexamethasone into the formulations. When the Size distribution of drug-loaded niosomes with %5 and %20 dexamethasone (Figure 4.2.3) was regarded, Part A provided more uniform Size distribution than Part B. So, the less amount of drug enabled better results.

The zeta potential of free niosomes and drug-loaded niosomes with %5, %10, and %20 dexamethasone was measured and compared. It can be said that the higher ratio

of dexamethasone gave less negative value and decreased the surface charge but there was no significant change in the zeta potential value between %5 and %10 dexamethasone-loaded niosomes. Because the higher zeta potential value provided higher stability, the %10 dexamethasone was selected for drug-loaded niosomes, attributing to higher stability, better Size and PDI results.

At the purification stage of drug-loaded niosomes loaded with %5, %10, and %20 dexamethasone, the ultrafiltration by centrifugation process was applied to remove non-encapsulated drug molecules and impurities in the solution and then, DLS results as size and PDI values were taken and presented at Table 4.2.14. After ultrafiltration, it was seen that PDI values were decreased by an increased ratio of dexamethasone and the ratio of %10 dexamethasone gave the best DLS result as size and PDI values among all drug-loaded niosomes.

For the drug content calculations for Dex-loaded niosomes, purified niosome solutions were burst with acetonitrile with 1:1 ratio by volume, and then analyzed with LC-MS/MS instrument. Firstly, different concentrations of drug solutions were prepared and at the molecular ion peak, intensity signals were related to these concentration values in ppm and the calibration curve was obtained as a linear graph with R2 value as %96.66. Prepared and burst noisome solutions were run with the same method and the free drug content was calculated. Also, drug release experiments conducted at two different pH values were evaluated with the same method. pH 7.4 PBS buffer solution was used to mimic healthy tissue condition and blood, whereas pH5.5 acetate buffer was used to simulate inflammation environment. Niosomes with 3 different drug concentrations were prepared as %5, 10 and 20, and subjected to dialysis membrane based method with the receptor solutions as stated below. At different time points, samples from the receptor solutions were withdrawn and these samples were analyzed by LC-MS/MS at the method specific to Dexamethasone. The obtained results were presented as percentages to the initial drug content, and once these graphs were compared, it can be clearly seen that for all 3 niosome types, release profile in acidic media was faster and higher, compared to the ones at pH7.4, which shows the pH responsiveness of these particles. Although there was a little difference

between buffers for %20 drug-loaded niosomes, %5 and %10 drug-loaded ones shows more, which can be attributed to the reached drug-carrier capacity of prepared niosomes for %20 drug loading. For 5% drug-loaded niosomes, there is a faster release of drug payload, especially at acidic pH, which might not be suitable for day-based therapy. For 10% drug-loaded niosomes, this difference can be seen clearly, there is almost 2 times more drug release for acidic pH, compared to neutral media with lower drug release percent. This points out to the slow and sustained release of drug from the niosomes with a dependent fashion.

At Section 4.5, targeted and drug-loaded niosomes were prepared with Span 60, PEG-distearate, and Cholesterol with the ratio of 0,75:0,25:0,25, together with dexamethasone and peptide. The ratio of dexamethasone and peptide was %10 of the total amount of formulations and the content of targeted and drug-loaded niosomes were indicated in Table 4.5.1. While N1 was empty-NP and N2 includes dexamethasone as an extra component, N3 includes peptide without drug and N4 includes both dexamethasone and peptide. According to DLS results as size and PDI values, loaded dru seems to decrease the Size and increase PDI value. After the ultrafiltration by centrifugation process was applied for purification, the size was seen to decrease slightly with a more uniform peak at Size distribution (Figure 4.5.1-Part F).

While N3 which included Span 60, PEG-distearate, Cholesterol, and peptide provided similar niosome size and PDI value compared to N1 and N2 after syringe filtration for 1 time, N3 had a smaller Size and PDI value after 1 and 5 times filtration followed by sonication. DLS and PDI results after ultrafiltration were similar and heterogeneous between N2 and N3, but N3 provided more heterogenous size distribution than N2. When the DLS results as Size and PDI values were evaluated in Table 4.5.4, the peptide and dexamethasone addition increased the Size and PDI values expectedly and the best result was obtained after filtration only once. Also, it has noticed that the sonication increased the Size and PDI value because niosomes can be separated from each other during sonication, and Figure 4.5.2 pointed out to more uniform Size distribution.

After the drug content and encapsulation efficiency values were measured and indicated in Table 4.5.5, similar results were obtained for N2 and N4, and the peptide slightly decreased the drug content and encapsulation efficiency.

When the zeta potential results for targeted empty and drug-loaded niosomes were considered at Table 4.5.7, drug-loaded ones were detected to bear more negative surface charge compared to the ones with peptide in their formulations. So, peptide would decrease the surface charge, without having a dramatic effect on stability of niosomes. It was also hopeful to see that the zeta potential graphic of N4 formulation which contains both drug and conjugated to the targeting peptide was more uniform.

6. CONCLUSION

As a conclusion, it will be possible to carry drugs only to cells where viral infection is present or at risk of being seen. So far, there is no example in the literature that includes niosome design targeted to the ACE2 receptor.

Therefore, this proposed noisome will reduce the possible and unwanted side effects of free drug molecules by slowing the release of drugs while circulating in the body (blood or mucus) thanks to its PEGylated and neutral surface. In fact, this system can both help the body to increase the fight against the virus and reduce the inflammation in the cells exposed to viral infection (with an anti-inflammatory drug). Moreover, It helps the cell to restore its natural and healthy functions, reduce viral damage, support the elimination of infection, reduce the mortality rate and increase the treatment efficiency. It can be considered as a new drug delivery platform with potential.

7. REFERENCES

1. J. Wanigasekara, C. Witharana, Applications of nanotechnology in drug delivery and design-an insight, Curr. Trends Biotechnol. Pharm. 10 (1) (2016) 78–91.

2. N.A. Ochekpe, P.O. Olorunfemi, N.C. Ngwuluka, Nanotechnology and drug delivery part 1: background and applications, Trop. J. Pharmaceut. Res. 8 (3) (2009).

3. M. Ghafarzadeh, M. Namdari, A. Eatemadi, Stem cell therapies for congenital heart disease, Biomed. Pharmacother. 84 (2016) 1163–1171.

4. M. Namdari, A. Eatemadi, B. Negahdari, Natriuretic peptides and their therapeutic potential in heart failure treatment: an updated review, Cell. Mol. Biol. 62 (11) (2016) 1–7.

5. K.K. Jain, Current status and future prospects of drug delivery systems, in: Drug Delivery System, vols. 1–56, Humana Press, New York, 2014.

6. R. Wang, G. Zhu, L. Mei, Y. Xie, H. Ma, M. Ye, F.-L. Qing, W. Tan, Automated modular synthesis of aptamer–drug conjugates for targeted drug delivery, J. Am. Chem. Soc. 136 (2014) 2731–2734.

7. M.A. Farooq et. al. Nanocarrier-mediated co-delivery systems for lung cancer therapy: recent developments and prospects, Environ. Chem. Lett. 17 (2019) 1565–1583.

8. X.-X. Xia, M. Wang, Y. Lin, Q. Xu, D.L. Kaplan, Hydrophobic drug-triggered selfassembly of nanoparticles from silk-elastin-like protein polymers for drug delivery, Biomacromolecules 15 (2014) 908–914.

9. W. She, N. Li, K. Luo, C. Guo, G. Wang, Y. Geng, Z. Gu, Dendronized heparin− doxorubicin conjugate based nanoparticle as pH-responsive drug delivery system for cancer therapy, Biomaterials 34 (2013) 2252–2264

10. A.Z. Mirza, F.A. Siddiqui, Nanomedicine and drug delivery: a mini review, Int. Nano Lett. 4 (2014) 94–100.

11. M.A. Heinrich, B. Martina, J. Prakash, Nanomedicine strategies to target coronavirus, Nano Today 35 (2020) 100961.

12. B. Maherani, et al., Liposomes: a review of manufacturing techniques and targeting strategies, Curr. Nanosci. 7 (3) (2011) 436–452.

13. Fang, J., Nakamura, H., Maeda, H., 2011. The EPR effect: unique features of tumor blood vessels for drug delivery, factors involved, and limitations and augmentation of the effect. Adv. Drug Deliv. Rev. 63, 136–151.

14. A. Capuano, C. Scavone, G. Racagni, F. Scaglione. NSAIDs in patients with viral infections, including Covid-19: victims or perpetrators? Pharmacol Res (April 29, 2020), p. 104849

15. L.L. Brunton, B.C. Knollmann, R. Hilal-Dandan. Goodman & gilman's the pharmacological basis of therapeutics(13th ed.), McGraw-Hill Education (2018)

16. E.K. McCreary, J.M. Pogue. Coronavirus disease 2019 treatment: a review of early and emerging options. Open forum infectious diseases, Vol. 7(4), Oxford University Press, Cary, NC (April 2020), p. ofaa105

17. M.J. Vincent, E. Bergeron, S. Benjannet, B.R. Erickson, P.E. Rollin, T.G. Ksiazek, N.G. Seidah, S.T. Nichol. Chloroquine is a potent inhibitor of SARS coronavirus infection and spread. J. Virol , 2 (1) (December 1, 2005), p. 69

18. Y. Furuta, B.B. Gowen, K. Takahashi, et al. Favipiravir (T-705), a novel viral RNA polymerase inhibitor Antiviral Res, 100 (2013), pp. 446-454

19. H. Maeda, G.Y. Bharate, J. Daruwalla, Polymeric drugs and nanomedicines for efficient tumor targeted drug delivery based on EPR-effect, Eur. J. Pharm. Biopharm. 71 (2009) 409–419.

20. H.Maeda, K. Greish, J. Fang, The EPR effect and polymeric drugs: a paradigm shift for cancer chemotherapy in the 21st century, Adv. Polym. Sci. 193 (2006) 103–121.

21. A.K. Iyer, K. Greish, J. Fang, H. Maeda, Exploiting the enhanced permeability and retention effect for tumor targeting, Drug Discov. Today 11 (2006) 812–818.

22. V. Torchilin, Tumor delivery of macromolecular drugs based on the EPR effect, Adv. Drug Deliv. Rev. 63 (2011) 131–135.

23. M.J. Vicent, H. Ringsdorf, R. Duncan, Polymer therapeutics: clinical applications and challenges for development, Adv. Drug Deliv. Rev. 61 (2009) 1117–1120.

24. R. Duncan, The dawning era of polymer therapeutics, Nat. Rev. Drug Discov. 2 (2003) 347–360.

25. Y. Matsumura, K. Kataoka, Preclinical and clinical studies of anticancer agentincorporating polymer micelles, Cancer Sci. 100 (2009) 572–579.;

26. J. Fang, T. Sawa, T. Akaike, H. Maeda, Tumor-targeted delivery of polyethylene glycol-conjugated D-amino acid oxidase for antitumor therapy via enzymatic generation of hydrogen peroxide, Cancer Res. 62 (2002) 3138–3143.

27. J. Fang, T. Sawa, T. Akaike, T. Akuta, S.K. Sahoo, K. Greish, A. Hamada, H. Maeda, In vivo antitumor activity of pegylated zinc protoporphyrin: targeted inhibition of heme oxygenase in solid tumor, Cancer Res. 63 (2003) 3567–3674.

28. A.K. Iyer, K. Greish, J. Fang, R. Murakami, H. Maeda, High-loading nanoSized micelles of copoly(styrene-maleic acid)-zinc protoporphyrin for targeted delivery of a potent heme oxygenase inhibitor, Biomaterials 28 (2007) 1871–1881.

29. K. Greish, A. Nagamitsu, J. Fang, H. Maeda, Copoly(styrene-maleic acid)- pirarubicin micelles: high tumor-targeting efficiency with little toxicity, Bioconjug. Chem. 16 (2005) 230–236.

30. K. Greish, T. Sawa, J. Fang, T. Akaike, H. Maeda, SMA-doxorubicin, a new polymeric micellar drug for effective targeting to solid tumours, J. Control. Release 97 (2004) 219–230.

31. H. Maeda, Y. Matsumura, Tumoritropic and lymphotropic principles of macromolecular drugs, Crit. Rev. Ther. Drug Carrier Syst. 6 (1989) 193–210.

32. A. Frère et.al. Polymeric Nanoparticles as siRNA Drug Delivery System for Cancer Therapy: The Long Road to Therapeutic Efficiency. Nanoarchitectonics for Smart Delivery and Drug Targeting, Nanoarchitectonics for Smart Delivery and Drug Targeting. 2016, Pages 503-540

33.Y. Noguchi, J. Wu, R. Duncan, J. Strohalm, K. Ulbrich, T. Akaike, H. Maeda, Early phase tumor accumulation of macromolecules: a great difference in clearance rate between tumor and normal tissues, Jpn. J. Cancer Res. 89 (1998) 307–314.

34. B. Maherani, et al., Liposomes: a review of manufacturing techniques and targeting strategies, Curr. Nanosci. 7 (3) (2011) 436–452.
35. Sun, C., Lee, J.S.H., Zhang, M., 2008. Magnetic nanoparticles in MR imaging and drug delivery. Adv. Drug Deliv. Rev. 60 (11), 1252–1265. https://doi.org/10.1016/j. addr.2008.03.018.
36. U. Arshad, H. et. al. Prioritization of anti-SARS-Cov-2 drug repurposing opportunities based on plasma and target site concentrations derived from their established human pharmacokinetics, Clin. Pharmacol. Ther. 108 (2020) 775–790
37. L. Chen, P. Liu, et. al. Inhalation of nitric oxide in the treatment of severe acute respiratory syndrome: a rescue trial in Beijing, Clin. Infect. Dis. 39 (2004) 1531–1535.
38. J.L. Rau, The inhalation of drugs: advantages and problems, Respir. Care 50 (2005) 367–382.
39. V.P. Torchilin, Recent advances with liposomes as pharmaceutical carriers, Nat. Rev. Drug Discov. 4 (2) (2005) 145–160.
40. M.R. Díaz, P.E. Vivas-Mejia, Nanoparticles as drug delivery systems in cancer medicine: emphasis on RNAi-containing nanoliposomes, Pharmaceuticals 6 (11) (2013) 1361–1380.
41. X. Chen, et al., The stability, sustained release and cellular antioxidant activity of curcumin nanoliposomes, Molecules 20 (8) (2015) 14293–14311.
42. M. Haghighi, et al., Design and fabrication of pectin-coated nanoliposomal delivery systems for a bioactive polyphenolic: Phloridzin, Int. J. Biol. Macromol. 112 (2018) 626–637.
43. K. Khosravi-Darani, M. Mozafari, Nanoliposome potentials in nanotherapy: a concise overview, Int. J. Nanosci. Nanotechnol. 6 (1) (2010) 3–13.
44. S. Hallaj-Nezhadi, M. Hassan, Nanoliposome-based antibacterial drug delivery, Drug Deliv. 22 (5) (2015) 581–589.
45. Y. Patil, et al., Targeting of folate-conjugated liposomes with co-entrapped drugs to prostate cancer cells via prostate-specific membrane antigen (PSMA), Nanomed. Nanotechnol. Biol. Med. 14 (4) (2018) 1407–1416.
46 A. Shakeri-Zadeh, et al., Folate receptor-targeted nanoprobes for molecular imaging of cancer: friend or foe? Nano Today 39 (2021) 101173.
47. B. Farran, et al., Folate-conjugated nanovehicles: strategies for cancer therapy, Mater. Sci. Eng. C 107 (2020) 110341.
48. M. Jaymand, et al., Radiolabeled carbon-based nanostructures: new radiopharmaceuticals for cancer therapy? Coord. Chem. Rev. 440 (2021) 213974.
49. Tan, Y., & McClements, D. (2021). Improving the bioavailability of oil-soluble vitamins by optimizing food matrix effects: A review. *Food Chemistry, 348*, 129–148.
50. Moel ler, H., Martin, D., Schrader, K., Hoffmann, W., & Lorenzen, P. C. (2018). Spray- or freeze-drying of casein micelles loaded with Vitamin D2: Studies on storage stability and in vitro digestibility. *Lebensmittel-Wissenschaft & Technologie, 97*, 87–93.
51. Cohen, Y., Levi, M., Lesmes, U., Margier, M., Reboul, E., & Livney, Y. D. (2017a). Re-assembled casein micelles improve in vitro bioavailability of vitamin D in a Caco-2 cell model. *Food & Function, 8*.

52. Tzankova, V., Gorinova, C., Kondeva-Burdina, M., Simeonova, R., Philipov, S., Konstantinov, S., et al. (2016). In vitro and in vivo toxicity evaluation of cationic PDMAEMA-PCL-PDMAEMA micelles as a carrier of curcumin. *Food Chem Toxicol, 97*, 1–10.

53. Kalhapure, R. S., & Renukuntla, J. (2018). Thermo- and pH dual responsive polymeric micelles and nanoparticles. *Chemico-Biological Interactions, 295*, 20–37

54. Lu, Y., Zhang, E., Yang, J., & Cao, Z. (2018). Strategies to improve micelle stability for drug delivery. Nano Res, 11, 4985–4998.

55. Almeida, A., Araújo, M., Novoa-Carballal, R., Andrade, F., Gonçalves, H., Reis, R. L., et al. (2020). Novel amphiphilic chitosan micelles as carriers for hydrophobic anticancer drugs. Materials Science and Engineering: C, 112, 110920.

56. Chen, T., Tu, L., Wang, G., Qi, N., Wu, W., Zhang, W., et al. (2020). Multi-functional chitosan polymeric micelles as oral paclitaxel delivery systems for enhanced bioavailability and anti-tumor efficacy. Int J Pharm, 578, 119105.

57. Ojogbo, E., Ogunsona, E. O., & Mekonnen, T. H. (2020). Chemical and physical modifications of starch for renewable polymeric materials. Materials Today Sustainability, 7–8, 100028.

58. Wusigale, Liang, L., & Luo, Y. (2020). Casein and pectin: Structures, interactions, and applications. Trends in Food Science & Technology, 97, 391–403.

59. Ranadheera, C. S., Liyanaarachchi, W. S., Chandrapala, J., Dissanayake, M., & Vasiljevic, T. (2016). Utilizing unique properties of caseins and the casein micelle for delivery of sensitive food ingredients and bioactives. Trends in Food Science & Technology, 57, 178–187.

60. Kumar, A. et. al. (2018). Mixed surfactant (altering chain length and head group) aggregates as an effective carrier for tuberculosis drug. Chemistry and Physics of Lipids, 215, 11–17.

61. Salvia-Trujillo, L., Verkempinck, S. H., Sun, L., Van Loey, A. M., Grauwet, T., & Hendrickx, M. E. (2017). Lipid digestion, micelle formation and carotenoid bioaccessibility kinetics: Influence of emulsion droplet Size. *Food Chemistry, 229*, 653–662.

62. Tuncer, E., & Bayramoglu, B. (2019). Characterization of the self-assembly and Size dependent structural properties of dietary mixed micelles by molecular dynamics simulations. Biophys Chem, 248, 16–27.

63. Gunzel, D. (2017). Claudins: Vital partners in transcellular and paracellular transport coupling. Pflügers Archiv, 469, 35–44.

64 Chen, S. et al. (2020). Nano-micelles based on hydroxyethyl starch-curcumin conjugates for improved stability, antioxidant and anticancer activity of curcumin. Carbohydrate Polymers, 228, 115398.

65. S. Khorasani, M. Danaei, M. Mozafari, Nanoliposome technology for the food and nutraceutical industries. Trends in Food Science & Technology, 79 (2018), pp. 106-115, 10.1016/j.tifs.2018.07.009

66. W. Liu, Y. Hou, Y. Jin, Y. Wang, X. Xu, J. Han. Research progress on liposomes: Application in food, digestion behavior and absorption mechanism. Trends in Food Science & Technology (2020),

67. Y. Xiao, et al., Engineering nanoparticles for targeted delivery of nucleic acid therapeutics in tumor, Mol. Ther. Methods Clin. Dev. 12 (2019) 1–18.

68. M.M. El-Hammadi, J.L. Arias, An update on liposomes in drug delivery: a patent review (2014-2018), Expert Opin. Ther. Pat. 29 (11) (2019) 891–907.
69. M. Alavi, N. Karimi, M. Safaei, Application of various types of liposomes in drug delivery systems, Adv. Pharmaceut. Bull. 7 (1) (2017) 3.
70. D. Sharma, A.A.E. Ali, L.R. Trivedi, An Updated Review on: liposomes as drug delivery system, PharmaTutor 6 (2) (2018) 50–62.
71. W.G. Pitt, G.A. Husseini, Ultrasound in Drug and Gene Delivery, Elsevier, 2008.
72. H. Takeuchi, et al., Passive targeting of doxorubicin with polymer coated liposomes in tumor bearing rats, Biol. Pharm. Bull. 24 (7) (2001) 795–799.
73. D.C. Drummond, et al., Development of a highly active nanoliposomal irinotecan using a novel intraliposomal stabilization strategy, Cancer Res. 66 (6) (2006) 3271–3277.
74. M. Mohammadabadi, M. Mozafari, Enhanced efficacy and bioavailability of thymoquinone using nanoliposomal dosage form, J. Drug Deliv. Sci. Technol. 47 (2018) 445–453.
75. B.-H. Chen, B. Stephen Inbaraj, Nanoemulsion and nanoliposome based strategies for improving anthocyanin stability and bioavailability, Nutrients 11 (5) (2019) 1052.
76. A. Shakeri-Zadeh, et al., Gold nanoparticle-mediated bubbles in cancer nanotechnology, J. Contr. Release 330 (2020) 49–60.
77. M. Namdari, A. Eatemadi, Nanofibrous bioengineered heart valve—application in paediatric medicine, Biomed. Pharmacother. 84 (2016) 1179–1188.
78. M.R. Mozafari, Nanocarrier Technologies: Frontiers of Nanotherapy, Springer, 2006.
79. Y. Li, C. Zhu, Enhanced hepatic-targeted delivery via oral administration using nanoliposomes functionalized with a novel DSPE–PEG–cholic acid conjugate, RSC Adv. 6 (33) (2016) 28110–28120.
80. M.R. Mozafari, et al., Encapsulation of food ingredients using nanoliposome technology, Int. J. Food Prop. 11 (4) (2008) 833–844.
81. H. Hwang, et al., PEGylated nanoliposomes encapsulating angiogenic peptides improve perfusion defects: radionuclide imaging-based study, Nucl. Med. Biol. 43 (9) (2016) 552–558.
82. A. Cern, et al., Effect of solubilizing agents on mupirocin loading into and release from PEGylated nanoliposomes, J. Pharmaceut. Sci. 103 (7) (2014) 2131–2138.
83. S. Sur, et al., Recent developments in functionalized polymer nanoparticles for efficient drug delivery system, Nano-Structures & Nano-Objects 20 (2019) 100397.
84. Niosomes: a novel approach in modern drug delivery systems Chapter · December 2017. Morteza Yaghoobian. Shahid Beheshti University of Medical Sciences
85. Khandare JN. et. al., Niosomes Novel Drug Delivery System. The Eastern Pharmacist. 1994, 37: 61-64.
86. Baillie AJ. et. al, The preparation and properties of niosomes non-ionic surfactant vesicles. J. Pharm. Pharmacol. 1985, 37: 863- 868. V. Pola Chandu
87. Rogerson A., Cummings J., Willmott N., Florence AT., The distribution of doxorubicin in mice following administration in niosomes. J. Pharm. Pharmacol. 1988, 40: 337-342

88. Ling et. Al. Niosomes: A review of their structure, properties, methods of preparation, and medical applications. Asian Biomedicine 11(4):301-314. March 2018.

89. Biju SS., Talegaonkar S., Misra PR., Khar RK., Vesicular systems: An overview. Indian J. Pharm. Sci. 2006, 68: 141-153.

90. Ijeoma F., Uchegbu., Suresh P., Vyas., Non-ionic surfactant based vesicles (niosomes) in drug delivery. Int. J. Pharm. 1998; 172: 33–70.

91. Malhotra M., Jain N.K., Niosomes as Drug Carriers. Indian Drugs. 1994, 31(3): 81-866.

92. Hall, D.G., 1987. Thermodynamics of micelle formation. In: Schick, J. (Ed.), Nonionic Surfactants: Physical Chemistry. In: Surfactant Science Series. Marcel Dekker, New York, pp. 233–296.

93. Giddi, H.S., Arunagirinathan, M.A., Bellare, J.R., 2007. Self-assembled surfactant nano-structures important in drug delivery. Indian J. Exp. Biol. 45 (2), 133–159.

94. Bouwstra, J.A., Van Hal, D.A., Hofland, H.E.J., 1997. Preparation and characterization of nonionic surfactant vesicles. Colloid Surf. A. 123-124, 71–80.

95. Hao, Y., Zhao, F., Li, N., Yang, Y., Li, K., 2002. Studies on a high encapsulation of colchicine by a niosome system. Int. J. Pharm. 244, 73–80.

96. Yoshida, H. et. al. 1992. Niosomes for oral delivery of peptide drugs. J. Control. Release 21, 145–153.

97. Nasseri, B., 2005. Effect of cholesterol and temperature on the elastic properties of niosomal membranes. Int. J. Pharm. 300 (1–2), 95–101.

98. Balakrishnan, P. et. al. 2009. Formulation and in vitro assessment of minoxidil niosomes for enhanced skin delivery. Int. J. Pharm. 244, 73–80.

99. Pardakhty, A. Et. al. 2011. Pharmacokinetic study of niosome-loaded insulin in diabetic rats. Daru 19 (6), 404–411.

100. Okore, V.C., Attama, A.A., Ofokansi, K.C., Esimone, C.O., Onuigbo, E.B., 2011. Formulation and Evaluation of Niosomes. Indian J. Pharm Sci. 73 (3), 323–328.

101. Hu, C., Rhodes, D.G., 2000. Proniosomes: a novel drug carrier preparation. Int. J. Pharm. 206, 110–122.

102. Manosroi, A. et. al. J., 2010. Transdermal absorption enhancement through rat skin of gallidermin loaded in niosomes. Int. J. Pharm. 392, 304–310.

103. Agrati, C., Marianecci, C., Sennato, S., Carafa, M., Bordoni, V., Cimini, E., Tempestilli, M., Pucillo, L.P., Turchi, F., Martini, F., Borioni, G., Bordi, F., 2011. Multicompartment vectors as novel drug delivery systems: selective activation of Tγδ lymphocytes after zoledronic acid delivery. Nanomedicine 7, 153–161.

104. Alsarra A., Bosela A,, Ahmed S.M,, Mahrous G.M., Proniosomes as a drug carrier for transdermal delivery of ketorolac. Eur. J. Pharm. and Biopharm. 2004; 2(1): 1-6.

105.Hu C., Rhodes D.G., Proniosomes: a novel drug carrier preparation. Int. J. Pharm. 1999, 185: 23-35.

106. Blazek-Walsh A.I., and Rhodes D.G., Pharm. Res. SEM imaging predicts quality of niosomes from maltodextrin-based proniosomes. 2001, 18: 656-661.

107. Yoshioka T., Stermberg B., Florence A.T., Preparation and properties of vesicles (niosomes) of sorbitan monoesters (Span 20, 40, 60, and 80) and a sorbitan triester (Span 85). Int. J Pharm. 1994; 105: 1-6

108. Karim Masud Kazi et. al. Niosome: A future of targeted drug delivery systems J Adv Pharm Technol Res. 2010 Oct-Dec; 1(4): 374–380.

109. Carter, K.C., Dolan, T.F., Baillie, A.J., MacColgan, C., 1989. Visceral leishmaniasis: drug carrier system characteristics and the ability to clear parasites from the liver, spleen and bone marrow in *Leishmania donovani* infected BALB/c mice. J. Pharm. Pharmcol. 41 (2), 87–91.

110. Kisan, R.J., Manoj, N.G., Ishaque, M.S., Vilarsrao, J.K., Sambjahi, S.P., 2007. Nasal drug delivery system-factors affecting and applications. Curr. Drug Therapy 2, 27–38.

111. Priyadarshi Aparajaya, Abhimanyu Dev. Department of Pharmaceutical Sciences & Technology, Birla Institute of Technology, Mesra, Ranchi, Jharkhand - 835215 (India). Functionalized niosomes as a smart delivery device in cancer and fungal infection. European Journal of Pharmaceutical Sciences Volume 168, 1 January 2022, 106052.

112. Guan Y et al. Isolation and characterization of viruses related to the SARS coronavirus from animals in southern China. Science 2003; 302:276–278.

113. Derdeyn CA. et. al. Sensitivity of human immunodeficiency virus type 1 to fusion inhibitors targeted to the gp41 first heptad repeat involves distinct regions of gp41 and is consistently modulated by gp120 interactions with the coreceptor. Journal of Virology 2001; 75:8605–8614.

114. Sia SK, Carr PA, Cochran AG, Malashkevich VN & Kim PS. Short constrained peptides that inhibit HIV-1 entry. Proceedings of the National Academy of Sciences, USA 2002; 99:14664–14669.

115. Medinas RJ, Lambert DM & Tompkins WA. C-terminal gp40 peptide analogs inhibit feline immunodeficiency virus: cell fusion and virus spread. Journal of Virology 2002; 76:9079–9086.

116. Pinon JD, Kelly SM, Price NC, Flanagan JU & Brighty DW. An antiviral peptide targets a coiled-coil domain of the human T-cell leukemia virus envelope glycoprotein. Journal of Virology 2003; 77:3281–3290.

117. Liu S, Xiao G et. al. Interaction between heptad repeat 1 and 2 regions in spike protein of SARS-associated coronavirus: implications for virus fusogenic mechanism and identification of fusion inhibitors. Lancet 2004; 363:938–947.

118. Bo-Jian Zheng1 et al. CY Woo1 , Hsiang-fu Kung2,3, Kwok-Yung Yuen1 and Jian-Dong Huang5†1 Department of Microbiology, 2 Institute of Molecular Biology, 4 Department of Chemistry and Open Laboratory of Chemical Biology, 5 Department of Biochemistry, University of Hong Kong, Pokfulam, Hong Kong SAR, China 3 Centre for Emerging Infectious Diseases, Faculty of Medicine, Chinese University of Hong Kong, Hong Kong SAR, China 6 Biomolecular Structure Research Centre, University of Siena, Siena, Italy Corresponding authors: *†

119.Synthetic peptides outside the spike protein heptad repeat regions as potent inhibitors of SARS-associated coronavirus. Antiviral Therapy 10:393–403

120. H. Lu, C.W. Stratton, Y.W. Tang, Outbreak of pneumonia of unknown etiology in Wuhan, China: the mystery and the miracle, J. Med. Virol. 92 (4) (2020) 401–402, https://doi.org/10.1002/jmv.25678.

121. Ye, Z.-W., Yuan, S., Yuen, K.-S., Fung, S.-Y., Chan, C.-P., Jin, D.-Y., 2020. Zoonotic origins of human coronaviruses. Int. J. Biol. Sci. 16, 1686.
122. N. Chen, M. Zhou, X. Dong, et al., Epidemiological and clinical characteristics of 99 cases of 2019 novel coronavirus pneumonia in Wuhan, China: a descriptive study, Lancet 395 (10223) (2020) 507–513, https://doi.org/10.1016/S0140- 6736(20)30211-7.
123. J.F. Chan, S.K. Lau, K.K. To, et al., Middle East respiratory syndrome coronavirus: another zoonotic betacoronavirus causing SARS-like disease, Clin. Microbiol. Rev. 28 (2015) 465–522. https://cmr.asm.org/content/28/2/465.
124. A.M. Zaki et al., Isolation of a novel coronavirus from a man with pneumonia in Saudi Arabia, N. Engl. J. Med. 367 (2012) 1814–1820. https://www.nejm.org/doi/full/10.1056/NEJM oa1211721.
125. Central Disaster and Safety Countermeasure Headquarters of the Republic of Korea, Rules and guidelines for distancing in daily life to control coronavirus disease 2019 in Korea: 3rd version, announced on July 3, 2020, J. Educ. Eval. Health. Prof. (2020) 17-20. https://www.jeehp.org/DOIx.php?id=10.3352/ jeehp.2020.17.20.
126. R. Lu, X. Zhao, J. Li, et al., Genomic characterisation and epidemiology of 2019 novel coronavirus: implications for virus origins and receptor binding, Lancet 395 (10224) (2020) 565–574, https://doi.org/10.1016/S0140-6736(20)30251-8.
127. M. Chan-Yeung, R. Xu, SARS: epidemiology, Respirology 8 (2003) S9–S14.
128. A.A. Rabaan, S.H. Al-Ahmed, S. Haque, et al., SARS-CoV-2, SARS-CoV, and MERSCoV: a comparative overview, L. Inf. in Med. 2 (2020) 174–184.
129. Jian Shang, Gang Ye, Ke Shi, Yushun Wan, Chuming Luo, Hideki Aihara, Qibin Geng, Ashley Auerbach, Fang Li, Structural basis of receptor recognition bySARS-CoV-2, Nat. 581 (7807) (2020) 221–224, https://doi.org/10.1038/ s41586-020-2179.
130. Filippo Scialo, Aurora Daniele, Felice Amato, Lucio Pastore, Maria Gabriella Matera, Mario Cazzola, Giuseppe Castaldo, Andrea Bianco, ACE2: The Major Cell Entry Receptor for SARS-CoV-2, Lung. 198 (6) (2020) 867–877, https://doi.org/10.1007/s00408-020-00408-4.
131. L. Wang, Y. Xiang, Spike Glycoprotein-Mediated Entryof SARS Coronaviruses, Viruses. 12 (2020) 1289, https://doi.org/10.3390/v12111289.
132. H.T. Nguyen, S. Zhang, Q. Wang, et al. (2020). Spike glycoprotein and host cell determinants. SARS-CoV-2 entry and cytopathic effects. J Virol.11, 95e02304-20. https://doi.org/10.1128/JVI.02304-20.
133. Li, W. et al. Bats are natural reservoirs of SARS-like coronaviruses. Science 310, 676–679 (2005).
134. Ge, X.-Y. et al. Isolation and characterization of a bat SARS-like coronavirus that uses the ACE2 receptor. Nature 503, 535–538 (2013).
135. Yang, L. et al. Novel SARS-like betacoronaviruses in bats, China, 2011. Emerg. Infect. Dis. 19, 989–991 (2013).
136. Hu, B. et al. Discovery of a rich gene pool of bat SARS-related coronaviruses provides new insights into the origin of SARS coronavirus. PLoS Pathog. 13, e1006698 (2017).

137. Drosten, C. et al. Identification of a novel coronavirus in patients with severe acute respiratory syndrome. N. Engl. J. Med. 348, 1967–1976 (2003).
138. Zaki, A. M., van Boheemen, S., Bestebroer, T. M., Osterhaus, A. D. M. E. & Fouchier, R. A. M. Isolation of a novel coronavirus from a man with pneumonia in Saudi Arabia. N. Engl. J. Med. 367, 1814–1820 (2012).
139. Cui, J., Li, F. & Shi, Z. L. Origin and evolution of pathogenic coronaviruses. Nat. Rev. Microbiol. 17, 181–192 (2019).
140. Fan, Y., Zhao, K., Shi, Z.-L. & Zhou, P. Bat coronaviruses in China. Viruses 11, 210 (2019).
141. Wuhan Municipal Health Commission. Press statement related to novel coronavirus infection (in Chinese) http://wjw.wuhan.gov.cn/front/web/showDetail/2020012709194 (2020).
142. Andrew G. Harrison, Tao Lin, Penghua Wang, Mechanisms of SARS-CoV-2 Transmission and pathogenesis, T. in Immunol. 41 (12) (2020) 1100–1115, https://doi.org/10.1016/j.it.2020.10.004.
143. Shumpei Yokota, Takako Miyamae, Yoshiyuki Kuroiwa, Kusuki Nishioka, Novel Coronavirus Disease 2019 (COVID-19) and Cytokine Storms for More Effective Treatments from anInflammatory Pathophysiology, J. Clin. Med. 10 (4) (2021) 801, https://doi.org/10.3390/jcm10040801.
144. Li, W. et al. Angiotensin-converting enzyme 2 is a functional receptor for the SARS coronavirus. Nature 426, 450–454 (2003).
145. K. Kuba, Y. Imai, S. Rao, et al., A crucial role of angiotensin converting enzyme 2 (ACE2) in SARS coronavirus-induced lung injury, Nat. Med. 11 (8) (2005) 875–879, https://doi.org/10.1038/nm1267.
146. W.S.D. Tan, W. Liao, S. Zhou, D. Mei, W.F. Wong, Targeting the renin-angiotensin system as novel therapeutic strategy for pulmonary diseases, Curr. Opin. Pharmacol. 40 (2018) 9–17, https://doi.org/10.1016/j.coph.2017.12.002.
147. Y. Imai, K. Kuba, S. Rao, et al., Angiotensin-converting enzyme 2 protects from severe acute lung failure, Nature 436 (7047) (2005) 112–116, https://doi.org/10. 1038/nature03712.
148. G. Li, Y. Fan, Y. Lai, et al., Coronavirus infections and immune responses, J. Med. Virol. 92 (4) (2020) 424–432, https://doi.org/10.1002/jmv.25685.
149. S.L. Smits, A. de Lang, J.M. van den Brand, et al., Exacerbated innate host response to SARS-CoV in aged non-human primates, PLoS Pathog. 6 (2) (2010) e1000756, , https://doi.org/10.1371/journal.ppat.1000756.
150. B.G. Chousterman, F.K. Swirski, G.F. Weber (Eds.), Cytokine Storm and Sepsis Disease Pathogenesis. Seminars in Immunopathology, Springer, 2017.
151. J.Y. Chien, P.R. Hsueh, W.C. Cheng, C.J. Yu, P.C. Yang, Temporal changes in cytokine/chemokine profiles and pulmonary involvement in severe acute respiratory syndrome, Respirology 11 (6) (2006) 715–722, https://doi.org/10. 1111/j.1440-1843.2006.00942.x.
152. I. Astuti, Severe acute respiratory syndrome coronavirus 2 (SARS-CoV-2): an overview of viral structure and host response, Diabetes. Metab. Syndr. 14 (2020) 407–412, https://doi.org/10.1016/j.dsx.2020.04.020.

153. M.A. Shereen, S. Khan, A. Kazmi, N. Bashir, R. Siddique, COVID-19 infection: origin, transmission, and characteristics of human coronaviruses, J. Adv. Res. 24 (2020) 91–98, https://doi.org/10.1016/j.jare.2020.03.005

154. P.A. Reyfman, J.M. Walter, N. Joshi, K.R. Anekalla, A.C. McQuattie-Pimentel, S. Chiu, R. Fernandez, M. Akbarpour, C.I. Chen, Z. Ren, R. Verma, Single-cell transcriptomic analysis of human lung provides insights into the pathobiology of pulmonary fibrosis, Am, J. Respir. Crit. Care Med. 199 (2019) 1517–1536, https://doi.org/10.1164/rccm.201712-2410OC.

155. M. Hoffmann, H. Et. al. SARS-CoV-2 cell entry depends on ACE2 and TMPRSS2 and is blocked by a clinically proven protease inhibitor, Cell 181 (2020) 271–280, https://doi.org/10.1016/j. cell.2020.02.052.

156. Y. Wan, J. Shang, R. Graham, R.S. Baric, F. Li, Receptor recognition by the novel coronavirus from Wuhan: an analysis based on decade-long structural studies of SARS coronavirus, J. Virol. 94 (2020), https://doi.org/10.1128/JVI.00127-20.

157. W. Sungnak et. al SARSCoV-2 entry factors are highly expressed in nasal epithelial cells together with innate immune genes, Nat. Med. 26 (2020) 681–687, https://doi.org/10.1038/ s41591-020-0868-6.

158. J. Shang, Y. Wan, C. Luo, G. Ye, Q. Geng, A. Auerbach, F. Li, Cell entry mechanisms of SARS-CoV-2, Proc. Natl. Acad. Sci. 117 (2020) 11727–11734, https://doi.org/10.1073/pnas.2003138117

159. R.J. Mason, Pathogenesis of COVID-19 from a cell biology perspective, Eur. Respir. J. 55 (2020), 2000607, https://doi.org/10.1183/13993003.00607-2020.

160. M.S. Yip, N.H. et. al. Antibody-dependent infection of human macrophages by severe acute respiratory syndrome coronavirus, Virol. J. 11 (2014) 1–11, https:// doi.org/10.1186/1743-422X-11-82.

161. K. Annen, T.E. Morrison, M.G. DomBourian, et al., Presence and short-term persistence of SARS-CoV-2 neutralizing antibodies in COVID-19 convalescent plasma donors, Transfusion. 61 (2021) 1148–1159, https://doi.org/10.1111/ trf.16261.

162. D. Nag, R. Chaudhry, M. Mishra, et al., A Prospective Study on Rapidly Declining SARS-CoV-2 IgG Antibodies Within One to Three Months of Testing IgG Positive: Can It Lead to Potential Reinfections? Cureus. 12 (2020), e11845 https://doi.org/ 10.7759/cureus.11845.

163. C.E. Gomez, ´ B. Perdiguero, M. Esteban, Emerging SARS-CoV-2 Variants and Impact in Global Vaccination Programs against SARS-CoV-2/COVID-19, Vaccines. 9 (2021) 243, https://doi.org/10.3390/vaccines9030243.

164. Xiaoying Shen et. al. SARS-CoV-2 variant B.1.1.7 is susceptible to neutralizing antibodies elicited by ancestral Spike vaccines, C. Host Microb. 29 (4) (2021) 529–539.e3, https://doi.org/10.1016/j.chom.2021.03.002.

165. J. Singh, S.A. Rahman, N.Z. Ehtesham, et al. (2021). SARS-CoV-2 variants of concern are emerging in India. Nat. Med. https://doi.org/10.1038/s41591-021- 01397-4.

166. Constantinos Kurt Wibmer et. al. SARS-CoV-2 501Y.V2 escapes neutralization by South African COVID-19 donor plasma, Nat. Med. 27 (4) (2021) 622–625, https://doi.org/10.1038/s41591-021-01285-x.

167. Markus Hoffmann et. al. S.ARS-CoV-2 variants B.1.351 and P.1 escape from neutralizing antibodies, Cell 184 (9) (2021) 2384–2393.e12, https://doi.org/ 10.1016/j.cell.2021.03.036.
168. WHO variants nomenclature announcement. https://www.who.int/en/activities/ tracking-SARS-CoV-2-variants/ (accessed in 10 June 2021).
169. C. Qin, L. Zhou, Z. Hu, et al., Dysregulation of immune response in patients with COVID-19 in Wuhan, China, Clin. Infect. Dis. (2020), https://doi.org/10.1093/ cid/ciaa248.
170. Chen G, Wu D, Guo W, et al. Clinical and immunological features of severe and moderate coronavirus disease 2019. J Clin Invest 2020;130:2620–9. https://doi.org/10.1172/JCI137244.
171. Zhou F, Yu T, Du R, et al. Clinical course and risk factors for mortality of adult inpatients with COVID-19 in Wuhan, China: a retrospective cohort study. Lancet (London, England) 2020;395:1054–62. https://doi.org/10.1016/S0140-6736(20)30566-3.
172. Henderson LA, et al. On the alert for cytokine storm: immunopathology in COVID-19. Arthritis Rheumatol 2020. https://doi.org/10.1002/art.41285.
173. Chaolin Huang et. al. Bin Cao, novel coronavirus in Wuhan, China. Lancet. 395 (10223) (2020) 497–506, https://doi.org/10.1016/S0140- 6736(20)30183-5.
174. F. Qi, S. Qian, S. Zhang, Z. Zhang, Single cell RNA sequencing of 13 human tissues identify cell types and receptors of human coronaviruses, Biochem. Biophys. Res. Commun. 526 (2020) 135–140, https://doi.org/10.1016/j.bbrc.2020.03.044.
175. L.A. Teuwen, V. Geldhof, A. Pasut, P. Carmeliet, COVID-19: the vasculature unleashed, Nat. Rev. Immunol. 20 (2020) 389–391, https://doi.org/10.1038/ s41577-020-0343-0.
176. M. Soy et. al. Cytokine storm in COVID-19: pathogenesis and overview of anti-inflammatory agents used in treatment, Clin. Rheumatol. 39 (2020) 2085–2094, https://doi.org/10.1007/ s10067-020-05190-5.
177. A.S. Hancock et. al. Transcriptome analysis of infected and bystander type 2 alveolar epithelial cells during influenza A virus infection reveals in vivo Wnt pathway downregulation, e01325-18, J. Virol. 92 (2018), https://doi.org/10.1128/JVI.01325-18.
178. N.L.S. Tang et. al. Lam, Early enhanced expression of interferon-inducible protein-10 (CXCL-10) and other chemokines predicts adverse outcome in severe acute respiratory syndrome, Clin. Chem. 51 (2005) 2333–2340, https://doi.org/ 10.1373/clinchem.2005.054460.
179. J. Wang, M.P et. al.Innate immune response to influenza A virus in differentiated human alveolar type II cells, Am. J. Respir. Cell Mol. Biol. 45 (2011) 582–591, https://doi.org/10.1165/rcmb.2010-0108OC.
180. M. Gracia-Hernandez, E.M. Sotomayor, A. Villagra, Targeting macrophages as a therapeutic option in COVID-19, Front. Pharmacol. 11 (2020) 1659, https://doi. org/10.3389/fphar.2020.577571.
181. E.J. Giamarellos-Bourboulis, et. al. M.E. Adami, P. Katsaounou, Ntaganou, Complex immune dysregulation in COVID-19 patients with severe respiratory failure, Cell. Host. Microbe. 27 (2020) 992–1000, https:// doi.org/10.1016/j.chom.2020.04.009.

182. M. Panigada, N.et. al. Hypercoagulability of COVID-19 patients in intensive care unit: a report of thromboelastography findings and other parameters of hemostasis, J. Thromb. Haemost. 18 (2020) 1738–1742, https://doi.org/10.1111/jth.14850.
183. L. Spiezia, A. et. al. COVID-19-related severe hypercoagulability in patients admitted to intensive care unit for acute respiratory failure, Thromb. Haemost. 120 (2020) 998, https://doi.org/10.1055/s-0040-1710018.
184. E. Terpos, I. et. al. Hematological findings and complications of COVID-19, Am. J. Hematol. 95 (2020) 834–847, https://doi.org/10.1002/ajh.25829.
185. Krammer F. SARS-CoV-2 vaccines in development. Nature 2020;586:516–27. doi: 10.1038/s41586-020-2798-3.
186. Bale S, Goebrecht G, Stano A, Wilson R, Ota T, Tran K, et al. Covalent Linkage of HIV-1 Trimers to Synthetic Liposomes Elicits Improved B Cell and Antibody Responses. J Virol 2017;91 e00443-17. doi: 10.1128/JVI.00443-17.
187. Thanh T et. al. Lipid-Based Nanoparticles in the Clinic and Clinical Trials From Cancer Nanomedicine to COVID-19 Vaccines. Vaccines 2021;9:359.
188. Editoral. Let's talk about lipid nanoparticles. Nat Rev Mater 2021;6. doi: 10.1038/ s41578-021-00281-4.
189. Gurtman A, Lockhart S, Perez JL, Marc GP, Moreira ED, Zerbini C, et al. Safety and Efficacy of the BNT162b2 mRNA Covid-19 Vaccine. N Engl J Med 2020;383:2603–15.
190. Baden LR et al. Efficacy and Safety of the mRNA-1273 SARS-CoV-2 Vaccine. N Engl J Med 2021;384:403–16.
191. Karik_o K, Muramatsu H, Welsh FA, Ludwig J, Kato H, Akira S, et al. Incorporation of pseudouridine into mRNA yields superior nonimmunogenic vector with increased translational capacity and biological stability. Mol Ther 2008;16:1833–40. doi: 10.1038/mt.2008.200.
192. CureVac. CureVac Provides Update on Phase 2b/3 Trial of First-Generation COVID-19 Vaccine Candidate, CVnCoVn.d.. https://www.curevac.com/en/2021/06/16/curevac-provides-update-on-phase-2b-3-
trial-of-first-generation-covid-19-vaccine-candidate-cvncov/(accessed October 21, 2021).
193. Medhi R, Srinoi P, Ngo N, Tran H, Lee TR. Nanoparticle-Based Strategies to Combat COVID-19. ACS Appl Nano Mater 2020;3:8557–80.
194. Renu S, Feliciano-ruiz N, Patil V. Immunity and Protective Efficacy of Mannose Conjugated Chitosan-Based Influenza Nanovaccine in Maternal Antibody Positive Pigs. Front Immunol 2021;12:516
195. Ortega-Rivera OA, Shin MD, Chen A, Beiss V, Moreno-Gonzalez MA, Lopez-Ramirez MA, et al. Trivalent Subunit Vaccine Candidates for COVID-19 and Their Delivery Devices. J Am Chem Soc 2021;143:14748–65. doi: 10.1021/jacs.1c06600.
196. Bangaru S, Ozorowski G, Turner HL, Antanasijevic A, Huang D, Wang X, et al. Structural analysis of full-length SARS-CoV-2 spike protein from an advanced vaccine candidate. Science (80-) 2020;370:1089–94. doi: 10.1126/science.abe1502

197. Joyce MG, King HAD, Naouar IE, Ahmed A, Peachman KK, Cincotta CM, et al. Efficacy of a Broadly Neutralizing SARS-CoV-2 Ferritin Nanoparticle Vaccine in Nonhuman Primates. BioRxiv 2021. doi: 10.1101/2021.03.24.436523.

198. Huang WC, Zhou S, He X, Chiem K, Mabrouk MT, Nissly RH, et al. SARS-CoV-2 RBD Neutralizing Antibody Induction is Enhanced by Particulate Vaccination. Adv Mater 2020;32:2005637.

199. Mathieu E, Ritchie H, Ortiz-Ospina E, Roser M, Hasell J, Appel C, et al. A global database of COVID-19 vaccinations. Nat Hum Behav 2021;5:947–53.

200. Dyer O. Covid-19: Countries are learning what others paid for vaccines. BMJ Bristish Med J 2021;372:n281.

201. Pollet J, Chen WH, Strych U. Recombinant protein vaccines, a proven approach against coronavirus pandemics. Adv Drug Deliv Rev 2021;170:71–82. doi: 10.1016/j.addr.2021.01.001.

202. Blumenthal KG, Phadke NA, Bates DW. Safety Surveillance of COVID-19 mRNA Vaccines Through the Vaccine Safety Datalink. JAMA 2021;326:1375–7. doi: 10.1001/jama.2021.14808.

203. Merad, M.&Martin, J. C. Pathological infammation in patients with COVID-19: a key role for monocytes and macrophages. Nat. Rev. Immunol. 20, 355–362 (2020).

204. Vabret, N. et al. Advancing scientifc knowledge in times of pandemics. Nat. Rev. Immunol. 20, 338 (2020).

205. Mehta, P. et al. COVID-19: consider cytokine storm syndromes and immunosuppression. Lancet 395, 1033–1034 (2020).

206. Ruan, Q., Yang, K., Wang, W., Jiang, L. & Song, J. Clinical predictors of mortality due to COVID-19 based on an analysis of data of 150 patients from Wuhan, China. Intensive Care Med. 46, 846–848 (2020).

207. Wu, C. et al. Risk factors associated with acute respiratory distress syndrome and death in patients with coronavirus disease 2019 pneumonia in Wuhan, China. JAMA Intern. Med. https://doi.org/10.1001/jamainternmed.2020.0994 (2020).

208. Herold, T. et al. Elevated levels of IL-6 and CRP predict the need for mechanical ventilation in COVID-19. J. Allergy Clin. Immunol. 146, 128–136 (2020).

209. Yang, Y. et al. Exuberant elevation of IP-10, MCP-3 and IL-1ra during SARS-CoV-2 infection is associated with disease severity and fatal outcome. Preprint at https://doi.org/10.1101/2020.03.02.20029975 (2020).

210. Zhang X. et al. Viral and host factors related to the clinical outcome of COVID-19. Nature 583, 437–440 (2020).

211. Fehr, A. R., Channappanavar, R. & Perlman, S. Middle East respiratory syndrome: emergence of a pathogenic human coronavirus. Annu. Rev. Med. 68, 387–399 (2017).

212. Ledford, H. Coronavirus breakthrough: dexamethasone is frst drug shown to save lives. Nature 582, 469 (2020).

213. Coperchini, F. Et. al. M., 2020. The cytokine storm in COVID-19: an overview of the involvement of the chemokine/chemokine-receptor system. Cytokine Growth Factor Rev. 53, 25–32. Wang, F., Nie,

J., Wang, H., Zhao, Q., Xiong, Y., Deng, L., Song, S., Ma, Z., Mo, P., Zhang, Y., 2020. Characteristics of peripheral lymphocyte subset alteration in COVID-19 pneumonia. J. Infect. Dis. 221, 1762–1769.
214. Bhatia, M., Zemans, R.L., Jeyaseelan, S., 2012. Role of chemokines in the pathogenesis of acute lung injury. Am. J. Resp. Cell Mol. 46, 566–572.
215. Channappanavar, R., Perlman, S., 2017. Pathogenic Human Coronavirus Infections: Causes and Consequences of Cytokine Storm and Immunopathology. Semin Immunopathol. Springer, pp. 529–539.
216. Huang, C., et. al. 2020. Clinical features of patients infected with 2019 novel coronavirus in Wuhan, China. Lancet 395, 497–506.
217. Goswami J, MacArthur TA, Sridharan M, et al. A review of pathophysiology, clinical features, and management options of COVID-19 associated coagulopathy. Shock 2020. https://doi. Org / 10.1097/SHK.0000000000001680.
218. Magro C, Mulvey JJ, Berlin D, et al. Complement associated microvascular injury and thrombosis in the pathogenesis of severe COVID-19 infection: a report of five cases. Transl Res 2020; 220:1–13. https://doi.org/10.1016/j.trsl.2020.04.007.
219. Tisoncik, J.R. et al. (2012) Into the eye of the cytokine storm. Microbiol. Mol. Biol. Rev. 76, 16–32
220. Fajgenbaum, D.C. and June, C.H. (2020) Cytokine storm. N. Engl. J. Med. 383, 2255–2273
221. Rhen, T. and Cidlowski, J.A. (2005) Antiinflammatory action of glucocorticoids new mechanisms for old drugs. N. Engl. J. Med. 353, 1711–1723
222. RECOVERY Collaborative Group (2021) Dexamethasone in hospitalized patients with Covid-19. N. Engl. J. Med. 384, 693–704.
223. Xu, Z., Shi, L., Wang, Y., Zhang, J., Huang, L., Zhang, C., Liu, S., Zhao, P., Liu, H., Zhu, L., 2020. Pathological findings of COVID-19 associated with acute respiratory distress syndrome. Lancet Respir. Med. 8, 420–422.
224.. Zhou, W. et. al. 2020. Potential benefits of precise corticosteroids therapy for severe 2019-nCoV pneumonia. Signal Transduct Tar. 5, 1–3.
225. Mccreary, E.K., Pogue, J.M., 2020. Coronavirus disease 2019 treatment: a review of early and emerging options. Open Forum Infectious Diseases. Oxford University Press US, ofaa105.
226. Armitage, L.C., Brettell, R., 2020. Inhaled corticosteroids: a rapid review of the evidence for treatment or prevention of COVID-19. https://www.cebm.net/covid-19/inhaledcorticosteroids-a-rapid-review-of-the-evidence-for-treatment-or-prevention-ofcovid-19/. (Accessed 3 July 2020).
227. Sanders, J.M., Monogue, M.L., Jodlowski, T.Z., Cutrell, J.B., 2020. Pharmacologic treatments for coronavirus disease 2019 (COVID-19): a review. J. Am. Med. Assoc. 323, 1824–1836.
228. Patel, S.K. et. al. 2020. Dexamethasone: a boon for critically ill COVID-19 patients? Trav. Med. Infect. Dis. 37.
229. Nicosia, R.F., Ligresti, G., Caporarello, N., Akilesh, S., Ribatti, D., 2021. COVID-19 vasculopathy: mounting evidence for an indirect mechanism of endothelial injury. Am. J. Pathol. 9 (8), 1374–1384 (08).

230. Leentjens, J., van Haaps, T.F., Wessels, P.F., Schutgens, R.E.G., Middeldorp, S., 2021. COVID-19-associated coagulopathy, and antithrombotic agents-lessons after one year. Lancet Haematol. 8 (7) (Apr 27).
231. Del Valle, et al., 2020. An inflammatory cytokine signature predicts COVID-19 severity and survival. Nat. Med. 26 (10), 1636–1643.
232. Andrianto, Al-Farabi M.J., Nugraha, R.A., Marsudi, B.A., Azmi, Y., 2021. Biomarkers of endothelial dysfunction and outcomes in coronavirus disease 2019 (COVID-19) patients: a systematic review and meta-analysis. Microvasc. Res. 138, 104224 (Nov).
233. Krüger-Genge, A., Block, A., Franke, R.-P., Jung, F., 2019. Vascular endothelial cell biology: an update. Int. J. Mol. Sci. 20 (18) (Sep 7).
234. Anderson, T.J., 1999. Assessment and treatment of endothelial dysfunction in humans. J. Am. Coll. Cardiol. 34 (3), 631–638 (Sep).
235. Pober, J.S., Sessa, W.C., 2007. Evolving functions of endothelial cells in inflammation. Nat Rev Immunol. 7 (10), 803–815 (Oct).
236. Seymour, C.W. et al., 2017. Time to treatment and mortality during mandated emergency care for sepsis. N. Engl. J. Med. 376 (23), 2235–2244 (Jun 8) https://doi.org/10.1016/S2213-2600(20)30560-9.
237. Van der Poll, T., van de Veerdonk, F.L., Scicluna, B.P., Netea, M.G., 2017. The immunopathology of sepsis and potential therapeutic targets. Nat Rev Immunol. 17 (7), 407–420 (Jul).
238. Ince, C., Mayeux, P.R., Nguyen, T., Gomez, H., Kellum, J.A., Ospina-Tascon, ´ G.A., et al., 2016. The endothelium in sepsis. Shock. 45 (3), 259–270 (Mar).
239. Amanda Baroutjian, Carol Sanchez, Dessy Boneva, Mark McKenney, Adel Elkbuli, SARS-CoV-2 pharmacologic therapies and their safety/effectiveness according to level of evidence, A. J. Emerg. Med. 38 (11) (2020) 2405–2415, https://doi.org/ 10.1016/j.ajem.2020.08.091.
240. Yang Wang, Xiaofan Lu, Yongsheng Li, Hui Chen, Taige Chen, Nan Su, Fang Huang, Jing Zhou, Bing Zhang, Fangrong Yan, Jun Wang, Clinical Course and Outcomes of 344 Intensive Care Patients with COVID-19, Am. J. Respir. Crit. Care Med. 201 (11) (2020) 1430–1434, https://doi.org/10.1164/rccm.202003- 0736LE.
241. S.U. Kumar, N. Madhana Priya, S.R. Nithya, et al, (2021). A review of novel coronavirus disease (COVID-19): based on genomic structure, phylogeny, current shreds of evidence, candidate vaccines, and drug repurposing. Biotech.11, 198. https://doi.org/10.1007/s13205-021-02749-0.
242. Vanitha Sampath et. al. Vaccines and Allergic reactions: the past, the current COVID-19 pandemic, and future perspectives, Allergy. 76 (6) (2021) 1640–1660, https://doi.org/10.1111/all.v76.610.1111/all.14840.
243. Camila B.P. da Costa, et. al. COVID-19 and Hyperimmune sera: A feasible plan B to fight against coronavirus, I. Immunopharm. 90 (2021) 107220, https://doi.org/10.1016/j. intimp.2020.107220.
244. E. Pairo-Castineira, S. Clohisey, L. Klaric, et al, Genetic mechanisms of critical illness in COVID-19, Nat.591 (2021) 92–98. https://doi.org/10.1038/s41586- 020-03065-y.

245. Sarah Al-Beltagi et. al. Thapsigargin Is a Broad-Spectrum Inhibitor of Major Human Respiratory Viruses: Coronavirus, Respiratory Syncytial Virus and Influenza A Virus, Viruses 13 (2) (2021) 234, https://doi.org/10.3390/v13020234.

246. S. Yuan, X. et al. (2021). Clofazimine broadly inhibits coronaviruses including SARS-CoV-2. Nat.https://doi.org/10.1038/s41586-021-03431-4.

247. W.P. Painter, W. Holman, J.A. Bush, et al. Human Safety, Tolerability, and Pharmacokinetics of Molnupiravir, a Novel Broad-2 Spectrum Oral Antiviral Agent with Activity Against SARS-CoV-2. Antimicrob. Agents Chemother. doi: 10.1128/AAC.02428-20.

248. Maxwell T. Finkelstein, et. al. Structural Analysis of Neutralizing Epitopes of the SARS-CoV-2 Spike to Guide Therapy and Vaccine Design Strategies, Viruses. 13 (1) (2021) 134, https://doi.org/10.3390/v13010134.

249. J. Hussen, M. Kandeel, M.G. Hemida, et al. (2020) Antibody-Based Immunotherapeutic Strategies for COVID-19. Pathogens.9, 917. https://doi.org/ 10.3390/pathogens9110917.

250. Shibo Jiang, Xiujuan Zhang, Yang Yang, Peter J. Hotez, Lanying Du, Neutralizing antibodies for the treatment ofCOVID-19, Nat. Biomed. Eng. 4 (12) (2020) 1134–1139, https://doi.org/10.1038/s41551-020-00660-2.

251. F. Levi-Schaffer, A. de Marco. (2021). COVID-19 and the revival of passive immunization: Antibody therapy for inhibiting SARS-CoV-2 and preventing host cell infection: IUPHAR review: 31. Br. J. Pharmacol.https://doi.org/10.1111/ bph.15359.

252. Daniele Focosi, Massimo Franchini, COVID-19 neutralizing antibody-based therapies in humoral immune deficiencies: A narrative review, Transfus. Apher. Sci. 60 (3) (2021) 103071, https://doi.org/10.1016/j.transci.2021.103071.

253. R.T.S. Cabral, E.M. Klumb, M. Couto, S. Carneiro, Evaluation of toxic retinopathy caused by antimalarial medications with spectral domain optical coherence tomography, Arq. Bras. Oftalmol. 82 (1) (2019) 12–17, https://doi.org/10.5935/ 0004-2749.20190002.

254. B.E. van den Borne, et. al. Chloroquine and hydroxychloroquine equally affect tumor necrosis factor-alpha, interleukin 6, and interferon-gamma production by peripheral blood mononuclear cells, J. Rheumatol. 24 (1) (1997) 55–60.,

255. Mentor Ali Ber Lucien, et. al. Antibiotics and antimicrobial resistance in the COVID-19 era: Perspective from resource-limited settings, Int. J. Infect. Dis. 104 (2021) 250–254, https://doi.org/10.1016/j.ijid.2020.12.087.

256. H. Li, Y. Zhou, M. Zhang, et al., Updated approaches against SARS-CoV-2, Antimicrob. Agents Chemother. 64 (2020) e00483–e520, https://doi.org/ 10.1128/AAC.

257. RECOVERY Collaborative Group H, Horby P, Lim WS, et al. Dexamethasone in Hospitalized Patients with Covid-19- Preliminary Report. N Engl J Med 2020. https://doi.org/10.1056/NEJMoa2021436.

258. Angus DC, Derde L, Al-Beidh F, et al. Effect of hydrocortisone on mortality and organ support in patients with severe COVID19: the REMAP-CAP COVID-19 corticosteroid domain randomized clinical trial. JAMA 2020; 324:1317–29. https://doi.org/ 10.1001/jama.2020.17022.

259. WHO Rapid Evidence Appraisal for COVID-19 Therapies (REACT) Working Group S, Sterne JAC, Murthy S, et al. Association between administration of systemic corticosteroids and mortality among critically ill patients with COVID-19: a metaanalysis. JAMA 2020; 324:1330–41. https://doi.org/10.1001/ jama.2020.17023.

260. Prevention C for DC and. Interim clinical guidance for management of patients with confirmed coronavirus disease (COVID-19). Available at: https://www.cdc.gov/coronavirus/2019-ncov/hcp/clinicalguidance-management-patients.html. Accessed December 23, 2020.

261. A.E. Coutinho, K.E. Chapman, The anti-inflammatory and immunosuppressive effects of glucocorticoids, recent developments and mechanistic insights, Mol. Cell. Endocrinol. 335 (1) (2011) 2–13, https://doi.org/10.1016/j.mce.2010.04. 005.

262. P. Horby, W.S. Lim, J. Emberson, et al., Effect of Dexamethasone in Hospitalized Patients With COVID-19: Preliminary Report, (2020), https://doi.org/10.1101/ 2020.06.22.20137273 %J medRxiv 2020.06.22.20137273.

263. G. Cevc, G. Blume, Hydrocortisone and dexamethasone in very deformable drug carriers have increased biological potency, prolonged effect, and reduced therapeutic dosage, Biochim. Biophys. Acta 1663 (1–2) (2004) 61–73, https://doi.org/ 10.1016/j.bbamem.2004.01.006.

264. Lingbo Shen. Enhanced topical corticosteroids delivery to the eye: A trade-off in strategy choice. Journal of Controlled Release. Volume 339, 10 November 2021, Pages 91-113

265. S.S. Chrai, M.C. Makoid, S.P. Eriksen, J.R. Robinson Drop Size and initial dosing frequency problems of topically applied ophthalmic drugs J. Pharm. Sci., 63 (1974), pp. 333-338, 10.1002/jps.2600630304

266. F.G. Senjoti et. al. J. Optimizing ophthalmic delivery of a poorly water soluble drug from an aqueous in situ gelling system Eur. J. Pharm. Biopharm., 154 (2020), pp. 1-7.

267. S. Kalepu, V. Nekkanti. Insoluble drug delivery strategies: Review of recent advances and business prospects j. Acta Pharm. Sin. B., 5 (2015), pp. 442-453

268. K.T. Savjani, A.K. Gajjar, J.K. Savjani. Drug Solubility: Importance and Enhancement Techniques. ISRN Pharm., 2012 (2012), pp. 1-10

269. A. Farkouh, P. Frigo, M. Czejka. Systemic side effects of eye drops: a pharmacokinetic perspective Clin. Ophthalmol., 10 (2016), pp. 2433-2441,

270. J. Möschwitzer, R. Müller. Nanocrystal formulations for improved delivery of poorly soluble drugs Nanomedicine Heal. Dis., 79 (2011), pp. 79-99,

271. S.M. Dizaj, Z. et al. Nanosizing of drugs: effect on dissolution rate. Res. Pharm. Sci., 10 (2015), pp. 95-108

272. T.C. Theoharides, P. Conti, Dexamethasone for COVID-19? Not so fast, J. Biol. Regul. Homeost. Agents 34 (3) (2020 Jun 4) 1–5, https://doi.org/10.23812/20- Edıtorıal_1-5.

273. Sahin, A.R. et. al. 2020. 2019 novel coronavirus (COVID-19) outbreak: a review of the current literature. EJMO 4, 1–7.

274. Villar, J., Ferrando, C., Martínez, D., Ambros, ´ A., Munoz, ˜ T., Soler, J.A., Aguilar, G., Alba, F., Gonzalez-Higueras, ´ E., Conesa, L.A., 2020a. Dexamethasone treatment for the acute respiratory distress syndrome: a multicentre, randomised controlled trial. Lancet. Respir. Med. 8, 267–276.

275. N. Abdolahi, E. Kaheh, R. Golsha, et al., Letter to the editor: efficacy of different methods of combination regimen administrations including dexamethasone, intravenous immunoglobulin, and interferon-beta to treat critically ill COVID-19 patients: a structured summary of a study protocol for a randomized controlled trial, Trials 21 (1) (2020 Jun 19) 549, https://doi.org/10.1186/s13063-020-04499-5.

276. Health, N.I.O., 2017. LiverTox: clinical and research information on drug-induced liver injury. Nih. gov. https://livertox.nih.gov.

277. Bethesda, 2012. Corticosteroids. LiverTox: Clinical and Research Information on Drug-Induced Liver Injury. National Institute of Diabetes and Digestive and Kidney Diseases; 2021 May 7.

278. Rhen, T., Cidlowski, J.A., 2005. Antiinflammatory action of glucocorticoids—new mechanisms for old drugs. N. Engl. J. Med. 353, 1711–1723.

279. Broccoli, M.C., Pigoga, J.L., Nyirenda, M., Wallis, L., Hynes, E.C., 2018. Essential medicines for emergency care in Africa. Afr. J. Emerg. Med. 8, 110–117.

280. Gulick, R.M., Sobieszczyk, M.E., Landry, D.W., Hollenberg, A.N., 2020. Prioritizing clinical research studies during the COVID-19 pandemic: lessons from New York City. J. Clin. Invest. 130 (9).

281. M.A. Lim, R. Pranata, Worrying situation regarding the use of dexamethasone for COVID-19, Ther. Adv. Respir. Dis. 14 (2020 Jan-Dec), https://doi.org/10.1177/ 1753466620942131, 1753466620942131.

282. T. Rhen, J.A. Cidlowski, Antiinflammatory action of glucocorticoids–new mechanisms for old drugs, N. Engl. J. Med. 353 (16) (2005 Oct 20) 1711–1723, https:// doi.org/10.1056/NEJMra050541.

283. V. Selvaraj, K. Dapaah-Afriyie, A. Finn, et al., Short-term dexamethasone in sarsCoV-2 patients, R. I. Med. J. 103 (6) (2020 Jun 19) 39–43.

284. N. Nagai et. al. A nanoparticle-based ophthalmic formulation of dexamethasone enhances corneal permeability of the drug and prolongs its corneal residence time. Biol. Pharm. Bull., 40 (2017), pp. 1055-1062

285. Lingbo Shen. Enhanced topical corticosteroids delivery to the eye: A trade-off in strategy choice. Journal of Controlled Release. Volume 339, 10 November 2021, Pages 91-113

286. News,2020a. Potential coronavirus vaccine. http://www.abc23.com/News/NewsDetails.asp?NewsID=30346.

287. Chen, Y., Li, L., 2020. SARS-CoV-2: virus dynamics and host response. Lancet Infect. Dis. 20, 515–516.

288. RECOVERY Collaborative Group, P. Horby, W.S. Lim, et al., Dexamethasone in hospitalized patients with covid-19- preliminary report, N. Engl. J. Med. (2020 Jul 17), https://doi.org/10.1056/NEJMoa2021436. Epub ahead of print. PMID: 32678530; PMCID: PMC7383595.

289. Group, R.C. tl. al. 2020. Dexamethasone in hospitalized patients with covid-19—preliminary report. Effect of dexamethasone in hospitalized patients with COVID-19: preliminary report. MedRxiv.
290. R.M. Johnson, J.M. Vinetz, Dexamethasone in the management of covid -19, BMJ 370 (2020 Jul 3) m2648, https://doi.org/10.1136/bmj.m2648.
291. Yong, S.J., 2020a. Biology of dexamethasone: the first lifesaving drug for covid-19.
292. Soy, M. et.al. 2020. Cytokine storm in COVID-19: pathogenesis and overview of anti-inflammatory agents used in treatment. Clin. Rheumatol. 39, 2085–2094.
293. Who, 2020. Coronavirus Disease (COVID-19): Dexamethasone.
294. Mahase, E., 2020b. Covid-19: Low Dose Steroid Cuts Death in Ventilated Patients by One Third, Trial Finds. British Medical Journal Publishing Group.

8. CURRICULUM VITAE